Fundamental Optics 1

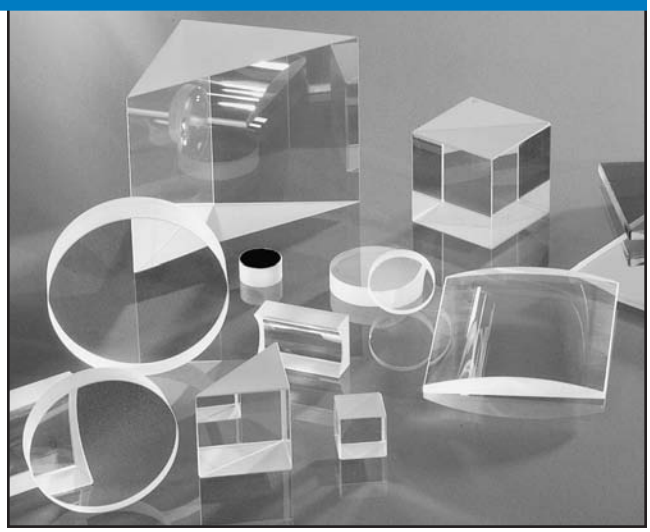

Introduction

The process of solving virtually any optical engineering problem can be broken down into two main steps. First, paraxial calculations (first order) are made to determine critical parameters such as magnification, focal length(s), clear aperture (diameter), and object and image position. These paraxial calculations are covered in the next section of this chapter.

Second, actual components are chosen based on these paraxial values, and their actual performance is evaluated with special attention paid to the effects of aberrations. A truly rigorous performance analysis for all but the simplest optical systems generally requires computer ray tracing, but simple generalizations can be used, especially when the lens selection process is confined to a limited range of component shapes.

In practice, the second step may reveal conflicts with design constraints, such as component size, cost, or product availability. System parameters may therefore require modification.

Because some of the terms used in this chapter may not be familiar to all readers, a glossary of terms is provided in *Definition of Terms*.

Finally, it should be noted that the discussion in this chapter relates only to systems with uniform illumination; optical systems for Gaussian beams are covered in *Gaussian Beam Optics*.

Engineering Support

CVI Melles Griot maintains a staff of knowledgeable, experienced applications engineers at each of our facilities worldwide. The information given in this chapter is sufficient to enable the user to select the most appropriate catalog lenses for the most commonly encountered applications. However, when additional optical engineering support is required, our applications engineers are available to provide assistance. Do not hesitate to contact us for help in product selection or to obtain more detailed specifications on CVI Melles Griot products.

THE OPTICAL ENGINEERING PROCESS

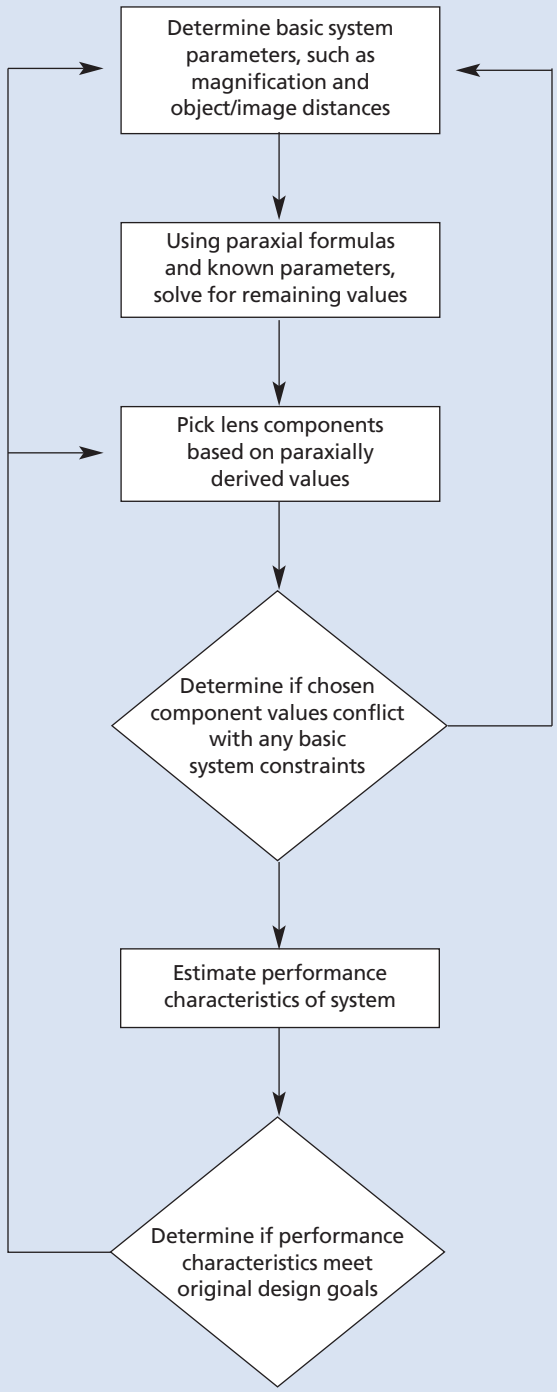

Paraxial Formulas

Sign Conventions

The validity of the paraxial lens formulas is dependent on adherence to the following sign conventions:

For lenses: (refer to figure 1.1)

s is + for object to left of H (the first principal point)

s is − for object to right of H

s'' is + for image to right of H″ (the second principal point)

s'' is − for image to left of H″

m is + for an inverted image

m is − for an upright image

For mirrors:

f is + for convex (diverging) mirrors

f is − for concave (converging) mirrors

s is + for object to left of H

s is − for object to right of H

s'' is − for image to right of H″

s'' is + for image to left of H″

m is + for an inverted image

m is − for an upright image

When using the thin-lens approximation, simply refer to the left and right of the lens.

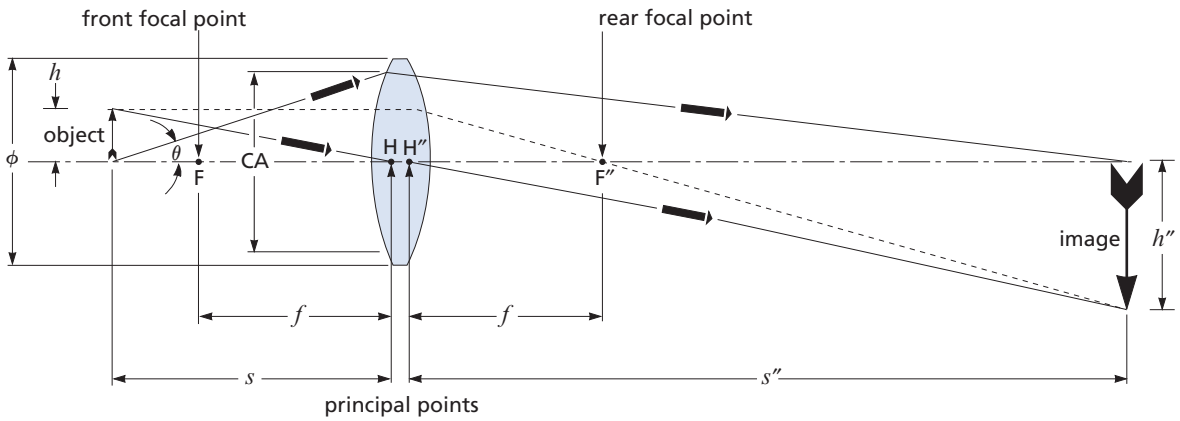

Note location of object and image relative to front and rear focal points.

ϕ = lens diameter

CA = clear aperture (typically 90% of ϕ)

f = effective focal length (EFL) which may be positive (as shown) or negative. f represents both FH and H″F″, assuming lens is surrounded by medium of index 1.0

m = $s''/s = h''/h$ = magnification or conjugate ratio, said to be infinite if either s'' or s is infinite

θ = arcsin (CA/2s)

s = object distance, positive for object (whether real or virtual) to the left of principal point H

s'' = image distance (s and s'' are collectively called conjugate distances, with object and image in conjugate planes), positive for image (whether real or virtual) to the right of principal point H″

h = object height

h'' = image height

Figure 1.1 **Sign conventions**

Typically, the first step in optical problem solving is to select a system focal length based on constraints such as magnification or conjugate distances (object and image distance). The relationship among focal length, object position, and image position is given by

$$\frac{1}{f} = \frac{1}{s} + \frac{1}{s''} \tag{1.1}$$

This formula is referenced to figure 1.1 and the sign conventions given in *Sign Conventions*.

By definition, magnification is the ratio of image size to object size or

$$m = \frac{s''}{s} = \frac{h''}{h}. \tag{1.2}$$

This relationship can be used to recast the first formula into the following forms:

$$f = m\frac{(s+s'')}{(m+1)^2} \tag{1.3}$$

$$f = \frac{sm}{m+1} \tag{1.4}$$

$$f = \frac{s+s''}{m+2+\frac{1}{m}} \tag{1.5}$$

$$s(m+1) = s+s'' \tag{1.6}$$

where $(s+s'')$ is the approximate object-to-image distance.

With a real lens of finite thickness, the image distance, object distance, and focal length are all referenced to the principal points, not to the physical center of the lens. By neglecting the distance between the lens' principal points, known as the hiatus, $s+s''$ becomes the object-to-image distance. This simplification, called the thin-lens approximation, can speed up calculation when dealing with simple optical systems.

Example 1: Object outside Focal Point

A 1-mm-high object is placed on the optical axis, 200 mm left of the left principal point of a LDX-25.0-51.0-C ($f = 50$ mm). Where is the image formed, and what is the magnification? (See figure 1.2.)

$$\frac{1}{s''} = \frac{1}{f} - \frac{1}{s}$$

$$\frac{1}{s''} = \frac{1}{50} - \frac{1}{200}$$

$$s'' = 66.7 \text{ mm}$$

$$m = \frac{s''}{s} = \frac{66.7}{200} = 0.33$$

or real image is 0.33 mm high and inverted.

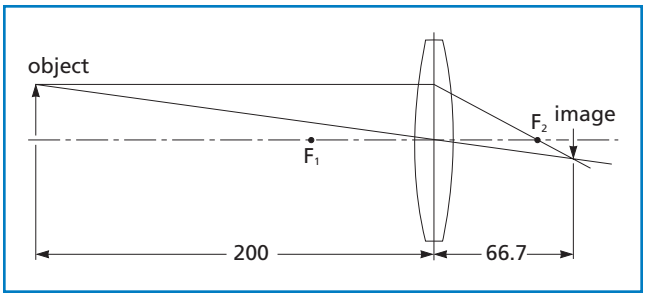

Figure 1.2 **Example 1** ($f = 50$ mm, $s = 200$ mm, $s'' = 66.7$ mm)

Example 2: Object inside Focal Point

The same object is placed 30 mm left of the left principal point of the same lens. Where is the image formed, and what is the magnification? (See figure 1.3.)

$$\frac{1}{s''} = \frac{1}{50} - \frac{1}{30}$$

$$s'' = -75 \text{ mm}$$

$$m = \frac{s''}{s} = \frac{-75}{30} = -2.5$$

or virtual image is 2.5 mm high and upright.

In this case, the lens is being used as a magnifier, and the image can be viewed only back through the lens.

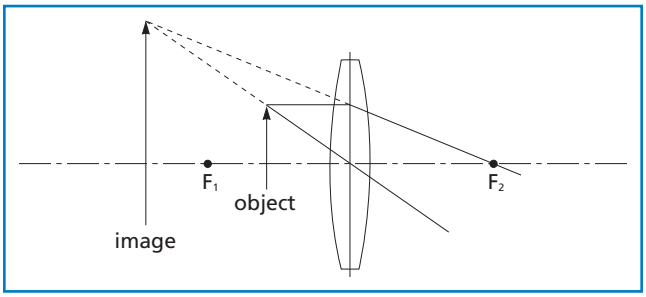

Figure 1.3 **Example 2** ($f = 50$ mm, $s = 30$ mm, $s'' = -75$ mm)

Example 3: Object at Focal Point

A 1-mm-high object is placed on the optical axis, 50 mm left of the first principal point of an LDK-50.0-52.2-C ($f = -50$ mm). Where is the image formed, and what is the magnification? (See figure 1.4.)

$$\frac{1}{s''} = \frac{1}{-50} - \frac{1}{50}$$

$$s'' = -25 \text{ mm}$$

$$m = \frac{s''}{s} = \frac{-25}{50} = -0.5$$

or virtual image is 0.5 mm high and upright.

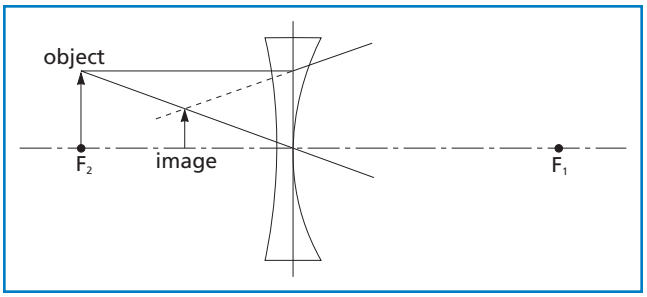

Figure 1.4 **Example 3** ($f = -50$ mm, $s = 50$ mm, $s' = -25$ mm)

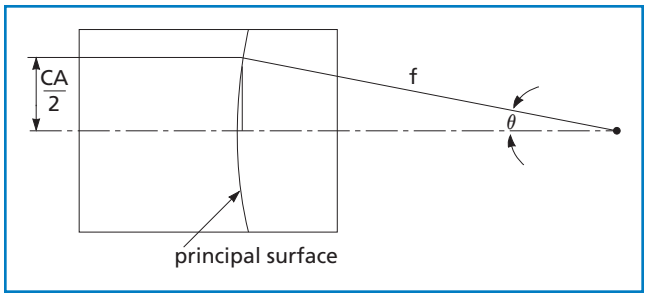

Figure 1.5 **F-number and numerical aperture**

A simple graphical method can also be used to determine paraxial image location and magnification. This graphical approach relies on two simple properties of an optical system. First, a ray that enters the system parallel to the optical axis crosses the optical axis at the focal point. Second, a ray that enters the first principal point of the system exits the system from the second principal point parallel to its original direction (i.e., its exit angle with the optical axis is the same as its entrance angle). This method has been applied to the three previous examples illustrated in figures 1.2 through 1.4. Note that by using the thin-lens approximation, this second property reduces to the statement that a ray passing through the center of the lens is undeviated.

F-NUMBER AND NUMERICAL APERTURE

The paraxial calculations used to determine the necessary element diameter are based on the concepts of focal ratio (f-number or f/#) and numerical aperture (NA). The f-number is the ratio of the focal length of the lens to its "effective" diameter, the clear aperture (CA).

$$\text{f-number} = \frac{f}{\text{CA}}. \qquad (1.7)$$

To visualize the f-number, consider a lens with a positive focal length illuminated uniformly with collimated light. The f-number defines the angle of the cone of light leaving the lens which ultimately forms the image. This is an important concept when the throughput or light-gathering power of an optical system is critical, such as when focusing light into a monochromator or projecting a high-power image.

The other term used commonly in defining this cone angle is numerical aperture. The NA is the sine of the angle made by the marginal ray with the optical axis. By referring to figure 1.5 and using simple trigonometry, it can be seen that

$$\text{NA} = \sin\theta = \frac{\text{CA}}{2f} \qquad (1.8)$$

and

$$\text{NA} = \frac{1}{2(\text{f-number})}. \qquad (1.9)$$

Ray f-numbers can also be defined for any arbitrary ray if its conjugate distance and the diameter at which it intersects the principal surface of the optical system are known.

NOTE

Because the sign convention given previously is not used universally in all optics texts, the reader may notice differences in the paraxial formulas. However, results will be correct as long as a consistent set of formulas and sign conventions is used.

Imaging Properties of Lens Systems

THE OPTICAL INVARIANT

To understand the importance of the NA, consider its relation to magnification. Referring to figure 1.6,

$$\text{NA (object side)} = \sin\theta = \frac{\text{CA}}{2s} \tag{1.10}$$

$$\text{NA}'' \text{ (image side)} = \sin\theta'' = \frac{\text{CA}}{2s''} \tag{1.11}$$

which can be rearranged to show

$$\text{CA} = 2s\ \sin\theta \tag{1.12}$$

and

$$\text{CA} = 2s''\sin\theta'' \tag{1.13}$$

leading to

$$\frac{s''}{s} = \frac{\sin\theta}{\sin\theta''} = \frac{\text{NA}}{\text{NA}''}. \tag{1.14}$$

Since $\frac{s''}{s}$ is simply the magnification of the system,

we arrive at

$$m = \frac{\text{NA}}{\text{NA}''}. \tag{1.15}$$

The magnification of the system is therefore equal to the ratio of the NAs on the object and image sides of the system. This powerful and useful result is completely independent of the specifics of the optical system, and it can often be used to determine the optimum lens diameter in situations involving aperture constraints.

When a lens or optical system is used to create an image of a source, it is natural to assume that, by increasing the diameter (ϕ) of the lens, thereby increasing its CA, we will be able to collect more light and thereby produce a brighter image. However, because of the relationship between magnification and NA, there can be a theoretical limit beyond which increasing the diameter has no effect on light-collection efficiency or image brightness.

Since the NA of a ray is given by CA/2s, once a focal length and magnification have been selected, the value of NA sets the value of CA. Thus, if one is dealing with a system in which the NA is constrained on either the object or image side, increasing the lens diameter beyond this value will increase system size and cost but will not improve performance (i.e., throughput or image brightness). This concept is sometimes referred to as the optical invariant.

SAMPLE CALCULATION

To understand how to use this relationship between magnification and NA, consider the following example.

Example: System with Fixed Input NA

Two very common applications of simple optics involve coupling light into an optical fiber or into the entrance slit of a monochromator. Although these problems appear to be quite different, they both have the same limitation — they have a fixed NA. For monochromators, this limit is usually expressed in terms of the f-number. In addition to the fixed NA, they both have a fixed entrance pupil (image) size.

Suppose it is necessary, using a singlet lens, to couple the output of an incandescent bulb with a filament 1 mm in diameter into an optical fiber as shown in figure 1.7. Assume that the fiber has a core diameter of 100 μm and an NA of 0.25, and that the design requires that the total distance from the source to the fiber be 110 mm. Which lenses are appropriate?

By definition, the magnification must be 0.1. Letting $s + s''$ total 110 mm (using the thin-lens approximation), we can use equation 1.3,

$$f = m\frac{(s+s'')}{(m+1)^2}, \qquad \textit{(see eq. 1.3)}$$

to determine that the focal length is 9.1 mm. To determine the conjugate distances, s and s'', we utilize equation 1.6,

$$s(m+1) = s + s'', \qquad \textit{(see eq. 1.6)}$$

and find that $s = 100$ mm and $s'' = 10$ mm.

We can now use the relationship NA = CA/2s or NA$''$ = CA/2s'' to derive CA, the optimum clear aperture (effective diameter) of the lens.

With an image NA of 0.25 and an image distance (s'') of 10 mm,

$$0.25 = \frac{\text{CA}}{20}$$

and

$$\text{CA} = 5 \text{ mm}.$$

Accomplishing this imaging task with a single lens therefore requires an optic with a 9.1-mm focal length and a 5-mm diameter. Using a larger diameter lens will not result in any greater system throughput because of the limited input NA of the optical fiber. The singlet lenses in this catalog that meet these criteria are LPX-5.0-5.2-C, which is plano-convex, and LDX-6.0-7.7-C and LDX-5.0-9.9-C, which are biconvex.

Making some simple calculations has reduced our choice of lenses to just three. The following chapter, *Gaussian Beam Optics*, discusses how to make a final choice of lenses based on various performance criteria.

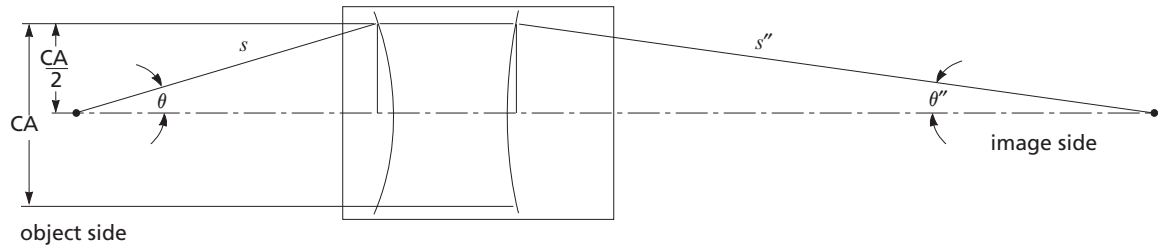

Figure 1.6 **Numerical aperture and magnification**

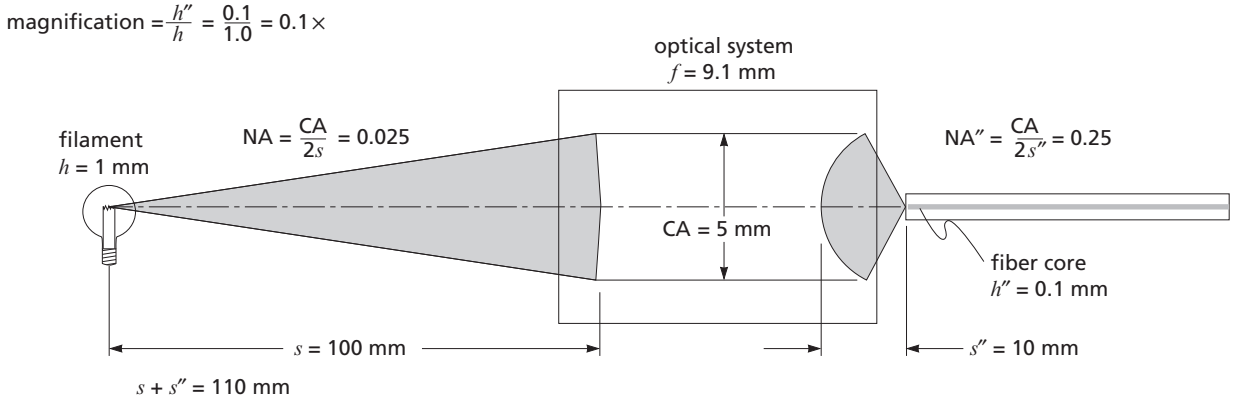

Figure 1.7 **Optical system geometry for focusing the output of an incandescent bulb into an optical fiber**

Lens Combination Formulas

Many optical tasks require several lenses in order to achieve an acceptable level of performance. One possible approach to lens combinations is to consider each image formed by each lens as the object for the next lens and so on. This is a valid approach, but it is time consuming and unnecessary.

It is much simpler to calculate the effective (combined) focal length and principal-point locations and then use these results in any subsequent paraxial calculations (see figure 1.8). They can even be used in the optical invariant calculations described in the preceding section.

EFFECTIVE FOCAL LENGTH

The following formulas show how to calculate the effective focal length and principal-point locations for a combination of any two arbitrary components. The approach for more than two lenses is very simple: Calculate the values for the first two elements, then perform the same calculation for this combination with the next lens. This is continued until all lenses in the system are accounted for.

The expression for the combination focal length is the same whether lens separation distances are large or small and whether f_1 and f_2 are positive or negative:

$$f = \frac{f_1 f_2}{f_1 + f_2 - d}. \qquad (1.16)$$

This may be more familiar in the form

$$\frac{1}{f} = \frac{1}{f_1} + \frac{1}{f_2} - \frac{d}{f_1 f_2}. \qquad (1.17)$$

Notice that the formula is symmetric with respect to the interchange of the lenses (end-for-end rotation of the combination) at constant *d*. The next two formulas are not.

COMBINATION FOCAL-POINT LOCATION

For all values of f_1, f_2, and d, the location of the focal point of the combined system (s_2''), measured from the secondary principal point of the second lens (H_2''), is given by

$$s_2'' = \frac{f_2(f_1 - d)}{f_1 + f_2 - d}. \qquad (1.18)$$

This can be shown by setting $s_1 = d - f_1$ (see figure 1.8a), and solving

$$\frac{1}{f_2} = \frac{1}{s_1} + \frac{1}{s_2''}$$

for s_2''.

Symbols

f_c = combination focal length (EFL), positive if combination final focal point falls to the right of the combination secondary principal point, negative otherwise (see figure 1.8c).

f_1 = focal length of the first element (see figure 1.8a).

f_2 = focal length of the second element.

d = distance from the secondary principal point of the first element to the primary principal point of the second element, positive if the primary principal point is to the right of the secondary principal point, negative otherwise (see figure 1.8b).

s_1'' = distance from the primary principal point of the first element to the final combination focal point (location of the final image for an object at infinity to the right of both lenses), positive if the focal point is to left of the first element's primary principal point (see figure 1.8d).

s_2'' = distance from the secondary principal point of the second element to the final combination focal point (location of the final image for an object at infinity to the left of both lenses), positive if the focal point is to the right of the second element's secondary principal point (see figure 1.8b).

z_H = distance to the combination primary principal point measured from the primary principal point of the first element, positive if the combination secondary principal point is to the right of secondary principal point of second element (see figure 1.8d).

z_H'' = distance to the combination secondary principal point measured from the secondary principal point of the second element, positive if the combination secondary principal point is to the right of the secondary principal point of the second element (see figure 1.8c).

Note: *These paraxial formulas apply to* ***coaxial*** *combinations of both thick and thin lenses immersed in air or any other fluid with refractive index independent of position. They assume that light propagates from left to right through an optical system.*

COMBINATION SECONDARY PRINCIPAL-POINT LOCATION

Because the thin-lens approximation is obviously highly invalid for most combinations, the ability to determine the location of the secondary principal point is vital for accurate determination of d when another element is added. The simplest formula for this calculates the distance from the secondary principal point of the final (second) element to the secondary principal point of the combination (see figure 1.8b):

$$z = s_2'' - f \,. \qquad (1.19)$$

COMBINATION EXAMPLES

It is possible for a lens combination or system to exhibit principal planes that are far removed from the system. When such systems are themselves combined, negative values of d may occur. Probably the simplest example of a negative d-value situation is shown in figure 1.9. Meniscus lenses with steep surfaces have external principal planes. When two of these lenses are brought into contact, a negative value of d can occur. Other combined-lens examples are shown in figures 1.10 through 1.13.

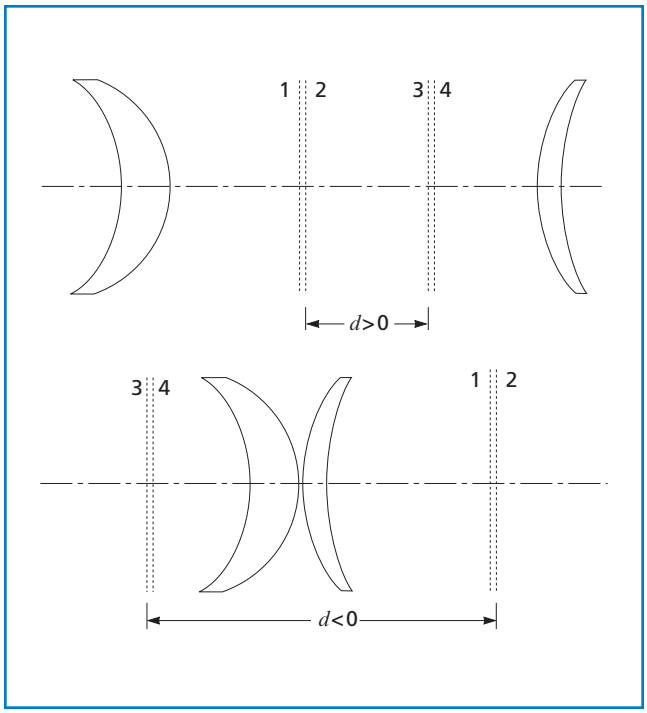

Figure 1.9 **"Extreme" meniscus-form lenses with external principal planes** (drawing not to scale)

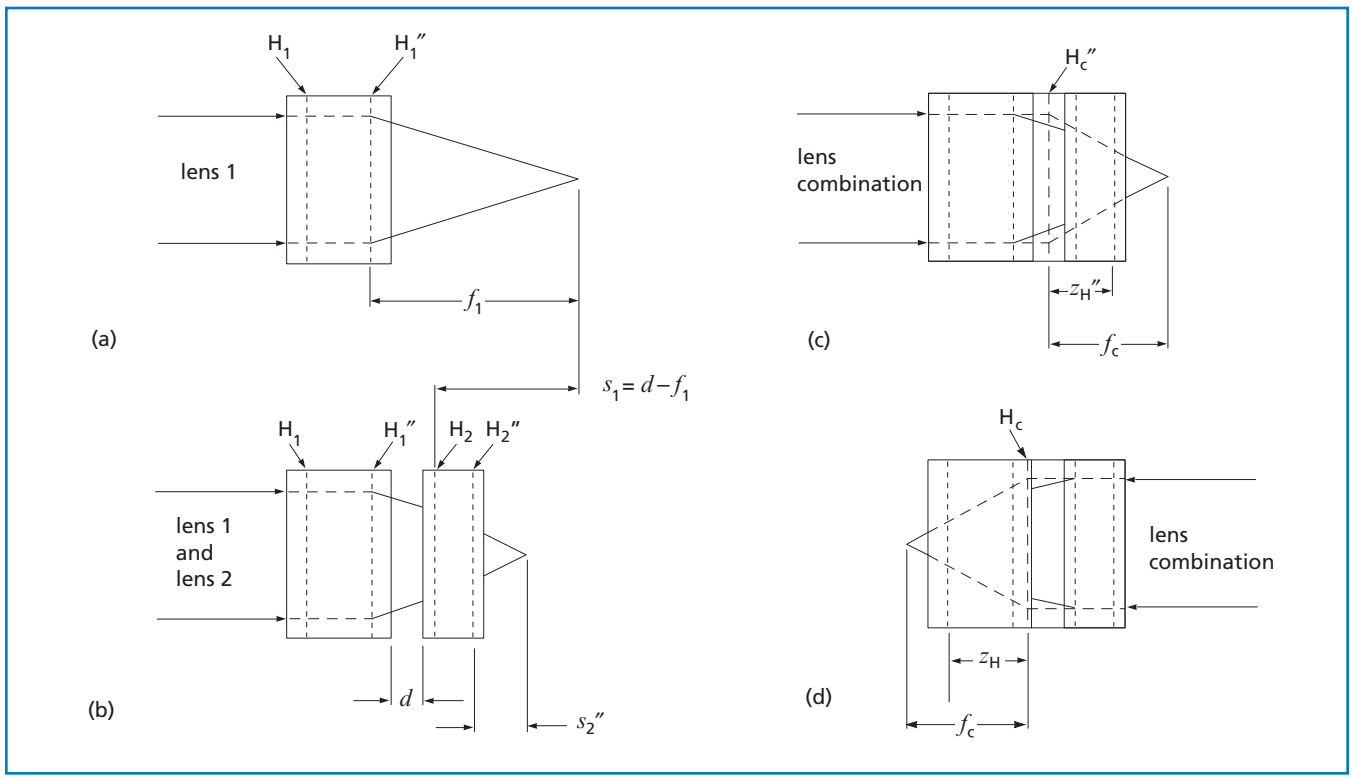

Figure 1.8 **Lens combination focal length and principal planes**

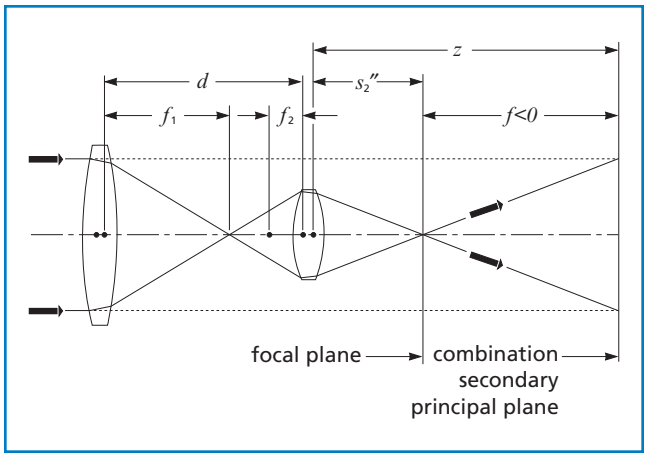

Figure 1.10 **Positive lenses separated by distance greater than $f_1 + f_2$:** f is negative and both s_2'' and z are positive. Lens symmetry is not required.

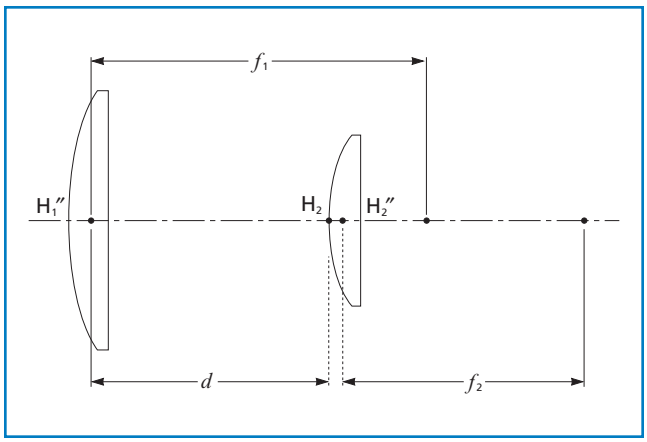

Figure 1.11 **Achromatic combinations:** Air-spaced lens combinations can be made nearly achromatic, even though both elements are made from the same material. Achieving achromatism requires that, in the thin-lens approximation,

$$d = \frac{(f_1 + f_2)}{2}.$$

This is the basis for Huygens and Ramsden eyepieces.

This approximation is adequate for most thick-lens situations. The signs of f_1, f_2, and d are unrestricted, but d must have a value that guarantees the existence of an air space. Element shapes are unrestricted and can be chosen to compensate for other aberrations.

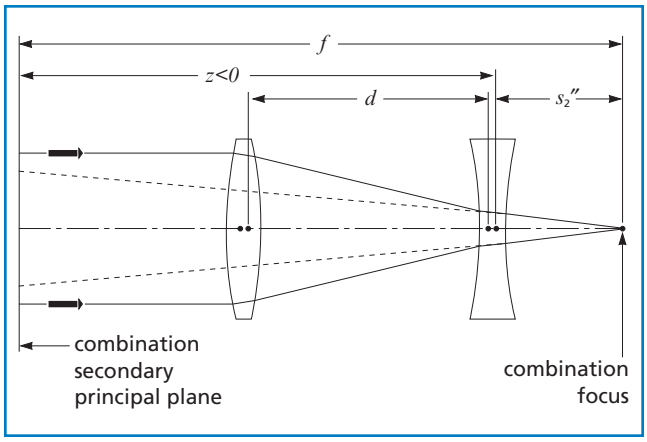

Figure 1.12 **Telephoto combination:** The most important characteristic of the telephoto lens is that the EFL, and hence the image size, can be made much larger than the distance from the first lens surface to the image would suggest by using a positive lens followed by a negative lens (but not necessarily the lens shapes shown in the figure). For example, f_1 is positive and $f_2 = -f_1/2$. Then f is negative for d less than $f_1/2$, infinite for $d = f_1/2$ (Galilean telescope or beam expander), and positive for d larger than $f_1/2$. To make the example even more specific, catalog lenses LDX-50.8-130.4-C and LDK-42.0-52.2-C, with $d = 78.2$ mm, will yield $s_2'' = 2.0$ m, $f = 5.2$ m, and $z = 43.2$ m.

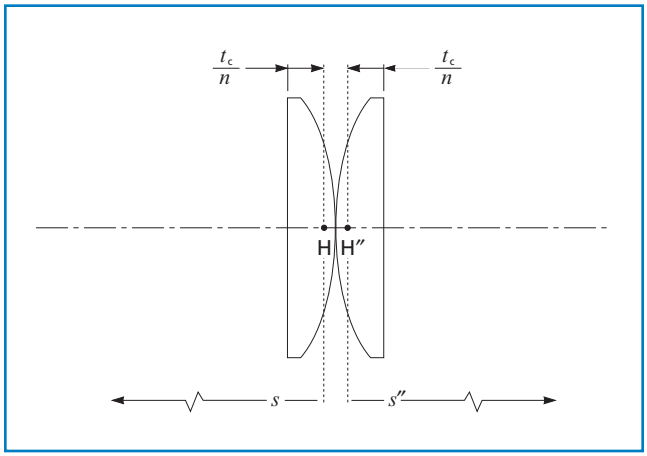

Figure 1.13 **Condenser configuration:** The convex vertices of a pair of identical plano-convex lenses are on contact. (The lenses could also be plano aspheres.) Because $d = 0$, $f = f_1/2 = f_2/2$, $f_1/2 = s_2''$, and $z = 0$. The secondary principal point of the second element and the secondary principal point of the combination coincide at H″, at depth t_c/n beneath the vertex of the plano surface of the second element, where t_c is the element center thickness and n is the refractive index of the element. By symmetry, the primary principal point of the combination is similarly located in the first element. Combination conjugate distances must be measured from these points.

Performance Factors

After paraxial formulas have been used to select values for component focal length(s) and diameter(s), the final step is to select actual lenses. As in any engineering problem, this selection process involves a number of tradeoffs, including performance, cost, weight, and environmental factors.

The performance of real optical systems is limited by several factors, including lens aberrations and light diffraction. The magnitude of these effects can be calculated with relative ease.

Numerous other factors, such as lens manufacturing tolerances and component alignment, impact the performance of an optical system. Although these are not considered explicitly in the following discussion, it should be kept in mind that if calculations indicate that a lens system only just meets the desired performance criteria, in practice it may fall short of this performance as a result of other factors. In critical applications, it is generally better to select a lens whose calculated performance is significantly better than needed.

DIFFRACTION

Diffraction, a natural property of light arising from its wave nature, poses a fundamental limitation on any optical system. Diffraction is always present, although its effects may be masked if the system has significant aberrations. When an optical system is essentially free from aberrations, its performance is limited solely by diffraction, and it is referred to as diffraction limited.

In calculating diffraction, we simply need to know the focal length(s) and aperture diameter(s); we do not consider other lens-related factors such as shape or index of refraction.

Since diffraction increases with increasing f-number, and aberrations decrease with increasing f-number, determining optimum system performance often involves finding a point where the combination of these factors has a minimum effect.

ABERRATIONS

To determine the precise performance of a lens system, we can trace the path of light rays through it, using Snell's law at each optical interface to determine the subsequent ray direction. This process, called ray tracing, is usually accomplished on a computer. When this process is completed, it is typically found that not all the rays pass through the points or positions predicted by paraxial theory. These deviations from ideal imaging are called lens aberrations.

The direction of a light ray after refraction at the interface between two homogeneous, isotropic media of differing index of refraction is given by Snell's law:

$$n_1 \sin\theta_1 = n_2 \sin\theta_2 \qquad (1.20)$$

where θ_1 is the angle of incidence, θ_2 is the angle of refraction, and both angles are measured from the surface normal as shown in figure 1.14.

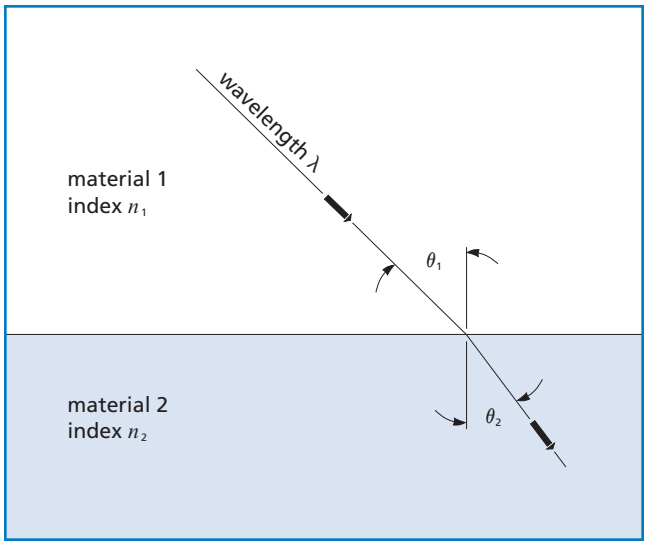

Figure 1.14 **Refraction of light at a dielectric boundary**

APPLICATION NOTE

Technical Assistance

Detailed performance analysis of an optical system is accomplished by using computerized ray-tracing software. CVI Melles Griot applications engineers are able to provide a ray-tracing analysis of simple catalog-component systems. If you need assistance in determining the performance of your optical system, or in selecting optimum components for your particular application, please contact your nearest CVI Melles Griot office.

Even though tools for the precise analysis of an optical system are becoming easier to use and are readily available, it is still quite useful to have a method for quickly estimating lens performance. This not only saves time in the initial stages of system specification, but can also help achieve a better starting point for any further computer optimization.

The first step in developing these rough guidelines is to realize that the sine functions in Snell's law can be expanded in an infinite Taylor series:

$$\sin\theta_1 = \theta_1 - \theta_1^3/3! + \theta_1^5/5! - \theta_1^7/7! + \theta_1^9/9! - \ldots \qquad (1.21)$$

The first approximation we can make is to replace all the sine functions with their arguments (i.e., replace $\sin\theta_1$ with θ_1 itself and so on). This is called first-order or paraxial theory because only the first terms of the sine expansions are used. Design of any optical system generally starts with this approximation using the paraxial formulas.

The assumption that $\sin\theta = \theta$ is reasonably valid for θ close to zero (i.e., high f-number lenses). With more highly curved surfaces (and particularly marginal rays), paraxial theory yields increasingly large deviations from real performance because $\sin\theta \neq \theta$. These deviations are known as aberrations. Because a perfect optical system (one without any aberrations) would form its image at the point and to the size indicated by paraxial theory, aberrations are really a measure of how the image differs from the paraxial prediction.

As already stated, exact ray tracing is the only rigorous way to analyze real lens surfaces. Before the advent of electronic computers, this was excessively tedious and time consuming. Seidel* addressed this issue by developing a method of calculating aberrations resulting from the ${\theta_1}^3/3!$ term. The resultant third-order lens aberrations are therefore called Seidel aberrations.

To simplify these calculations, Seidel put the aberrations of an optical system into several different classifications. In monochromatic light they are spherical aberration, astigmatism, field curvature, coma, and distortion. In polychromatic light there are also chromatic aberration and lateral color. Seidel developed methods to approximate each of these aberrations without actually tracing large numbers of rays using all the terms in the sine expansions.

In actual practice, aberrations occur in combinations rather than alone. This system of classifying them, which makes analysis much simpler, gives a good description of optical system image quality. In fact, even in the era of powerful ray-tracing software, Seidel's formula for spherical aberration is still widely used.

* *Ludwig von Seidel, 1857.*

SPHERICAL ABERRATION

Figure 1.15 illustrates how an aberration-free lens focuses incoming collimated light. All rays pass through the focal point F″. The lower figure shows the situation more typically encountered in single lenses. The farther from the optical axis the ray enters the lens, the nearer to the lens it focuses (crosses the optical axis). The distance along the optical axis between the intercept of the rays that are nearly on the optical axis (paraxial rays) and the rays that go through the edge of the lens (marginal rays) is called longitudinal spherical aberration (LSA). The height at which these rays intercept the paraxial focal plane is called transverse spherical aberration (TSA). These quantities are related by

$$\text{TSA} = \text{LSA} \times \tan(u'') \qquad (1.22)$$

Spherical aberration is dependent on lens shape, orientation, and conjugate ratio, as well as on the index of refraction of the materials present. Parameters for choosing the best lens shape and orientation for a given task are presented later in this chapter. However, the third-

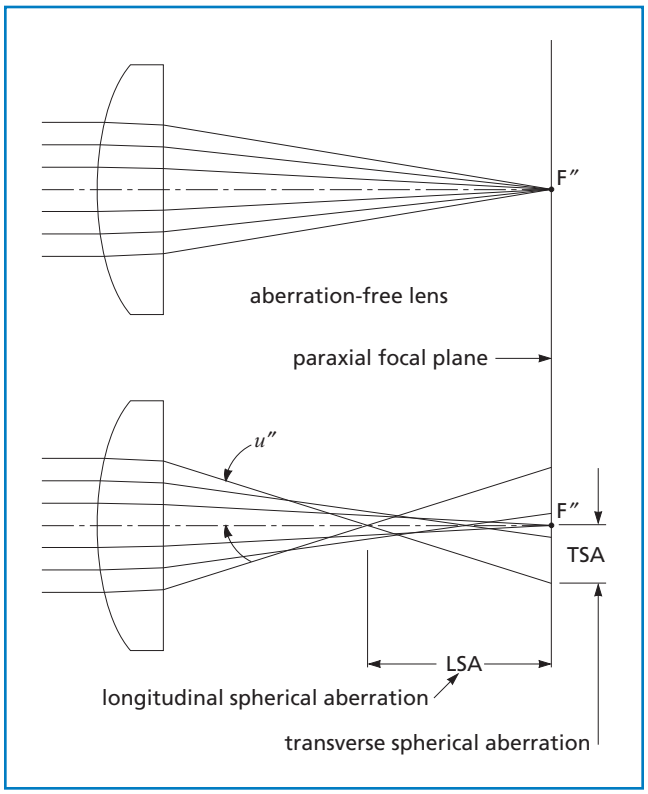

Figure 1.15 **Spherical aberration of a plano-convex lens**

order, monochromatic, spherical aberration of a plano-convex lens used at infinite conjugate ratio can be estimated by

$$\text{spot size due to spherical aberration} = \frac{0.067\, f}{\text{f/\#}^3}. \qquad (1.23)$$

Theoretically, the simplest way to eliminate or reduce spherical aberration is to make the lens surface(s) with a varying radius of curvature (i.e., an aspheric surface) designed to exactly compensate for the fact that $\sin\theta \neq \theta$ at larger angles. In practice, however, most lenses with high surface accuracy are manufactured by grinding and polishing techniques that naturally produce spherical or cylindrical surfaces. The manufacture of aspheric surfaces is more complex, and it is difficult to produce a lens of sufficient surface accuracy to eliminate spherical aberration completely. Fortunately, these aberrations can be virtually eliminated, for a chosen set of conditions, by combining the effects of two or more spherical (or cylindrical) surfaces.

In general, simple positive lenses have undercorrected spherical aberration, and negative lenses usually have overcorrected spherical aberration. By combining a positive lens made from low-index glass with a negative lens made from high-index glass, it is possible to produce a combination in which the spherical aberrations cancel but the focusing powers do not. The simplest examples of this are cemented doublets, such as the LAO series which produce minimal spherical aberration when properly used.

ASTIGMATISM

When an off-axis object is focused by a spherical lens, the natural asymmetry leads to astigmatism. The system appears to have two different focal lengths.

As shown in figure 1.16, the plane containing both optical axis and object point is called the tangential plane. Rays that lie in this plane are called tangential, or meridional, rays. Rays not in this plane are referred to as skew rays. The chief, or principal, ray goes from the object point through the center of the aperture of the lens system. The plane perpendicular to the tangential plane that contains the principal ray is called the sagittal or radial plane.

The figure illustrates that tangential rays from the object come to a focus closer to the lens than do rays in the sagittal plane. When the image is evaluated at the tangential conjugate, we see a line in the sagittal direction. A line in the tangential direction is formed at the sagittal conjugate. Between these conjugates, the image is either an elliptical or a circular blur. Astigmatism is defined as the separation of these conjugates.

The amount of astigmatism in a lens depends on lens shape only when there is an aperture in the system that is not in contact with the lens itself. (In all optical systems there is an aperture or stop, although in many cases it is simply the clear aperture of the lens element itself.) Astigmatism strongly depends on the conjugate ratio.

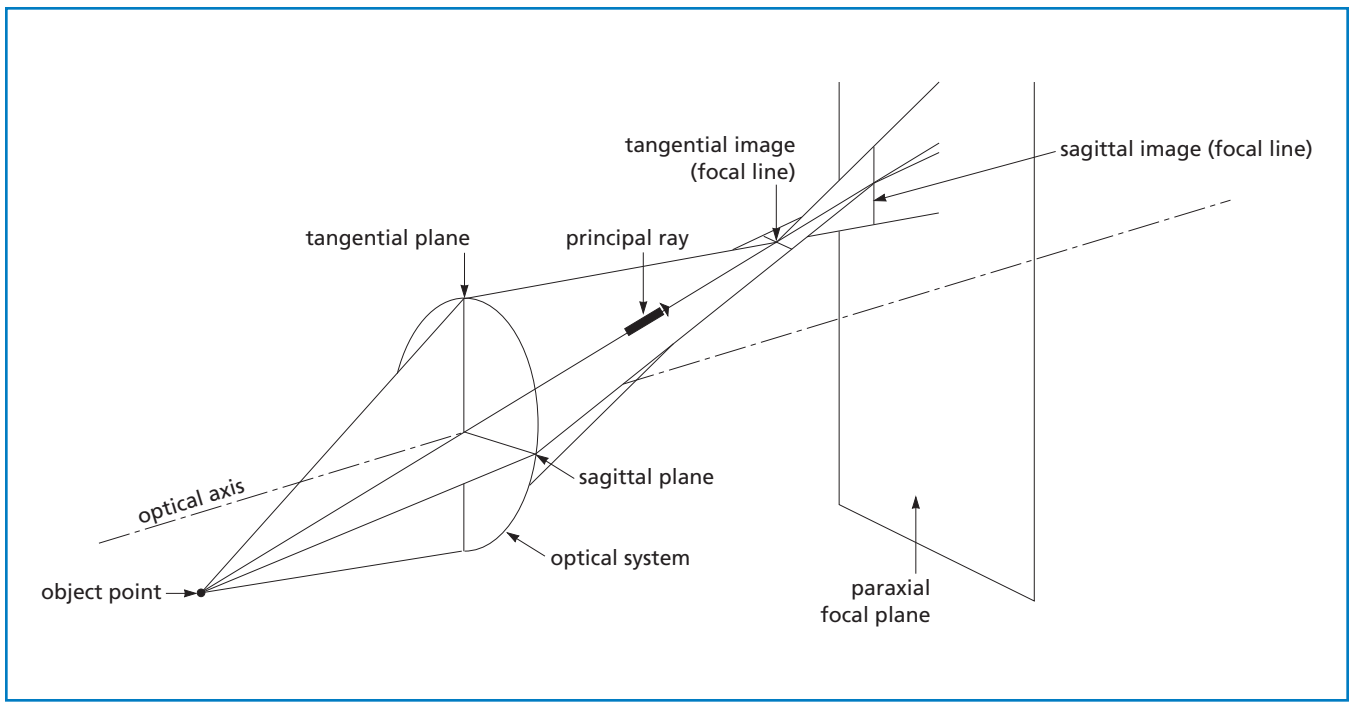

Figure 1.16 **Astigmatism represented by sectional views**

COMA

In spherical lenses, different parts of the lens surface exhibit different degrees of magnification. This gives rise to an aberration known as coma. As shown in figure 1.17, each concentric zone of a lens forms a ring-shaped image called a comatic circle. This causes blurring in the image plane (surface) of off-axis object points. An off-axis object point is not a sharp image point, but it appears as a characteristic comet-like flare. Even if spherical aberration is corrected and the lens brings all rays to a sharp focus on axis, a lens may still exhibit coma off axis. See figure 1.18.

As with spherical aberration, correction can be achieved by using multiple surfaces. Alternatively, a sharper image may be produced by judiciously placing an aperture, or stop, in an optical system to eliminate the more marginal rays.

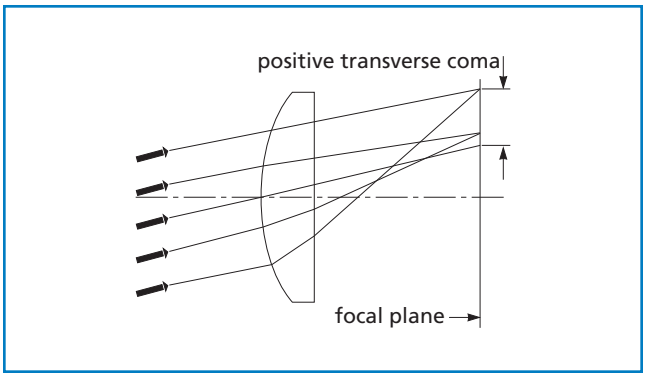

Figure 1.18 **Positive transverse coma**

FIELD CURVATURE

Even in the absence of astigmatism, there is a tendency of optical systems to image better on curved surfaces than on flat planes. This effect is called field curvature (see figure 1.19). In the presence of astigmatism, this problem is compounded because two separate astigmatic focal surfaces correspond to the tangential and sagittal conjugates.

Field curvature varies with the square of field angle or the square of image height. Therefore, by reducing the field angle by one-half, it is possible to reduce the blur from field curvature to a value of 0.25 of its original size.

Positive lens elements usually have inward curving fields, and negative lenses have outward curving fields. Field curvature can thus be corrected to some extent by combining positive and negative lens elements.

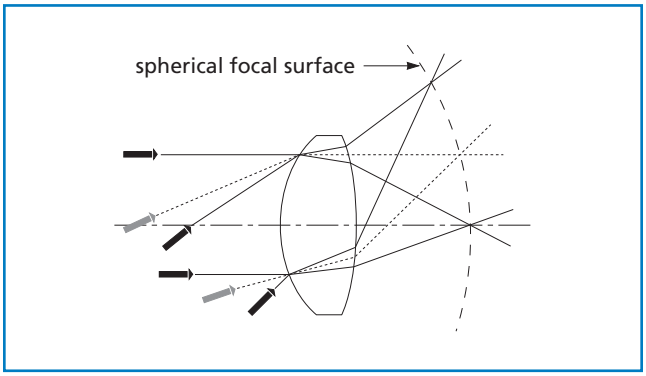

Figure 1.19 **Field curvature**

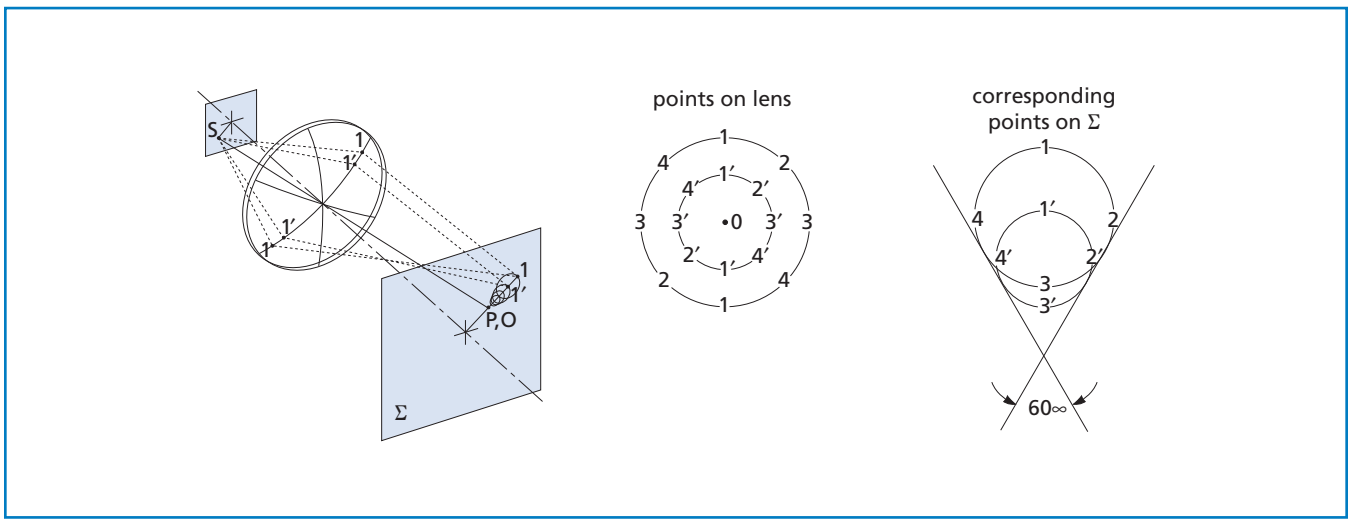

Figure 1.17 **Imaging an off-axis point source by a lens with positive transverse coma**

DISTORTION

The image field not only may have curvature but may also be distorted. The image of an off-axis point may be formed at a location on this surface other than that predicted by the simple paraxial equations. This distortion is different from coma (where rays from an off-axis point fail to meet perfectly in the image plane). Distortion means that even if a perfect off-axis point image is formed, its location on the image plane is not correct. Furthermore, the amount of distortion usually increases with increasing image height. The effect of this can be seen as two different kinds of distortion: pincushion and barrel (see figure 1.20). Distortion does not lower system resolution; it simply means that the image shape does not correspond exactly to the shape of the object. Distortion is a separation of the actual image point from the paraxially predicted location on the image plane and can be expressed either as an absolute value or as a percentage of the paraxial image height.

It should be apparent that a lens or lens system has opposite types of distortion depending on whether it is used forward or backward. This means that if a lens were used to make a photograph, and then used in reverse to project it, there would be no distortion in the final screen image. Also, perfectly symmetrical optical systems at 1:1 magnification have no distortion or coma.

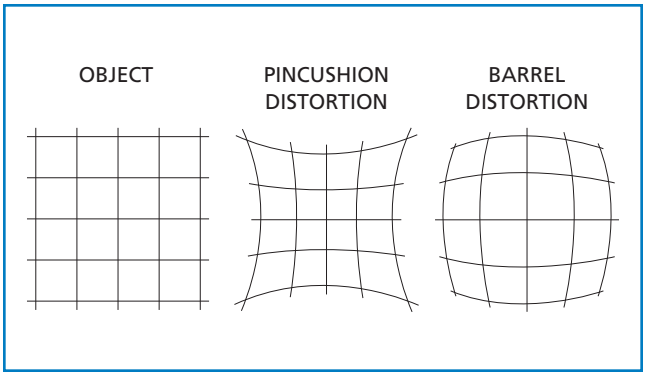

Figure 1.20 **Pincushion and barrel distortion**

CHROMATIC ABERRATION

The aberrations previously described are purely a function of the shape of the lens surfaces, and they can be observed with monochromatic light. Other aberrations, however, arise when these optics are used to transform light containing multiple wavelengths. The index of refraction of a material is a function of wavelength. Known as dispersion, this is discussed in *Material Properties*. From Snell's law (see equation 1.20), it can be seen that light rays of different wavelengths or colors will be refracted at different angles since the index is not a constant. Figure 1.21 shows the result when polychromatic collimated light is incident on a positive lens element. Because the index of refraction is higher for shorter wavelengths, these are focused closer to the lens than the longer wavelengths. Longitudinal chromatic aberration is defined as the axial distance from the nearest to the farthest focal point. As in the case of spherical aberration, positive and negative elements have opposite signs of chromatic aberration. Once again, by combining elements of nearly opposite aberration to form a doublet, chromatic aberration can be partially corrected. It is necessary to use two glasses with different dispersion characteristics, so that the weaker negative element can balance the aberration of the stronger, positive element.

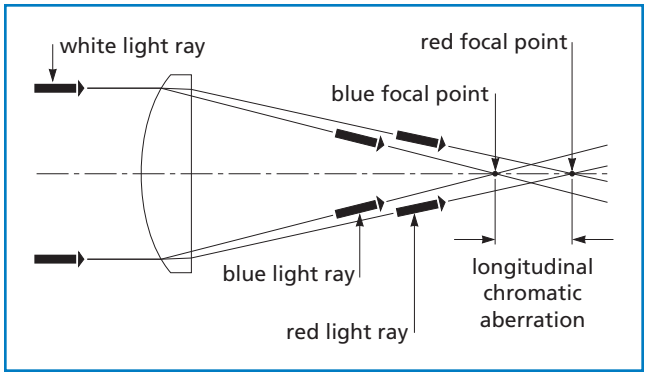

Figure 1.21 **Longitudinal chromatic aberration**

Variations of Aberrations with Aperture, Field Angle, and Image Height

Aberration	Aperture (ϕ)	Field Angle (θ)	Image Height (y)
Lateral Spherical	ϕ^3	—	—
Longitudinal Spherical	ϕ^2	—	—
Coma	ϕ^2	θ	y
Astigmatism	ϕ	θ^2	y^2
Field Curvature	ϕ	θ^2	y^2
Distortion	—	θ^3	y^3
Chromatic	—	—	—

LATERAL COLOR

Lateral color is the difference in image height between blue and red rays. Figure 1.22 shows the chief ray of an optical system consisting of a simple positive lens and a separate aperture. Because of the change in index with wavelength, blue light is refracted more strongly than red light, which is why rays intercept the image plane at different heights. Stated simply, magnification depends on color. Lateral color is very dependent on system stop location.

For many optical systems, the third-order term is all that may be needed to quantify aberrations. However, in highly corrected systems or in those having large apertures or a large angular field of view, third-order theory is inadequate. In these cases, exact ray tracing is absolutely essential.

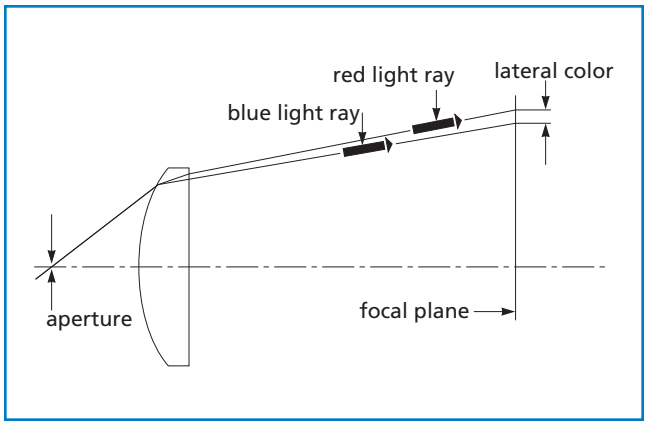

Figure 1.22 **Lateral Color**

APPLICATION NOTE

Achromatic Doublets Are Superior to Simple Lenses

Because achromatic doublets correct for spherical as well as chromatic aberration, they are often superior to simple lenses for focusing collimated light or collimating point sources, even in purely monochromatic light.

Although there is no simple formula that can be used to estimate the spot size of a doublet, the tables in *Spot Size* give sample values that can be used to estimate the performance of catalog achromatic doublets.

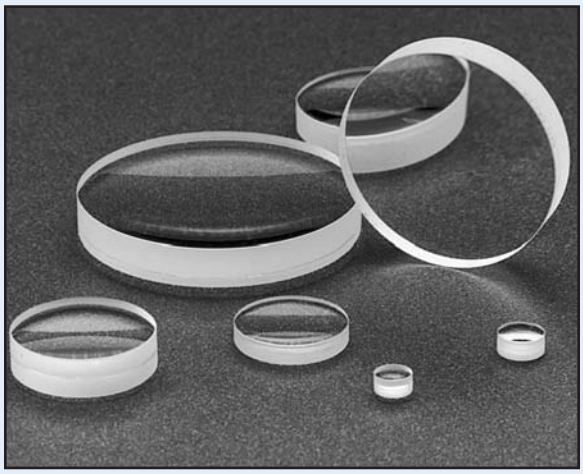

Lens Shape

Aberrations described in the preceding section are highly dependent on application, lens shape, and material of the lens (or, more exactly, its index of refraction). The singlet shape that minimizes spherical aberration at a given conjugate ratio is called best-form. The criterion for best-form at any conjugate ratio is that the marginal rays are equally refracted at each of the lens/air interfaces. This minimizes the effect of $\sin\theta \neq \theta$. It is also the criterion for minimum surface-reflectance loss. Another benefit is that absolute coma is nearly minimized for best-form shape, at both infinite and unit conjugate ratios.

To further explore the dependence of aberrations on lens shape, it is helpful to make use of the Coddington shape factor, q, defined as

$$q = \frac{(r_2 + r_1)}{(r_2 - r_1)}. \qquad (1.24)$$

Figure 1.23 shows the transverse and longitudinal spherical aberrations of a singlet lens as a function of the shape factor, q. In this particular instance, the lens has a focal length of 100 mm, operates at f/5, has an index of refraction of 1.518722 (BK7 at the mercury green line, 546.1 nm), and is being operated at the infinite conjugate ratio. It is also assumed that the lens itself is the aperture stop. An asymmetric shape that corresponds to a q-value of about 0.7426 for this material and wavelength is the best singlet shape for on-axis imaging. It is important to note that the best-form shape is dependent on refractive index. For example, with a high-index material, such as silicon, the best-form lens for the infinite conjugate ratio is a meniscus shape.

At infinite conjugate with a typical glass singlet, the plano-convex shape ($q = 1$), with convex side toward the infinite conjugate, performs nearly as well as the best-form lens. Because a plano-convex lens costs much less to manufacture than an asymmetric biconvex singlet, these lenses are quite popular. Furthermore, this lens shape exhibits near-minimum total transverse aberration and near-zero coma when used off axis, thus enhancing its utility.

For imaging at unit magnification ($s = s'' = 2f$), a similar analysis would show that a symmetric biconvex lens is the best shape. Not only is spherical aberration minimized, but coma, distortion, and lateral chromatic aberration exactly cancel each other out. These results are true regardless of material index or wavelength, which explains the utility of symmetric convex lenses, as well as symmetrical optical systems in general. However, if a remote stop is present, these aberrations may not cancel each other quite as well.

For wide-field applications, the best-form shape is definitely not the optimum singlet shape, especially at the infinite conjugate ratio, since it yields maximum field curvature. The ideal shape is determined by the situation and may require rigorous ray-tracing analysis. It is possible to achieve much better correction in an optical system by using more than one element. The cases of an infinite conjugate ratio system and a unit conjugate ratio system are discussed in the following section.

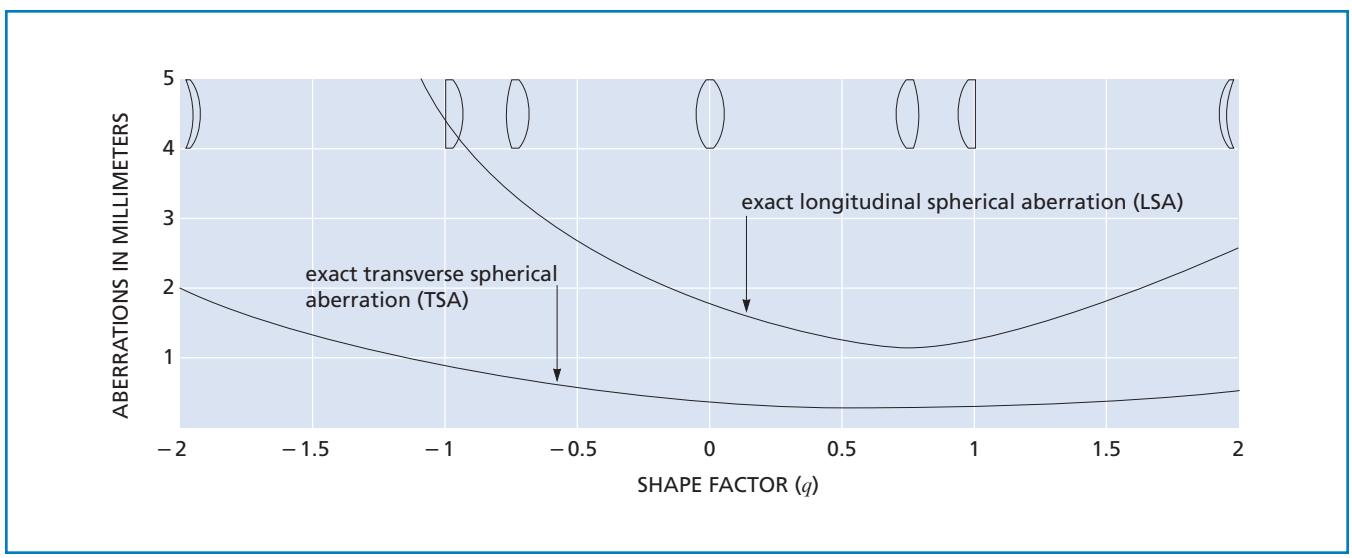

Figure 1.23 **Aberrations of positive singlets at infinite conjugate ratio as a function of shape**

Lens Combinations

INFINITE CONJUGATE RATIO

As shown in the previous discussion, the best-form singlet lens for use at infinite conjugate ratios is generally nearly plano-convex. Figure 1.24 shows a plano-convex lens (LPX-15.0-10.9-C) with incoming collimated light at a wavelength of 546.1 nm. This drawing, including the rays traced through it, is shown to exact scale. The marginal ray (ray f-number 1.5) strikes the paraxial focal plane significantly off the optical axis.

This situation can be improved by using a two-element system. The second part of the figure shows a precision achromat (LAO-21.0-14.0), which consists of a positive low-index (crown glass) element cemented to a negative meniscus high-index (flint glass) element. This is drawn to the same scale as the plano-convex lens. No spherical aberration can be discerned in the lens. Of course, not all of the rays pass exactly through the paraxial focal point; however, in this case, the departure is measured in micrometers, rather than in millimeters, as in the case of the plano-convex lens. Additionally, chromatic aberration (not shown) is much better corrected in the doublet. Even though these lenses are known as achromatic doublets, it is important to remember that even with monochromatic light the doublet's performance is superior.

Figure 1.24 also shows the f-number at which singlet performance becomes unacceptable. The ray with f-number 7.5 practically intercepts the paraxial focal point, and the f/3.8 ray is fairly close. This useful drawing, which can be scaled to fit a plano-convex lens of any focal length, can be used to estimate the magnitude of its spherical aberration, although lens thickness affects results slightly.

UNIT CONJUGATE RATIO

Figure 1.25 shows three possible systems for use at the unit conjugate ratio. All are shown to the same scale and using the same ray f-numbers with a light wavelength of 546.1 nm. The first system is a symmetric biconvex lens (LDX-21.0-19.2-C), the best-form singlet in this application. Clearly, significant spherical aberration is present in this lens at f/2.7. Not until f/13.3 does the ray closely approach the paraxial focus.

A dramatic improvement in performance is gained by using two identical plano-convex lenses with convex surfaces facing and nearly in contact. Those shown in figure 1.25 are both LPX-20.0-20.7-C. The combination of these two lenses yields almost exactly the same focal length as the biconvex lens. To understand why this configuration improves performance so dramatically, consider that if the biconvex lens were split down the middle, we would have two identical plano-convex lenses, each working at an infinite conjugate ratio, but with the convex surface toward the focus. This orientation is opposite to that shown to be optimum for this shape lens. On the other hand, if these lenses are reversed, we have the system just described but with a better correction of the spherical aberration.

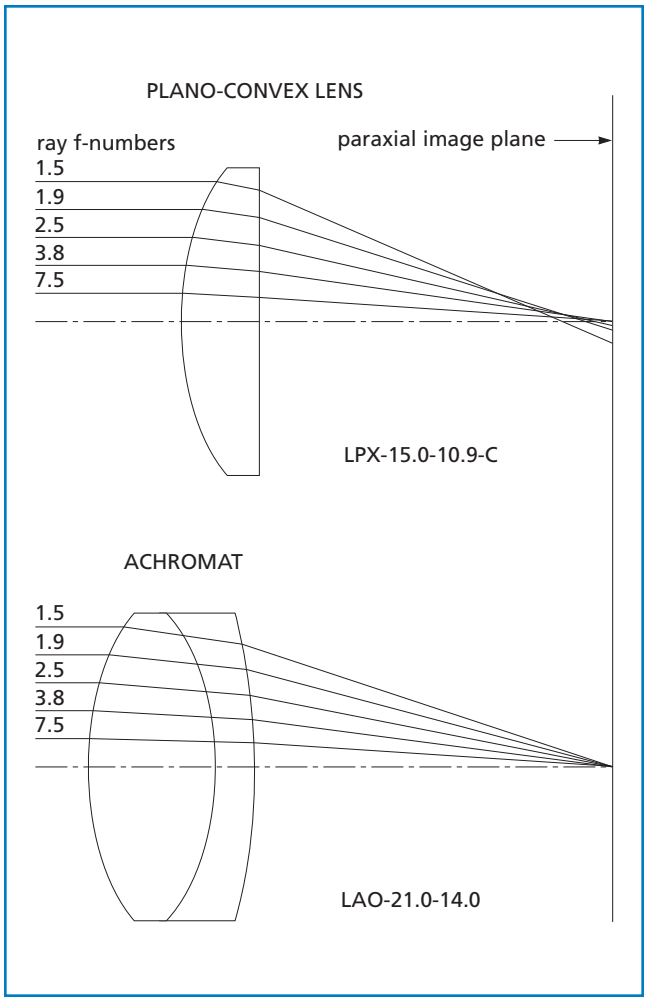

Figure 1.24 **Single-element plano-convex lens compared with a two-element achromat**

Previous examples indicate that an achromat is superior in performance to a singlet when used at the infinite conjugate ratio and at low f-numbers. Since the unit conjugate case can be thought of as two lenses, each working at the infinite conjugate ratio, the next step is to replace the plano-convex singlets with achromats, yielding a four-element system. The third part of figure 1.25 shows a system composed of two LAO-40.0-18.0 lenses. Once again, spherical aberration is not evident, even in the f/2.7 ray.

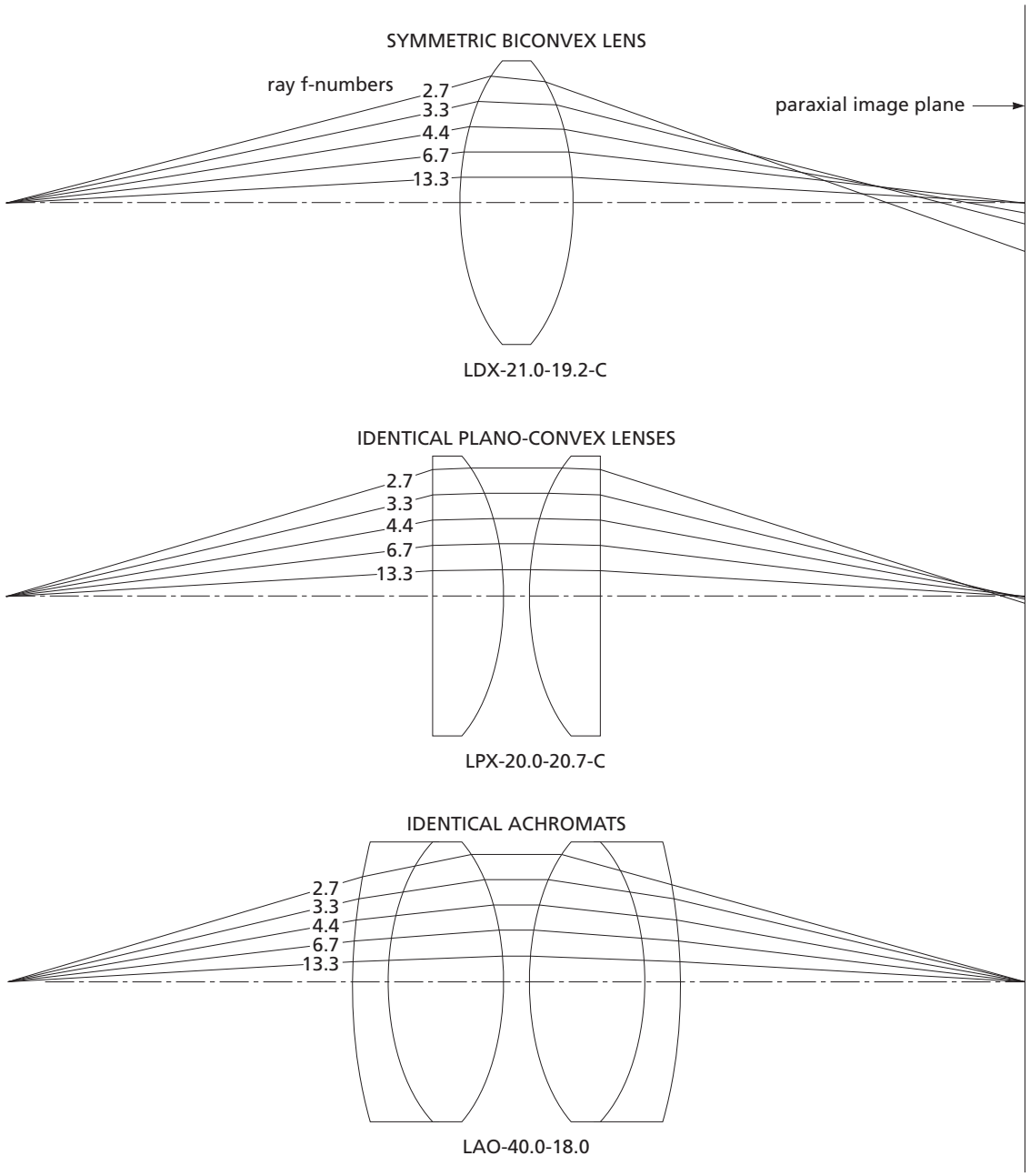

Figure 1.25 **Three possible systems for use at the unit conjugate ratio**

Diffraction Effects

In all light beams, some energy is spread outside the region predicted by geometric propagation. This effect, known as diffraction, is a fundamental and inescapable physical phenomenon. Diffraction can be understood by considering the wave nature of light. Huygens' principle (figure 1.26) states that each point on a propagating wavefront is an emitter of secondary wavelets. The propagating wave is then the envelope of these expanding wavelets. Interference between the secondary wavelets gives rise to a fringe pattern that rapidly decreases in intensity with increasing angle from the initial direction of propagation. Huygens' principle nicely describes diffraction, but rigorous explanation demands a detailed study of wave theory.

Diffraction effects are traditionally classified into either Fresnel or Fraunhofer types. Fresnel diffraction is primarily concerned with what happens to light in the immediate neighborhood of a diffracting object or aperture. It is thus only of concern when the illumination source is close to this aperture or object, known as the near field. Consequently, Fresnel diffraction is rarely important in most classical optical setups, but it becomes very important in such applications as digital optics, fiber optics, and near-field microscopy.

Fraunhofer diffraction, however, is often important even in simple optical systems. This is the light-spreading effect of an aperture when the aperture (or object) is illuminated with an infinite source (plane-wave illumination) and the light is sensed at an infinite distance (far-field) from this aperture.

From these overly simple definitions, one might assume that Fraunhofer diffraction is important only in optical systems with infinite conjugate, whereas Fresnel diffraction equations should be considered at finite conjugate ratios. Not so. A lens or lens system of finite positive focal length with plane-wave input maps the far-field diffraction pattern of its aperture onto the focal plane; therefore, it is Fraunhofer diffraction that determines the limiting performance of optical systems. More generally, at any conjugate ratio, far-field angles are transformed into spatial displacements in the image plane.

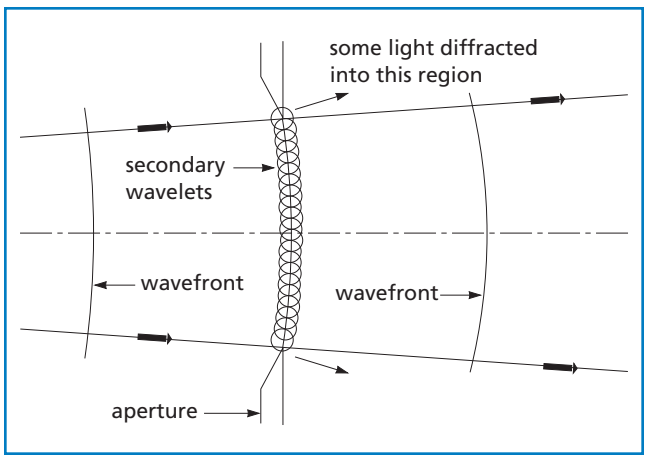

Figure 1.26 **Huygens' principle**

CIRCULAR APERTURE

Fraunhofer diffraction at a circular aperture dictates the fundamental limits of performance for circular lenses. It is important to remember that the spot size, caused by diffraction, of a circular lens is

$$d = 2.44\lambda(f/\#) \qquad (1.25)$$

where d is the diameter of the focused spot produced from plane-wave illumination and λ is the wavelength of light being focused. Notice that it is the f-number of the lens, not its absolute diameter, that determines this limiting spot size.

The diffraction pattern resulting from a uniformly illuminated circular aperture actually consists of a central bright region, known as the Airy disc (see figure 1.27), which is surrounded by a number of much fainter rings. Each ring is separated by a circle of zero intensity. The irradiance distribution in this pattern can be described by

$$I_x = I_0 \left[\frac{2J_1(x)}{x}\right]^2 \qquad (1.26)$$

where

I_0 = peak irradiance in the image

$J_1(x)$ = Bessel function of the first kind of order unity

$$= x\sum_{n=1}^{\infty}(-1)^{n+1}\frac{x^{2n-2}}{(n-1)!n!2^{2n-1}}$$

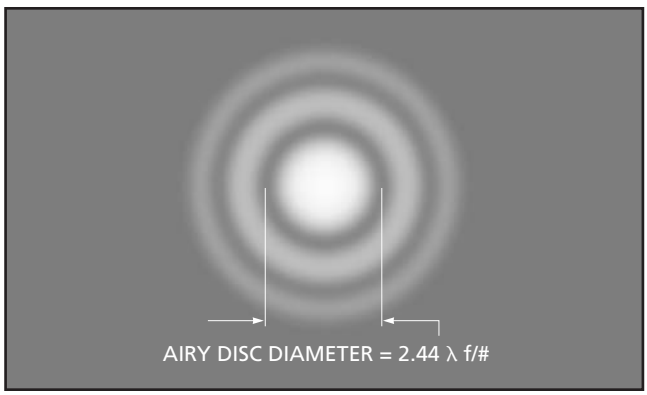

Figure 1.27 **Center of a typical diffraction pattern for a circular aperture**

and

$$x = \frac{\pi D}{\lambda}\sin\theta$$

where

λ = wavelength

D = aperture diameter

θ = angular radius from the pattern maximum.

This useful formula shows the far-field irradiance distribution from a uniformly illuminated circular aperture of diameter D.

SLIT APERTURE

A slit aperture, which is mathematically simpler, is useful in relation to cylindrical optical elements. The irradiance distribution in the diffraction pattern of a uniformly illuminated slit aperture is described by

$$I_x = I_0\left[\frac{\sin x}{x}\right]^2 \qquad (1.27)$$

where I_0 = peak irradiance in image

$$x = \frac{\pi w \sin\theta}{\lambda}$$

where λ = wavelength

w = slit width

θ = angular deviation from pattern maximum.

APPLICATION NOTE

Rayleigh Criterion

In imaging applications, spatial resolution is ultimately limited by diffraction. Calculating the maximum possible spatial resolution of an optical system requires an arbitrary definition of what is meant by resolving two features. In the Rayleigh criterion, it is assumed that two separate point sources can be resolved when the center of the Airy disc from one overlaps the first dark ring in the diffraction pattern of the second. In this case, the smallest resolvable distance, d, is

$$d = \frac{0.61\lambda}{NA} = 1.22\lambda(f/\#)$$

ENERGY DISTRIBUTION TABLE

The accompanying table shows the major features of pure (unaberrated) Fraunhofer diffraction patterns of circular and slit apertures. The table shows the position, relative intensity, and percentage of total pattern energy corresponding to each ring or band. It is especially convenient to characterize positions in either pattern with the same variable x. This variable is related to field angle in the circular aperture case by

$$\sin\theta = \frac{\lambda x}{\pi D} \qquad (1.28)$$

where D is the aperture diameter. For a slit aperture, this relationship is given by

$$\sin\theta = \frac{\lambda x}{\pi w} \qquad (1.29)$$

where w is the slit width, π has its usual meaning, and D, w, and λ are all in the same units (preferably millimeters). Linear instead of angular field positions are simply found from $r = s''\tan\theta$ where s'' is the secondary conjugate distance. This last result is often seen in a different form, namely the diffraction-limited spot-size equation, which, for a circular lens is

$$d = 2.44\,\lambda(f/\#) \qquad \text{(see eq. 1.25)}$$

This value represents the smallest spot size that can be achieved by an optical system with a circular aperture of a given f-number, and it is the diameter of the first dark ring, where the intensity has dropped to zero.

The graph in figure 1.28 shows the form of both circular and slit aperture diffraction patterns when plotted on the same normalized scale. Aperture diameter is equal to slit width so that patterns between x-values and angular deviations in the far-field are the same.

GAUSSIAN BEAMS

Apodization, or nonuniformity of aperture irradiance, alters diffraction patterns. If pupil irradiance is nonuniform, the formulas and results given previously do not apply. This is important to remember because most laser-based optical systems do not have uniform pupil irradiance. The output beam of a laser operating in the TEM_{00} mode has a smooth Gaussian irradiance profile. Formulas used to determine the focused spot size from such a beam are discussed in *Gaussian Beam Optics*. Furthermore, when dealing with Gaussian beams, the location of the focused spot also departs from that predicted by the paraxial equations given in this chapter. This is also detailed in *Gaussian Beam Optics*.

Energy Distribution in the Diffraction Pattern of a Circular or Slit Aperture

	Circular Aperture			Slit Aperture		
Ring or Band	Position (x)	Relative Intensity (I_x/I_0)	Energy in Ring (%)	Position (x)	Relative Intensity (I_x/I_0)	Energy in Band (%)
Central Maximum	0.0	1.0	83.8	0.0	1.0	90.3
First Dark	1.22π	0.0		1.00π	0.0	
First Bright	1.64π	0.0175	7.2	1.43π	0.0472	4.7
Second Dark	2.23π	0.0		2.00π	0.0	
Second Bright	2.68π	0.0042	2.8	2.46π	0.0165	1.7
Third Dark	3.24π	0.0		3.00π	0.0	
Third Bright	3.70π	0.0016	1.5	3.47π	0.0083	0.8
Fourth Dark	4.24π	0.0		4.00π	0.0	
Fourth Bright	4.71π	0.0008	1.0	4.48π	0.0050	0.5
Fifth Dark	5.24π	0.0		5.00π	0.0	

Note: Position variable (x) is defined in the text.

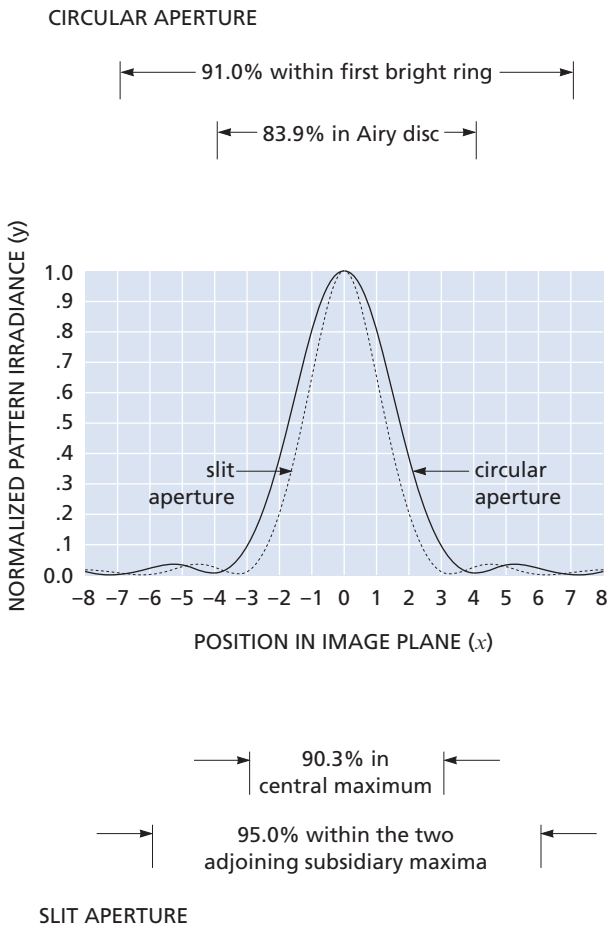

Figure 1.28 **Fraunhofer diffraction pattern of a singlet slit superimposed on the Fraunhofer diffraction pattern of a circular aperture**

Lens Selection

Having discussed the most important factors that affect the performance of a lens or a lens system, we will now address the practical matter of selecting the optimum catalog components for a particular task. The following useful relationships are important to keep in mind throughout the selection process:

- Diffraction-limited spot size = 2.44 λ f/#
- Approximate on-axis spot size of a plano-convex lens at the infinite conjugate resulting from spherical aberration = $\frac{0.067\,f}{\text{f}/\#^3}$
- Optical invariant = $m = \frac{\text{NA}}{\text{NA}''}$.

Example 1: Collimating an Incandescent Source

Produce a collimated beam from a quartz halogen bulb having a 1-mm-square filament. Collect the maximum amount of light possible and produce a beam with the lowest possible divergence angle.

This problem, illustrated in figure 1.29, involves the typical tradeoff between light-collection efficiency and resolution (where a beam is being collimated rather than focused, resolution is defined by beam divergence). To collect more light, it is necessary to work at a low f-number, but because of aberrations, higher resolution (lower divergence angle) will be achieved by working at a higher f-number.

In terms of resolution, the first thing to realize is that the minimum divergence angle (in radians) that can be achieved using any lens system is the source size divided by system focal length. An off-axis ray (from the edge of the source) entering the first principal point of the system exits the second principal point at the same angle. Therefore, increasing the system focal length improves this limiting divergence because the source appears smaller.

An optic that can produce a spot size of 1 mm when focusing a perfectly collimated beam is therefore required. Since source size is inherently limited, it is pointless to strive for better resolution. This level of resolution can be achieved easily with a plano-convex lens.

While angular divergence decreases with increasing focal length, spherical aberration of a plano-convex lens increases with increasing focal length. To determine the appropriate focal length, set the spherical aberration formula for a plano-convex lens equal to the source (spot) size:

$$\frac{0.067\,f}{\text{f}/\#^3} = 1\text{ mm}.$$

This ensures a lens that meets the minimum performance needed. To select a focal length, make an arbitrary f-number choice. As can be seen from the relationship, as we lower the f-number (increase collection efficiency), we decrease the focal length, which will worsen the resultant divergence angle (minimum divergence = 1 mm/*f*).

In this example, we will accept f/2 collection efficiency, which gives us a focal length of about 120 mm. For f/2 operation we would need a minimum diameter of 60 mm. The LPX-60.0-62.2-C fits this specification exactly. Beam divergence would be about 8 mrad.

Finally, we need to verify that we are not operating below the theoretical diffraction limit. In this example, the numbers (1-mm spot size) indicate that we are not, since

$$\text{diffraction-limited spot size} = 2.44 \times 0.5\ \mu\text{m} \times 2 = 2.44\ \mu\text{m}.$$

Example 2: Coupling an Incandescent Source into a Fiber

In *Imaging Properties of Lens Systems* we considered a system in which the output of an incandescent bulb with a filament of 1 mm in diameter was to be coupled into an optical fiber with a core diameter of 100 µm and a numerical aperture of 0.25. From the optical invariant and other constraints given in the problem, we determined that $f = 9.1$ mm, CA = 5 mm, $s = 100$ mm, $s'' = 10$ mm, NA″ = 0.25, and NA = 0.025 (or f/2 and f/20). The singlet lenses that match these specifications are the plano-convex LPX-5.0-5.2-C or biconvex lenses LDX-6.0-7.7-C and LDX-5.0-9.9-C. The closest achromat would be the LAO-10.0-6.0.

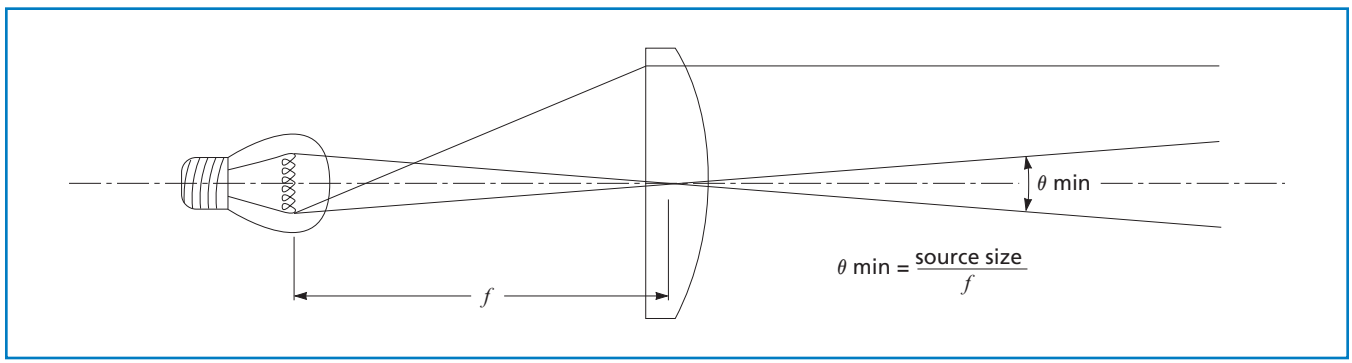

Figure 1.29 **Collimating an incandescent source**

We can immediately reject the biconvex lenses because of spherical aberration. We can estimate the performance of the LPX-5.0-5.2-C on the focusing side by using our spherical aberration formula:

$$\text{spot size} = \frac{0.067\ (10)}{2^3} = 84\ \mu\text{m}.$$

We will ignore, for the moment, that we are not working at the infinite conjugate.

This is slightly smaller than the 100-µm spot size we are trying to achieve. However, since we are not working at infinite conjugate, the spot size will be larger than that given by our simple calculation. This lens is therefore likely to be marginal in this situation, especially if we consider chromatic aberration. A better choice is the achromat. Although a computer ray trace would be required to determine its exact performance, it is virtually certain to provide adequate performance.

Example 3: Symmetric Fiber-to-Fiber Coupling

Couple an optical fiber with an 8-µm core and a 0.15 numerical aperture into another fiber with the same characteristics. Assume a wavelength of 0.5 µm.

This problem, illustrated in figure 1.30, is essentially a 1:1 imaging situation. We want to collect and focus at a numerical aperture of 0.15 or f/3.3, and we need a lens with an 8-µm spot size at this f-number. Based on the lens combination discussion in *Lens Combination Formulas*, our most likely setup is either a pair of identical plano-convex lenses or achromats, faced front to front. To determine the necessary focal length for a plano-convex lens, we again use the spherical aberration estimate formula:

$$\frac{0.067\ f}{3.3^3} = 0.008\ \text{mm}.$$

This formula yields a focal length of 4.3 mm and a minimum diameter of 1.3 mm. The LPX-4.2-2.3-BAK1 meets these criteria. The biggest problem with utilizing these tiny, short focal length lenses is the practical considerations of handling, mounting, and positioning them. Because using a pair of longer focal length singlets would result in unacceptable performance, the next step might be to use a pair of the slightly longer focal length, larger achromats, such as the LAO-10.0-6.0. The performance data, given in *Spot Size*, show that this combination does provide the required 8-μm spot diameter.

Because fairly small spot sizes are being considered here, it is important to make sure that the system is not being asked to work below the diffraction limit:

$$2.44 \times 0.5\ \mu\text{m} \times 3.3 = 4\ \mu\text{m}.$$

Since this is half the spot size caused by aberrations, it can be safely assumed that diffraction will not play a significant role here.

An entirely different approach to a fiber-coupling task such as this would be to use a pair of spherical ball lenses (LMS-LSFN series) or one of the gradient-index lenses (LGT series).

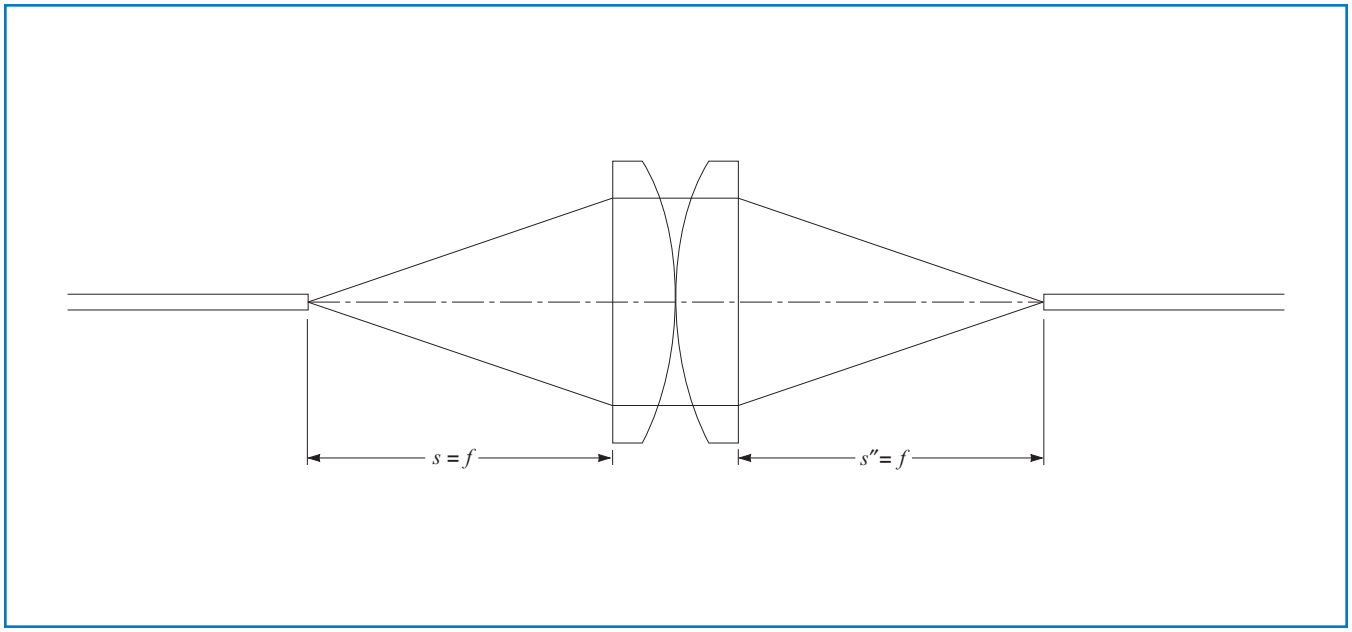

Figure 1.30 **Symmetric fiber-to-fiber coupling**

Example 4: Diffraction-Limited Performance

Determine at what f-number a plano-convex lens being used at an infinite conjugate ratio with 0.5-μm wavelength light becomes diffraction limited (i.e., the effects of diffraction exceed those caused by aberration).

To solve this problem, set the equations for diffraction-limited spot size and third-order spherical aberration equal to each other. The result depends upon focal length, since aberrations scale with focal length, while diffraction is solely dependent upon f-number. By substituting some common focal lengths into this formula, we get f/8.6 at $f = 100$ mm, f/7.2 at $f = 50$ mm, and f/4.8 at $f = 10$ mm.

$$2.44 \times 0.5\ \mu\text{m} \times \text{f/\#} = \frac{0.067 \times f}{\text{f/\#}^3}$$

or

$$\text{f/\#} = (54.9 \times f)^{1/4}.$$

When working with these focal lengths (and under the conditions previously stated), we can assume essentially diffraction-limited performance above these f-numbers. Keep in mind, however, that this treatment does not take into account manufacturing tolerances or chromatic aberration, which will be present in polychromatic applications.

APPLICATION NOTE

Spherical Ball Lenses for Fiber Coupling

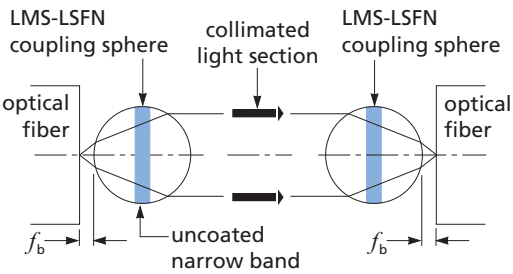

Spheres are arranged so that the fiber end is located at the focal point. The output from the first sphere is then collimated. If two spheres are aligned axially to each other, the beam will be transferred from one focal point to the other. Translational alignment sensitivity can be reduced by enlarging the beam. Slight negative defocusing of the ball can reduce the spherical aberration third-order contribution common to all coupling systems. Additional information can be found in "Lens Coupling in Fiber Optic Devices: Efficiency Limits," by A. Nicia, *Applied Optics*, vol. 20, no. 18, pp 3136–45, 1981. Off-axis aberrations are absent since the fiber diameters are so much smaller than the coupler focal length.

Spot Size

In general, the performance of a lens or lens system in a specific circumstance should be determined by an exact trigonometric ray trace. CVI Melles Griot applications engineers can supply ray-tracing data for particular lenses and systems of catalog components on request. In certain situations, however, some simple guidelines can be used for lens selection. The optimum working conditions for some of the lenses in this catalog have already been presented. The following tables give some quantitative results for a variety of simple and compound lens systems, which can be constructed from standard catalog optics.

In interpreting these tables, remember that these theoretical values obtained from computer ray tracing consider only the effects of ideal geometric optics. Effects of manufacturing tolerances have not been considered. Furthermore, remember that using more than one element provides a higher degree of correction but makes alignment more difficult. When actually choosing a lens or a lens system, it is important to note the tolerances and specifications clearly described for each CVI Melles Griot lens in the product listings.

The tables give the diameter of the spot for a variety of lenses used at several different f-numbers. All the tables are for on-axis, uniformly illuminated, collimated input light at 546.1 nm. They assume that the lens is facing in the direction that produces a minimum spot size. When the spot size caused by aberrations is smaller or equal to the diffraction-limited spot size, the notation "DL" appears next to the entry. The shorter focal length lenses produce smaller spot sizes because aberrations increase linearly as a lens is scaled up.

The effect on spot size caused by spherical aberration is strongly dependent on f-number. For a plano-convex singlet, spherical aberration is inversely dependent on the cube of the f-number. For doublets, this relationship can be even higher. On the other hand, the spot size caused by diffraction increases linearly with f-number. Thus, for some lens types, spot size at first decreases and then increases with f-number, meaning that there is some optimum performance point at which both aberrations and diffraction combine to form a minimum.

Unfortunately, these results cannot be generalized to situations in which the lenses are used off axis. This is particularly true of the achromat/aplanatic meniscus lens combinations because their performance degrades rapidly off axis.

Focal Length = 10 mm

	Spot Size (μm)*		
f/#	LDX-5.0-9.9-C	LPX-8.0-5.2-C	LAO-10.0-6.0
f/2	—	94	11
f/3	36	25	7
f/5	8	6.7 (DL)	6.7 (DL)
f/10	13.3 (DL)	13.3 (DL)	13.3 (DL)

**Diffraction-limited performance is indicated by DL.*

Focal Length = 30 mm

	Spot Size (μm)*		
f/#	LPX-18.5-15.6-C	LAO-30.0-12.5	LAO-50.0-18.0 & MENP-18.0-4.0-73.5-NSF8
f/2	295	—	3
f/3	79	7	4 (DL)
f/5	17	6.7 (DL)	6.9 (DL)
f/10	13.3 (DL)	13.3 (DL)	13.8 (DL)

**Diffraction-limited performance is indicated by DL.*

Focal Length = 60 mm

	Spot Size (μm)*			
f/#	LDX-50.0-60.0-C	LPX-30.0-31.1-C	LAO-60.0-30.0	LAO-100.0-31.5 & MENP-31.5-6.0-146.4-NSF8
f/2	816	600	—	—
f/3	217	160	34	4 (DL)
f/5	45	33	10	6.7 (DL)
f/10	13.3 (DL)	13.3 (DL)	13.3 (DL)	13.3 (DL)

**Diffraction-limited performance is indicated by DL.*

Aberration Balancing

To improve system performance, optical designers make sure that the total aberration contribution from all surfaces taken together sums to nearly zero. Normally, such a process requires computerized analysis and optimization. However, there are some simple guidelines that can be used to achieve this with lenses available in this catalog. This approach can yield systems that operate at a much lower f-number than can usually be achieved with simple lenses.

Specifically, we will examine how to null the spherical aberration from two or more lenses in collimated, monochromatic light. This technique will thus be most useful for laser beam focusing and expanding.

Figure 1.31 shows the third-order longitudinal spherical aberration coefficients for six of the most common positive and negative lens shapes when used with parallel, monochromatic incident light. The plano-convex and plano-concave lenses both show minimum spherical aberration when oriented with their curved surface facing the incident parallel beam. All other configurations exhibit larger amounts of spherical aberration. With these lens types, it is now possible to show how various systems can be corrected for spherical aberration.

A two-element laser beam expander is a good starting example. In this case, two lenses are separated by a distance that is the sum of their focal lengths, so that the overall system focal length is infinite. This system will not focus incoming collimated light, but it will change the beam diameter. By definition, each of the lenses is operating at the same f-number.

The equation for longitudinal spherical aberration shows that, for two lenses with the same f-number, aberration varies directly with the focal lengths of the lenses. The sign of the aberration is the same as focal length. Thus, it should be possible to correct the spherical aberration of this Galilean-type beam expander, which consists of a positive focal length objective and a negative diverging lens.

If a plano-convex lens of focal length f_1 oriented in the normal direction is combined with a plano-concave lens of focal length f_2 oriented in its reverse direction, the total spherical aberration of the system is

$$\mathrm{LSA} = \frac{0.272\, f_1}{\mathrm{f/\#}^2} + \frac{1.069\, f_2}{\mathrm{f/\#}^2}.$$

After setting this equation to zero, we obtain

$$\frac{f_1}{f_2} = -\frac{1.069}{0.272} = -3.93.$$

To make the magnitude of aberration contributions of the two elements equal so they will cancel out, and thus correct the system, select the focal length of the positive element to be 3.93 times that of the negative element.

Figure 1.32(a) shows a beam-expander system made up of catalog elements, in which the focal length ratio is 4:1. This simple system is corrected to about 1/6 wavelength at 632.8 nm, even though the objective is operating at f/4 with a 20-mm aperture diameter. This is remarkably good wavefront correction for such a simple system; one would normally assume that a doublet objective would be needed and a complex diverging lens as well. This analysis does not take into account manufacturing tolerances.

A beam expander of lower magnification can also be derived from this information. If a symmetric-convex objective is used together] with a reversed plano-concave diverging lens, the aberration coefficients are in the ratio of 1.069/0.403 = 2.65. Figure 1.32(b) shows a system of catalog lenses that provides a magnification of 2.7 (the closest possible given the available focal lengths). The maximum wavefront error in this case is only a quarter-wave, even though the objective is working at f/3.3.

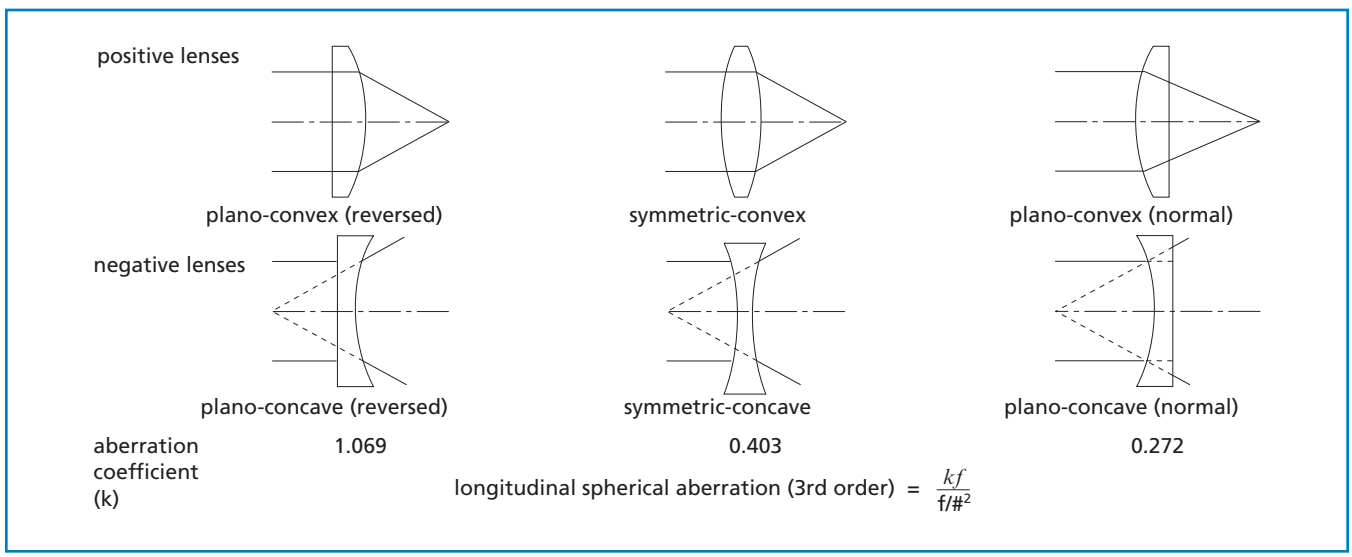

Figure 1.31 **Third-order longitudinal spherical aberration of typical lens shapes**

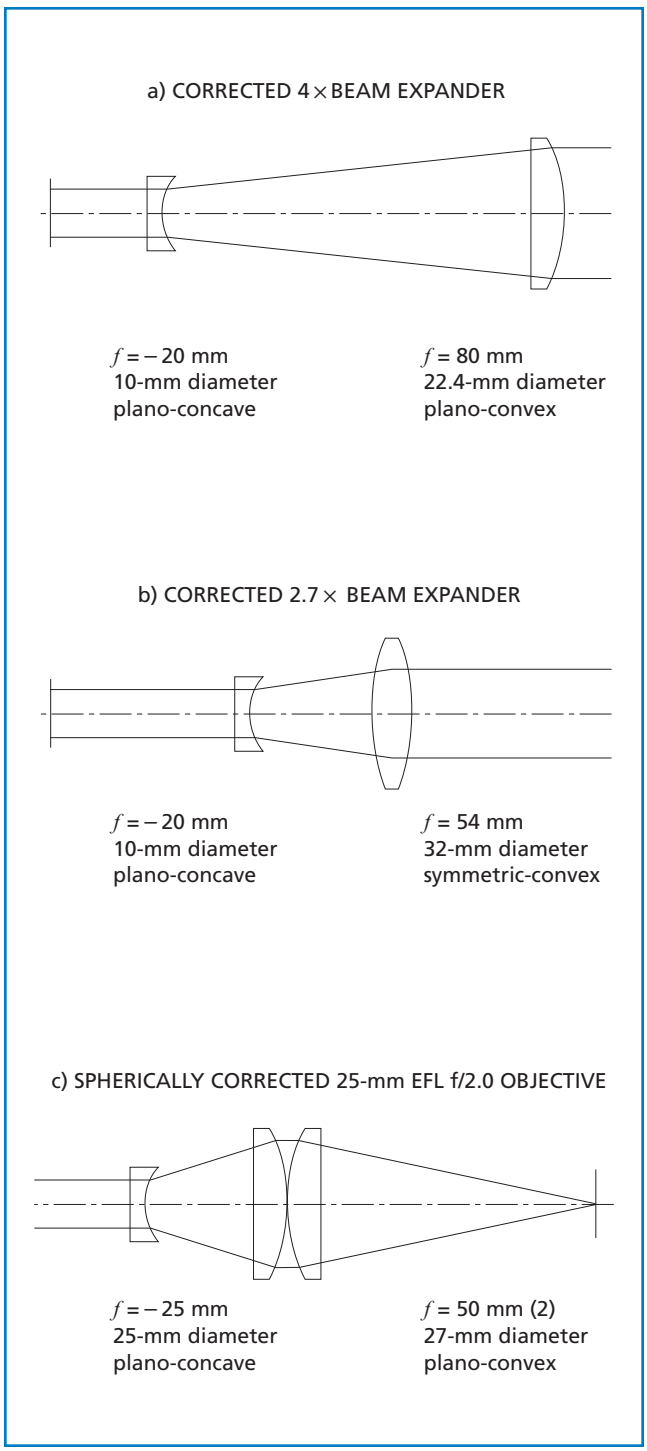

Figure 1.32 **Combining catalog lenses for aberration balancing**

The relatively low f numbers of these objectives is a great advantage in minimizing the length of these beam expanders. They would be particularly useful with Nd:YAG and argon-ion lasers, which tend to have large output beam diameters.

These same principles can be utilized to create high numerical aperture objectives that might be used as laser focusing lenses. Figure 1.32(c) shows an objective consisting of an initial negative element, followed by two identical plano-convex positive elements. Again, all of the elements operate at the same f-number, so that their aberration contributions are proportional to their focal lengths. To obtain zero total spherical aberration from this configuration, we must satisfy

$$1.069\, f_1 + 0.272\, f_2 + 0.272\, f_2 = 0$$

or

$$\frac{f_1}{f_2} = -0.51.$$

Therefore, a corrected system should result if the focal length of the negative element is just about half that of each of the positive lenses. In this case, $f_1 = 425$ mm and $f_2 = 50$ mm yield a total system focal length of about 25 mm and an f-number of approximately f/2. This objective, corrected to 1/6 wave, has the additional advantage of a very long working distance.

Definition of Terms

FOCAL LENGTH (f)

Two distinct terms describe the focal lengths associated with every lens or lens system. The effective focal length (EFL) or equivalent focal length (denoted f in figure 1.33) determines magnification and hence the image size. The term f appears frequently in lens formulas and in the tables of standard lenses. Unfortunately, because f is measured with reference to principal points which are usually inside the lens, the meaning of f is not immediately apparent when a lens is visually inspected.

The second type of focal length relates the focal plane positions directly to landmarks on the lens surfaces (namely the vertices) which are immediately recognizable. It is not simply related to image size but is especially convenient for use when one is concerned about correct lens positioning or mechanical clearances. Examples of this second type of focal length are the front focal length (FFL, denoted f_f in figure 1.33) and the back focal length (BFL, denoted f_b).

The convention in all of the figures (with the exception of a single deliberately reversed ray) is that light travels from left to right.

FOCAL POINT (F OR F″)

Rays that pass through or originate at either focal point must be, on the opposite side of the lens, parallel to the optical axis. This fact is the basis for locating both focal points.

PRIMARY PRINCIPAL SURFACE

Let us imagine that rays originating at the front focal point F (and therefore parallel to the optical axis after emergence from the opposite side of the lens) are singly refracted at some imaginary surface, instead of twice refracted (once at each lens surface) as actually happens. There is a unique imaginary surface, called the principal surface, at which this can happen.

To locate this unique surface, consider a single ray traced from the air on one side of the lens, through the lens and into the air on the other side. The ray is broken into three segments by the lens. Two of these are external (in the air), and the third is internal (in the glass). The external segments can be extended to a common point of intersection (certainly near, and usually within, the lens). The principal surface is the locus of all such

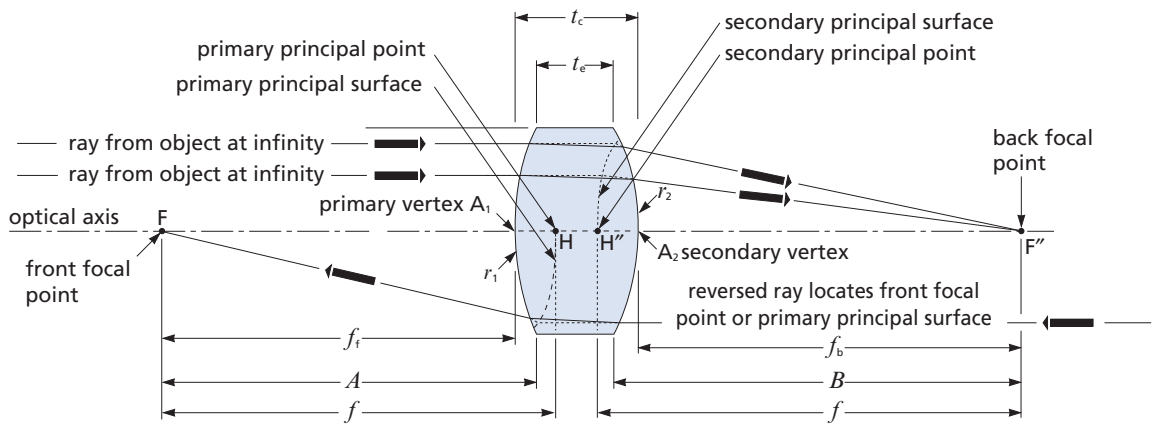

A = front focus to front edge distance

B = rear edge to rear focus distance

f = effective focal length; may be positive (as shown) or negative

f_f = front focal length

f_b = back focal length

t_e = edge thickness

t_c = center thickness

r_1 = radius of curvature of first surface (positive if center of curvature is to right)

r_2 = radius of curvature of second surface (negative if center of curvature is to left)

Figure 1.33 **Focal length and focal points**

points of intersection of extended external ray segments. The principal surface of a perfectly corrected optical system is a sphere centered on the focal point.

Near the optical axis, the principal surface is nearly flat, and for this reason, it is sometimes referred to as the principal plane.

SECONDARY PRINCIPAL SURFACE

This term is defined analogously to the primary principal surface, but it is used for a collimated beam incident from the left and focused to the back focal point F″ on the right. Rays in that part of the beam nearest the axis can be thought of as once refracted at the secondary principal surface, instead of being refracted by both lens surfaces.

PRIMARY PRINCIPAL POINT (H) OR FIRST NODAL POINT

This point is the intersection of the primary principal surface with the optical axis.

SECONDARY PRINCIPAL POINT (H″) OR SECONDARY NODAL POINT

This point is the intersection of the secondary principal surface with the optical axis.

CONJUGATE DISTANCES (s AND s'')

The conjugate distances are the object distance, s, and image distance, s''. Specifically, s is the distance from the object to H, and s'' is the distance from H″ to the image location. The term infinite conjugate ratio refers to the situation in which a lens is either focusing incoming collimated light or is being used to collimate a source (therefore, either s or s'' is infinity).

PRIMARY VERTEX (A_1)

The primary vertex is the intersection of the primary lens surface with the optical axis.

SECONDARY VERTEX (A_2)

The secondary vertex is the intersection of the secondary lens surface with the optical axis.

EFFECTIVE FOCAL LENGTH (EFL, f)

Assuming that the lens is surrounded by air or vacuum (refractive index 1.0), this is both the distance from the front focal point (F) to the primary principal point (H) and the distance from the secondary principal point (H″) to the rear focal point (F″). Later we use f to designate the paraxial EFL for the design wavelength (λ_0).

FRONT FOCAL LENGTH (f_f)

This length is the distance from the front focal point (F) to the primary vertex (A_1).

BACK FOCAL LENGTH (f_b)

This length is the distance from the secondary vertex (A_2) to the rear focal point (F″).

EDGE-TO-FOCUS DISTANCES (A AND B)

A is the distance from the front focal point to the primary vertex of the lens. B is the distance from the secondary vertex of the lens to the rear focal point. Both distances are presumed always to be positive.

REAL IMAGE

A real image is one in which the light rays actually converge; if a screen were placed at the point of focus, an image would be formed on it.

VIRTUAL IMAGE

A virtual image does not represent an actual convergence of light rays. A virtual image can be viewed only by looking back through the optical system, such as in the case of a magnifying glass.

F-NUMBER (f/#)

The f-number (also known as the focal ratio, relative aperture, or speed) of a lens system is defined to be the effective focal length divided by system clear aperture. Ray f-number is the conjugate distance for that ray divided by the height at which it intercepts the principal surface.

$$\text{f/\#} = \frac{f}{\text{CA}}. \qquad \textit{(see eq. 1.7)}$$

NUMERICAL APERTURE (NA)

The NA of a lens system is defined to be the sine of the angle, θ_1, that the marginal ray (the ray that exits the lens system at its outer edge) makes with the optical axis multiplied by the index of refraction (n) of the medium. The NA can be defined for any ray as the sine of the angle made by that ray with the optical axis multiplied by the index of refraction:

$$\text{NA} = n\sin\theta. \qquad \textit{(1.30)}$$

MAGNIFICATION POWER

Often, positive lenses intended for use as simple magnifiers are rated with a single magnification, such as 4 × . To create a virtual image for viewing with the human eye, in principle, any positive lens can be used at an infinite number of possible magnifications. However, there is usually a narrow range of magnifications that will be comfortable for the viewer. Typically, when the viewer adjusts the object distance so that the image appears to be essentially at infinity (which is a comfortable viewing distance for most individuals), magnification is given by the relationship

$$\text{magnification} = \frac{254\ \text{mm}}{f} \qquad (f \text{ in mm}). \qquad (1.31)$$

Thus, a 25.4-mm focal length positive lens would be a 10 × magnifier.

DIOPTERS

The term diopter is used to define the reciprocal of the focal length, which is commonly used for ophthalmic lenses. The inverse focal length of a lens expressed in diopters is

$$\text{diopters} = \frac{1000}{f} \qquad (f \text{ in mm}). \qquad (1.32)$$

Thus, the smaller the focal length is, the larger the power in diopters will be.

DEPTH OF FIELD AND DEPTH OF FOCUS

In an imaging system, depth of field refers to the distance in object space over which the system delivers an acceptably sharp image. The criteria for what is acceptably sharp is arbitrarily chosen by the user; depth of field increases with increasing f-number.

For an imaging system, depth of focus is the range in image space over which the system delivers an acceptably sharp image. In other words, this is the amount that the image surface (such as a screen or piece of photographic film) could be moved while maintaining acceptable focus. Again, criteria for acceptability are defined arbitrarily.

In nonimaging applications, such as laser focusing, depth of focus refers to the range in image space over which the focused spot diameter remains below an arbitrary limit.

APPLICATION NOTE

Technical Reference

For further reading about the definitions and formulas presented here, refer to the following publications:

Rudolph Kingslake, *Lens Design Fundamentals* (Academic Press)

Rudolph Kingslake, System Design (Academic Press)

Warren Smith, *Modern Optical Engineering* (McGraw Hill).

Donald C. O'Shea, *Elements of Modern Optical Design* (John Wiley & Sons)

Eugene Hecht, *Optics* (Addison Wesley)

Max Born, Emil Wolf, *Principles of Optics* (Cambridge University Press)

If you need help with the use of definitions and formulas presented in this guide, our applications engineers will be pleased to assist you.

Paraxial Lens Formulas

PARAXIAL FORMULAS FOR LENSES IN AIR

The following formulas are based on the behavior of paraxial rays, which are always very close and nearly parallel to the optical axis. In this region, lens surfaces are always very nearly normal to the optical axis, and hence all angles of incidence and refraction are small. As a result, the sines of the angles of incidence and refraction are small (as used in Snell's law) and can be approximated by the angles themselves (measured in radians).

The paraxial formulas do not include effects of spherical aberration experienced by a marginal ray — a ray passing through the lens near its edge or margin. All EFL values (f) tabulated in this catalog are paraxial values which correspond to the paraxial formulas. The following paraxial formulas are valid for both thick and thin lenses unless otherwise noted. The refractive index of the lens glass, n, is the ratio of the speed of light in vacuum to the speed of light in the lens glass. All other variables are defined in figure 1.33.

Focal Length

$$\frac{1}{f} = (n-1)\left(\frac{1}{r_1} - \frac{1}{r_2}\right) + \frac{(n-1)^2}{n}\,\frac{t_c}{r_1 r_2} \tag{1.33}$$

where n is the refractive index, t_c is the center thickness, and the sign convention previously given for the radii r_1 and r_2 applies. For thin lenses, $t_c \cong 0$, and for plano lenses either r_1 or r_2 is infinite. In either case the second term of the above equation vanishes, and we are left with the familiar lens maker's formula:

$$\frac{1}{f} = (n-1)\left(\frac{1}{r_1} - \frac{1}{r_2}\right). \tag{1.34}$$

Surface Sagitta and Radius of Curvature

(refer to figure 1.34)

$$r^2 = (r-s)^2 + \left(\frac{d}{2}\right)^2 \tag{1.35}$$

$$s = r - \sqrt{r^2 - \left(\frac{d}{2}\right)^2} > 0 \tag{1.36}$$

$$r = \frac{s}{2} + \frac{d^2}{8s}. \tag{1.37}$$

An often useful approximation is to neglect $s/2$.

Symmetric Lens Radii ($r_2 = -r_1$)

With center thickness constrained,

$$r_1 = (n-1)\left[f \pm \sqrt{f^2 - \left(\frac{f t_c}{n}\right)}\right] \tag{1.38}$$

$$= (n-1) f \left[1 + \sqrt{1 - \left(\frac{t_c}{nf}\right)}\right]$$

where, in the first form, the + sign is chosen for the square root if f is positive, but the − sign must be used if f is negative. In the second form, the + sign must be used regardless of the sign of f.

Plano Lens Radius

Since r_2 is infinite,

$$r_1 = (n-1) f. \tag{1.39}$$

Principal-Point Locations (signed distances from vertices)

$$\mathrm{A_2H''} = \frac{-r_2 t_c}{n(r_2 - r_1) + t_c(n-1)} \tag{1.40}$$

$$\mathrm{A_1H} = \frac{-r_1 t_c}{n(r_2 - r_1) + t_c(n-1)} \tag{1.41}$$

where the above sign convention applies.

For symmetric lenses ($r_2 = -r_1$),

$$\mathrm{A_1H} = -\mathrm{A_2H''} = \frac{r_1 t_c}{2nr_1 - t_c(n-1)}. \tag{1.42}$$

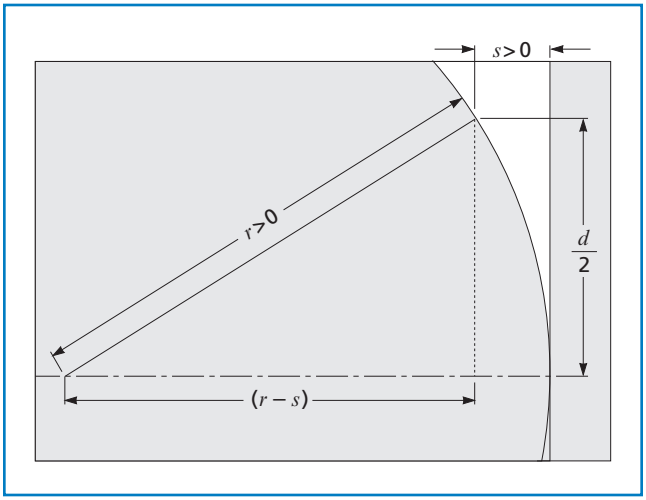

Figure 1.34 **Surface sagitta and radius of curvature**

If either r_1 or r_2 is infinite, l'Hôpital's rule from calculus must be used. Thus, referring to *Aberration Balancing*, for plano-convex lenses in the correct orientation,

$$\mathrm{A_1H} = 0$$

and

$$\mathrm{A_2H''} = -\frac{t_c}{n}. \tag{1.43}$$

For flat plates, by letting $r_1 \to \infty$ in a symmetric lens, we obtain $\mathrm{A_1H} = \mathrm{A_2H''} = t_c/2_n$. These results are useful in connection with the following paraxial lens combination formulas.

Hiatus or Interstitium (principal-point separation)

$$\mathrm{HH''} = t_c\left\{1 - \frac{f}{n}\left[\frac{1}{f} - \frac{(n-1)^2}{n}\frac{t_c}{r_1 r_2}\right]\right\} \tag{1.44}$$

which, in the thin-lens approximation (exact for plano lenses), becomes

$$\mathrm{HH''} = t_c\left(1 - \frac{1}{n}\right). \tag{1.45}$$

Solid Angle

The solid angle subtended by a lens, for an observer situated at an on-axis image point, is

$$\begin{aligned}\Omega &= 2\pi(1-\cos\theta)\\ &= 4\pi\sin^2\left(\frac{\theta}{2}\right)\end{aligned} \tag{1.46}$$

where this result is in steradians, and where

$$\theta = \arctan\left(\frac{\mathrm{CA}}{2s}\right) \tag{1.47}$$

is the apparent angular radius of the lens clear aperture. For an observer at an on-axis object point, use s instead of s''. To convert from steradians to the more intuitive sphere units, simply divide Ω by 4π. If the Abbé sine condition is known to apply, θ may be calculated using the arc sine function instead of the arctangent.

Back Focal Length

$$\begin{aligned}f_\mathrm{b} &= f'' + \mathrm{A_2H''}\\ &= f'' - \frac{r_2 t_\mathrm{c}}{n(r_2 - r_1) + t_\mathrm{c}(n-1)}\end{aligned} \tag{1.48}$$

where the sign convention presented above applies to $\mathrm{A_2H''}$ and to the radii. If r_2 is infinite, l'Hôpital's rule from calculus must be used, whereby

$$f_\mathrm{b} = f'' - \frac{t_\mathrm{c}}{n}. \tag{1.49}$$

Front Focal Length

$$\begin{aligned}f_\mathrm{f} &= f - \mathrm{A_1H}\\ &= f + \frac{r_1 t_c}{n(r_2 - r_1) + t_\mathrm{c}(n-1)}\end{aligned} \tag{1.50}$$

where the sign convention presented above applies to $\mathrm{A_1H}$ and to the radii. If r_1 is infinite, l'Hôpital's rule from calculus must be used, whereby

$$f_\mathrm{f} = f - \frac{t_\mathrm{c}}{n}. \tag{1.51}$$

Edge-to-Focus Distances

For positive lenses,

$$\mathrm{A} = f_\mathrm{f} + s_1 \tag{1.52}$$

and

$$\mathrm{B} = f_\mathrm{b} + s_2 \tag{1.53}$$

where s_1 and s_2 are the sagittas of the first and second surfaces. Bevel is neglected.

Magnification or Conjugate Ratio

$$\begin{aligned}m &= \frac{s''}{s}\\ &= \frac{f}{s - f}\\ &= \frac{s'' - f}{f}.\end{aligned} \tag{1.54}$$

PARAXIAL FORMULAS FOR LENSES IN ARBITRARY MEDIA

These formulas allow for the possibility of distinct and completely arbitrary refractive indices for the object space medium (refractive index n'), lens (refractive index n''), and image space medium (refractive index n). In this situation, the EFL assumes two distinct values, namely f in object space and f'' in image space. It is also necessary to distinguish the principal points from the nodal points. The lens serves both as a lens and as a window separating the object space and image space media.

The situation of a lens immersed in a homogenous fluid (figure 1.35) is included as a special case ($n = n''$). This case is of considerable practical importance. The two values f and f'' are again equal, so that the lens combination formulas are applicable to systems immersed in a common fluid. The general case (two different fluids) is more difficult, and it must be approached by ray tracing on a surface-by-surface basis.

Lens Constant (*k*)

This number appears frequently in the following formulas. It is an explicit function of the complete lens prescription (both radii, t_c and n') and both media indices (n and n''). This dependence is implicit anywhere that k appears.

$$k = \frac{n'-n}{r_1} + \frac{n''-n'}{r_2} - \frac{t_c(n'-n)(n''-n')}{n'r_1r_2}. \quad (1.55)$$

Effective Focal Lengths

$$f = \frac{n}{k} \qquad f'' = \frac{n''}{k}. \quad (1.56)$$

Lens Formula (Gaussian form)

$$\frac{n}{s} + \frac{n''}{s''} = k. \quad (1.57)$$

Lens Formula (Newtonian form)

$$xx'' = f''f = \frac{nn''}{k^2}. \quad (1.58)$$

Principal-Point Locations

$$A_1H = \frac{nt_c}{k}\left(\frac{n''-n'}{n'r_2}\right) \quad (1.59)$$

$$A_2H'' = \frac{-n''t_c}{k}\left(\frac{n'-n}{n'r_1}\right). \quad (1.60)$$

Object-to-First-Principal-Point Distance

$$s = \frac{ns''}{ks''-n''}. \quad (1.61)$$

Second Principal-Point-to-Image Distance

$$s'' = \frac{n''s}{ks-n}. \quad (1.62)$$

Magnification

$$m = \frac{ns''}{n''s}. \quad (1.63)$$

Lens Maker's Formula

$$\frac{n}{f} = \frac{n''}{f''} = k. \quad (1.64)$$

Nodal-Point Locations

$$A_1N = A_1H + HN \quad (1.65)$$

$$A_2N'' = A_2H'' + H''N''. \quad (1.66)$$

Separation of Nodal Point from Corresponding Principal Point

HN = H″N″ = $(n''-n)/k$, positive for N to right of H and N″ to right of H″.

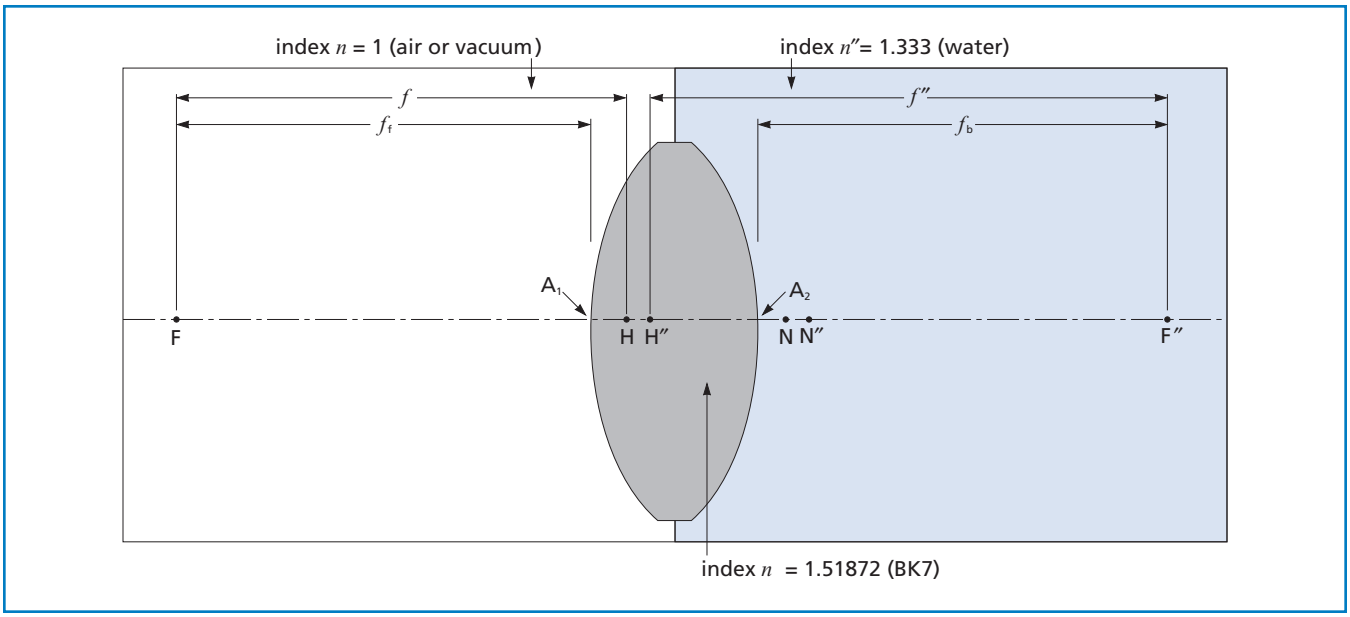

Figure 1.35 **Symmetric lens with disparate object and image space indexes**

Back Focal Length

$$f_b = f'' + A_2H''. \qquad \textit{(see eq. 1.48)}$$

Front Focal Length

$$f_f = f - A_1H. \qquad \textit{(see eq. 1.50)}$$

Focal Ratios

The focal ratios are f/CA and f''/CA, where CA is the diameter of the clear aperture of the lens.

Numerical Apertures

$$n \sin\theta$$

$$\text{where } \theta = \arcsin\left(\frac{CA}{2s}\right)$$

and

$$n'' \sin\theta''$$

$$\text{where } \theta'' = \arcsin\left(\frac{CA}{2s''}\right).$$

Solid Angles (in steradians)

$$\Omega = 2\pi(1-\cos\theta) \qquad \textit{(see eq. 1.46)}$$

$$= 4\pi \sin^2\left(\frac{\theta}{2}\right)$$

$$\text{where } \theta = \arctan\left(\frac{CA}{2s}\right)$$

$$\Omega = 2\pi(1-\cos\theta'')$$

$$= 4\pi \sin^2\left(\frac{\theta}{2}\right)$$

$$\text{where } \theta'' = \arctan\left(\frac{CA}{2s''}\right).$$

To convert from steradians to spheres, simply divide by 4π.

APPLICATION NOTE

For Quick Approximations

Much time and effort can be saved by ignoring the differences among f, f_b, and f_f in these formulas by assuming that $f = f_b = f_f$. Then s becomes the lens-to-object distance; s'' becomes the lens-to-image distance; and the sum of conjugate distances $s + s''$ becomes the object-to-image distance. This is known as the thin-lens approximation.

APPLICATION NOTE

Physical Significance of the Nodal Points

A ray directed at the primary nodal point N of a lens appears to emerge from the secondary nodal point N″ without change of direction. Conversely, a ray directed at N″ appears to emerge from N without change of direction. At the infinite conjugate ratio, if a lens is rotated about a rotational axis orthogonal to the optical axis at the secondary nodal point (i.e., if N″ is the center of rotation), the image remains stationary during the rotation. This fact is the basis for the nodal slide method for measuring nodal-point location and the EFL of a lens. The nodal points coincide with their corresponding principal points when the image space and object space refractive indices are equal ($n = n''$). This makes the nodal slide method the most precise method of principal-point location.

Principal-Point Locations

Figure 1.36 indicates approximately where the principal points fall in relation to the lens surfaces for various standard lens shapes. The exact positions depend on the index of refraction of the lens material, and on the lens radii, and can be found by formula. in extreme meniscus lens shapes (short radii or steep curves), it is possible that both principal points will fall outside the lens boundaries. For symmetric lenses, the principal points divide that part of the optical axis between the vertices into three approximately equal segments. For plano lenses, one principal point is at the curved vertex, and the other is approximately one-third of the way to the plane vertex.

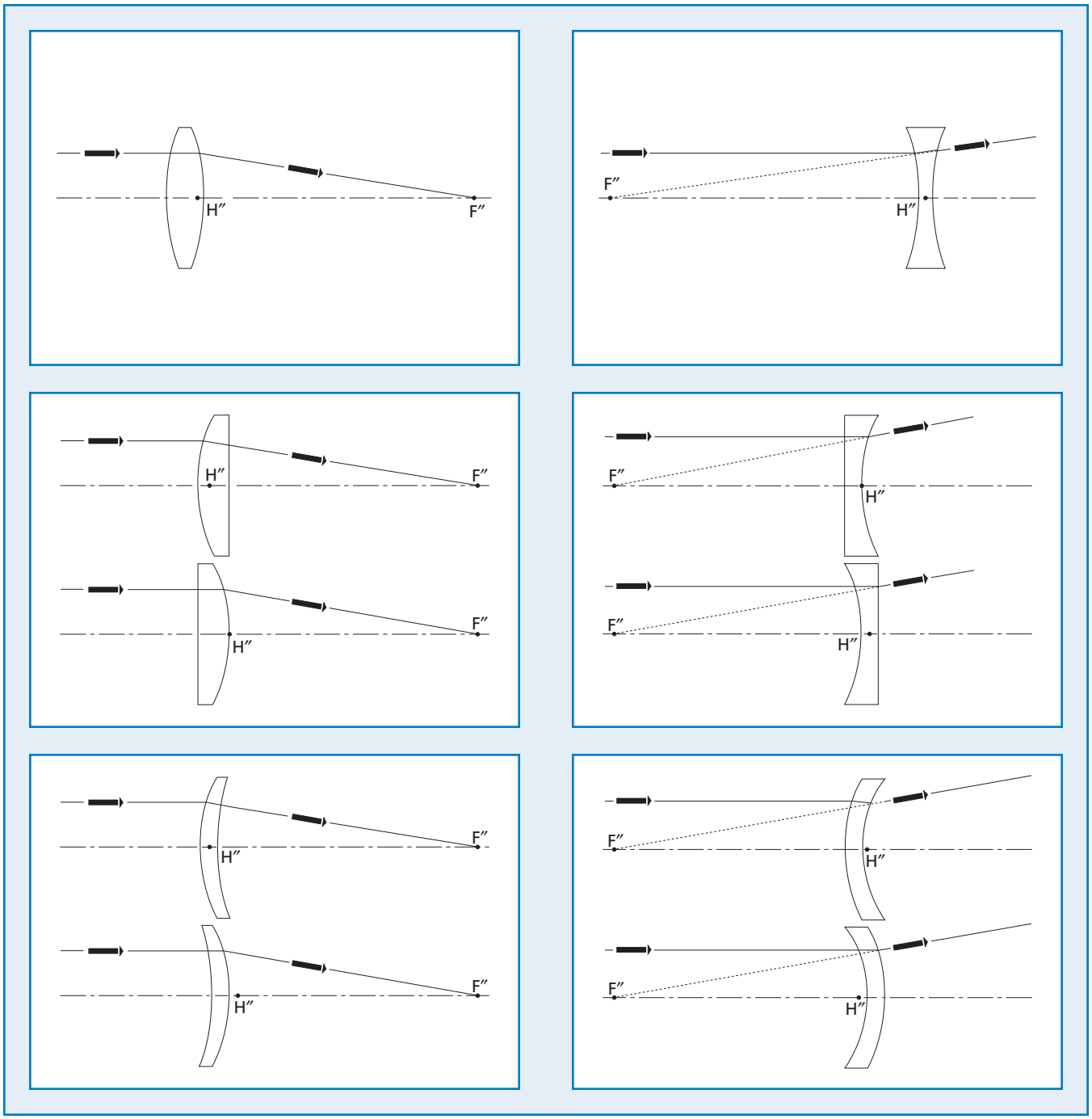

Figure 1.36 **Principal points of common lenses**

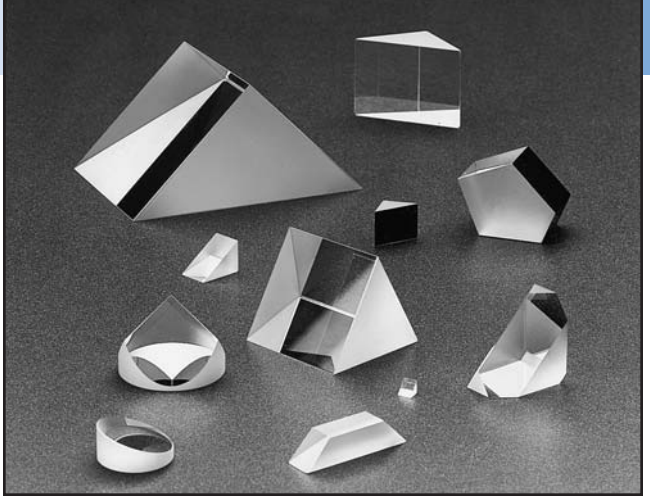

Prisms

Prisms are blocks of optical material whose flat, polished sides are arranged at precisely controlled angles to each other. Prisms may be used in an optical system to deflect or deviate a beam of light. They can invert or rotate an image, disperse light into its component wavelengths, and be used to separate states of polarization.

PRISM ORIENTATION

The orientation of a prism determines its effect on a beam of light or an image.

A viewer looks through a prism at an object and sees a virtual image (see Figure 1.37). This image may be displaced from the original object, or, if a dove prism is used, it may coincide with the object. Furthermore, image orientation may differ from the object; in the case of a right-angle prism, the image is reversed.

A real image (see Figure 1.38) can be formed only if imaging optics are present in the system. Without imaging optics, the image is virtual. A virtual image has the same orientation as the real image shown, but it can be viewed by the observer only by looking back through the prism system.

TOTAL INTERNAL REFLECTION

Rays incident upon a glass/air boundary (i.e., an internal reflection) at angles that exceed the critical angle are reflected with 100-percent efficiency regardless of their initial polarization state. The critical angle is given by

$$\theta_c(\lambda) = \arcsin\frac{1}{n_\lambda} \qquad (1.67)$$

and depends on the refractive index, which is a function of wavelength. If, at some wavelength, the refractive index should fall to less than $\sqrt{2} = 1.414$, the critical angle will exceed 45 degrees, and total internal reflection (TIR) will fail for a collimated beam internally incident at 45 degrees on the hypotenuse face of a right-angle prism. Reflectance decreases rapidly at angles of incidence smaller than the critical angle.

The index of BK7 is sufficiently high to guarantee the TIR of a collimated beam at 45 degrees internal incidence over the visible and near-infrared region. The possibility of significant TIR failure with convergent or divergent beams should be kept in mind if polarization is important. TIR can also fail if the hypotenuse face is not kept extremely clean. Even an almost invisible fingerprint can lead to TIR failure. An aluminum- or silver-coated hypotenuse is recommended for applications where the right-angle prism is frequently handled, or where convergent or divergent beams are used. There is a slight loss of reflectance at all internal angles with the coating, and no critical angle exists.

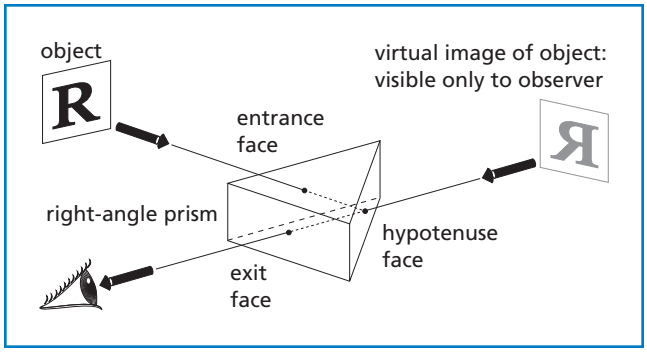

Figure 1.37 **Virtual imaging using a prism**

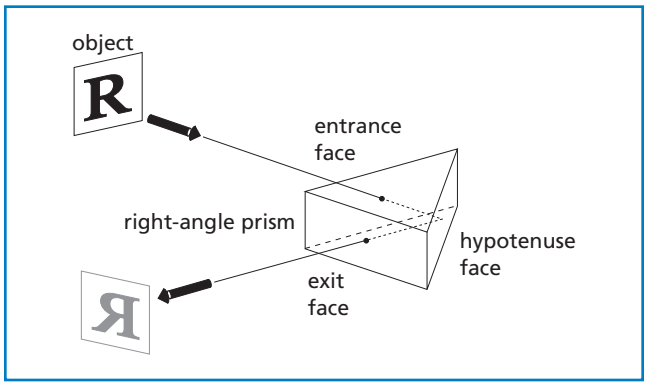

Figure 1.38 **Real imaging using a prism**

ABERRATIONS FOR PRISMS

Prisms will introduce aberrations when they are used with convergent or divergent beams of light. Using prisms with collimated or nearly collimated light will help minimize aberrations. Conjugate distances that include prisms should be long.

DISPERSING PRISMS

Dispersing prisms are used to separate a beam of white light into its component colors. Generally, the light is first collimated and then dispersed by the prism. A spectrum is then formed at the focal plane of a lens or curved mirror. In laser work, dispersing prisms are used to separate two wavelengths following the same beam path. Typically, the dispersed beams are permitted to travel far enough so the beams separate spatially.

A prism exhibits magnification in the plane of dispersion if the entrance and exit angles for a beam differ. This is useful in anamorphic (one-dimensional) beam expansion or compression, and may be used to correct or create asymmetric beam profiles.

As shown in Figure 1.39, a beam of width W_1 is incident at an angle α on the surface of a dispersing prism of apex angle A. The angle of refraction at the first surface, β, the angle of incidence at the second surface, γ, and the angle of refraction exiting the prism, δ, are easily calculated:

$$\beta = \sin^{-1}((\sin\alpha) / \eta)$$
$$\gamma = A - \beta$$
$$\delta = \sin^{-1}(\eta \sin\gamma)$$

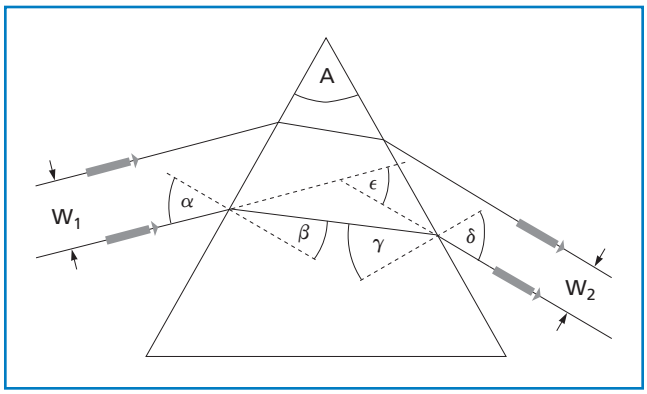

Figure 1.39 **Diagram of dispersing prism**

The beam deviation, ϵ, is of greatest importance. It is the angle the exit beam makes with its original direction.

$$\epsilon = \alpha + \delta - A \qquad (1.68)$$

The magnification W_2/W_1 is given by:

$$M = \frac{\cos\delta\cos\beta}{\cos\alpha\cos\gamma} \qquad (1.69)$$

The resolving power of a prism spectrometer angle α, the angular dispersion of the prism is given by:

$$\frac{d\delta}{d\lambda} = \left(\frac{\sin A}{\cos\delta\cos\beta}\right)\left(\frac{d\eta}{d\lambda}\right) \qquad (1.70)$$

If the spectrum is formed by a diffraction limited focal system of focal length f, the minimum spot size is $dx \sim f\lambda / W$. This corresponds to a minimum angular resolution $d\delta \sim \lambda/w$ for a beam of diameter w. The diffraction limited angular resolution at a given beam diameter sets the limit on the spectral resolving power of a prism. Setting the expression for $d\delta$ equal to the minimum angular resolution, we obtain:

$$RP = \frac{\lambda}{d\lambda} = \left(\frac{w_2 \sin A}{\cos\delta\cos\beta}\right)\left(\frac{d\eta}{d\lambda}\right) \qquad (1.71)$$

where RP is the resolving power of the prism.

At a given wavelength, the beam deviation ϵ is a minimum at an angle of incidence:

$$\alpha_{\text{min dev}} = \sin^{-1}[\eta \sin(A/2)] \qquad (1.72)$$

where η is the prism index of refraction at that wavelength. At this angle, the incident and exit angles are equal, the prism magnification is one, and the internal rays are perpendicular to the bisector of the apex angle.

By measuring the angle of incidence for minimum deviation, the index of refraction of a prism can be determined. Also, by proper choice of apex angle, the equal incident and exit angles may be made Brewster's angle, eliminating losses for p-polarized beams. The apex angle to choose is:

$$A = \pi - 2\theta_B \qquad (1.73)$$

If, in addition, the base angles of the prism are chosen as Brewster's angle, an isosceles Brewster prism results.

Another use is illustrated next.

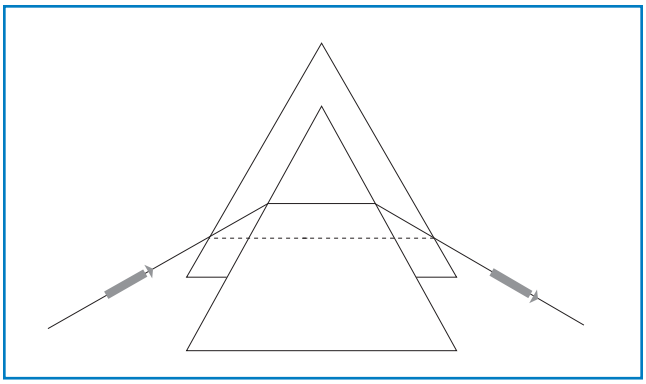

Figure 1.40 **Translation of a prism at minimum deviation**

At minimum deviation, translating a prism along the bisector of the apex angle does not disturb the direction of the output rays. See Figure 1.40. This is important in femtosecond laser design where intracavity prisms are used to compensate for group velocity dispersion. By aligning a prism for minimum deviation and translating it along its apex bisector, the optical path length in material may be varied with no misalignment, thus varying the contribution of the material to overall group velocity dispersion. Finally, it is possible to show that at minimum deviation

$$RP = (b_2 - b_1)\frac{d\eta}{d\lambda} \qquad (1.74)$$

where the relevant quantities are defined in Figure 1.41.

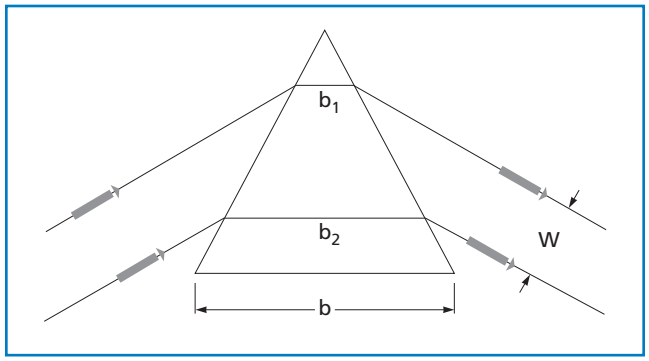

Figure 1.41 **Ray path lengths of a prism at minimum deviation**

If the beam is made to fill the prism completely, $b_1 = 0$, and $b_2 = b$, the base of the prism. So, we have the classical result that the resolving power of a prism spectrometer is equal to the base of the prism times the dispersion of the prism material.

As an example, consider CVI Melles Griot EDP-25-F2 prism, operating in minimum deviation at 590 nm. The angle of incidence and emergence are both then 54.09° and $d\eta/d\lambda$ is $-0.0854\ \mu m^{-1}$ for F2 glass at 590 nm. If the 25-mm prism is completely filled, the resolving power, $\lambda/d\lambda$, is 2135. This is sufficient to resolve the Sodium D lines.

PELLIN BROCA PRISMS

In a Pellin Broca prism, an ordinary dispersing prism is split in half along the bisector of the apex angle. Using a right angle prism, the two halves are joined to create a dispersing prism with an internal right angle bend obtained by total internal reflection, as shown in Figure 1.42.

In principle, one can split any type of dispersing prism to create a Pellin Broca prism. Typically the Pellin Broca prism is based on an Isosceles Brewster prism. Provided the light is *p*-polarized, the prism will be essentially lossless.

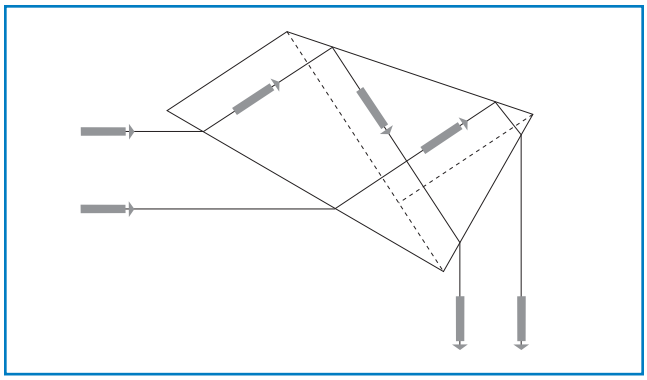

Figure 1.42 **One of the wavelengths deviates at exactly 90° to its initial direction**

Suppose wavelengths λ_1 and λ_2 are superimposed in a collimated beam, as at the output of a harmonic generating crystal, the diagram in Figure 1.42 suggests that it is always possible to find a rotation of the prism in its plane that ensures that one of the two wavelengths will operate at minimum deviation when refracting at the input face of the first of the half-dispersing prisms. This means that it will enter the right angle prism normal to one of its faces, be turned exactly 90°, be presented to the second half-dispersing prism in minimum deviation, and hence exit the Pellin Broca prism deviated at exactly 90° to its initial direction.

A simple dispersing prism always deviates the longer wavelength less than the shorter wavelength. In a Pellin Broca prism, whether the longer wavelength is deviated more or less depends on the orientation of the prism. This is an important consideration when designing a high power Pellin Broca beam separator, as shown in Figures 1.43 and 1.44.

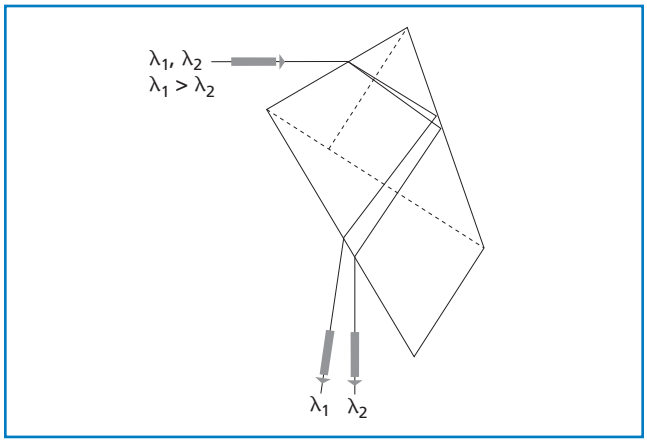

Figure 1.43 **Longer wavelength is deviated more than the shorter wavelength**

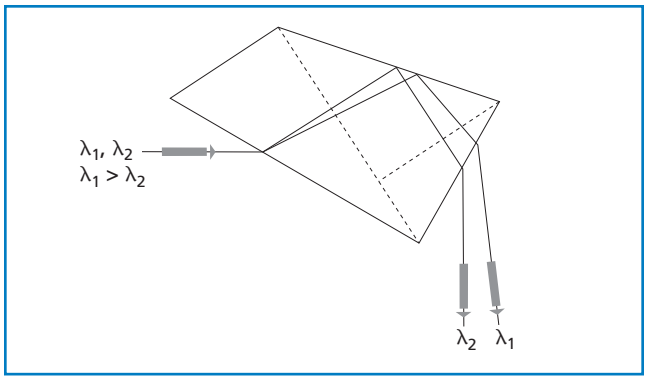

Figure 1.44 **Longer wavelength is deviated less than the shorter wavelength**

CVI Melles Griot offers Brewster angle Pellin Brocca prisms in a number of sizes and materials. BK7 prisms are used in the visible and near IR, and is the least expensive. UV-grade fused silica Pellin Broca prisms are used from 240 nm to 2000 nm. Excimer-grade prisms are used in the 180-nm to 240-nm region. Crystal-quartz Pellin Broca prisms are specifically designed for high-power Q-switched 266-nm laser pulses at fluence levels of 50 mJ/cm^2. Fused silica prisms track (i.e., suffer internal catastrophic damage) above this fluence, probably due to self-focusing.

PORRO PRISMS

A Porro prism, named for its inventor Ignazio Porro, is a type of reflection prism used to alter the orientation of an image. In operation, light enters the large face of the prism, undergoes total internal reflection twice from the 45° sloped faces, and exits again through the large face. An image traveling through a Porro prism is rotated by 180° and exits in the opposite direction offset from its entrance point, as shown in Figure 1.45. Since the image is reflected twice, the handedness of the image is unchanged. Porro prisms have rounded edges to minimize breakage and facilitate assembly.

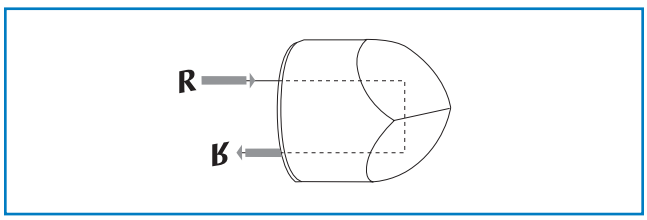

Figure 1.45 **Porro prisms retroreflect and invert the image**

Porro prisms are most often used in pairs, forming a double Porro prism, as shown in Figure 1.46. A second prism, rotated 90° with respect to the first, is placed such that the beam will traverse both prisms. The net effect of the prism system is a beam parallel to but displaced from its original direction, with the image rotated 180°. As before, the handedness of the image is unchanged.

Double Porro prism systems are used in small optical telescopes to reorient an inverted image and in many binoculars to both re-orient the image and provide a longer, folded distance between the objective lenses and the eyepieces.

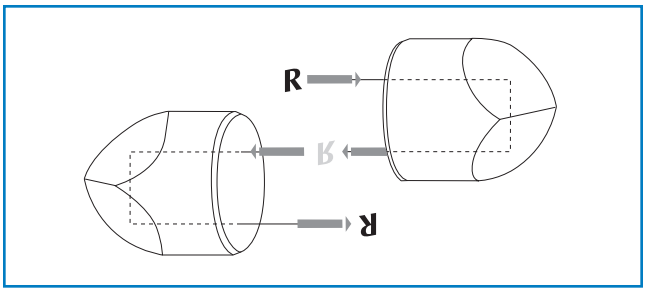

Figure 1.46 **Double porro prism results in a beam parallel to but displaced from its original direction, with the image rotated 180°**

Polarization

Polarization States

Four numbers are required to describe a single plane wave Fourier component traveling in the $+z$ direction. These can be thought of as the amplitude and phase shift of the field along two orthogonal directions.

1. CARTESIAN REPRESENTATION

In Cartesian coordinates, the propagation equation for an electric field is given by the formula

$$E(x,y,z) = (xE_x e^{i\phi_x} + yE_y e^{i\phi_y}) e^{i(kz-\omega t)} \quad (1.75)$$

where E_x, E_y, ϕ_x, and ϕ_y are real numbers defining the magnitude and the phase of the field components in the orthogonal unit vectors x and y. If the origin of time is irrelevant, only the relative phase shift

$$\phi = \phi_x - \phi_y \quad (1.76)$$

need be specified.

2. CIRCULAR REPRESENTATION

In the circular representation, we resolve the field into circularly polarized components. The basic states are represented by the complex unit vectors

$$e_+ = \left(1/\sqrt{2}\right)(x+iy) \text{ and} \quad (1.77)$$

$$e_- = \left(1/\sqrt{2}\right)(x-iy) \quad (1.78)$$

where e_+ is the unit vector for left circularly polarized light; for positive helicity light; for light that rotates counterclockwise in a fixed plane as viewed facing into the light wave; and for light whose electric field rotation obeys the right hand rule with thumb pointing in the direction of propagation.

APPLICATION NOTE

Polarization Convention

Historically, the orientation of a polarized electromagnetic wave has been defined in the optical regime by the orientation of the electric vector. This is the convention used by CVI Melles Griot.

e_- is the unit vector for right circularly polarized light; for negative helicity light; for light that rotates clockwise in a fixed plane as viewed facing into the light wave; and for light whose electric field rotation disobeys the right hand rule with thumb pointing in the direction of propagation.

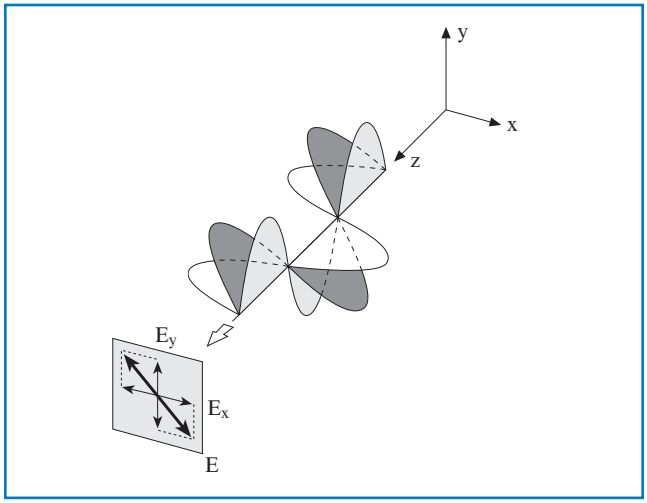

Figure 1.47 **Linearly polarized light. E_x and E_y are in phase**

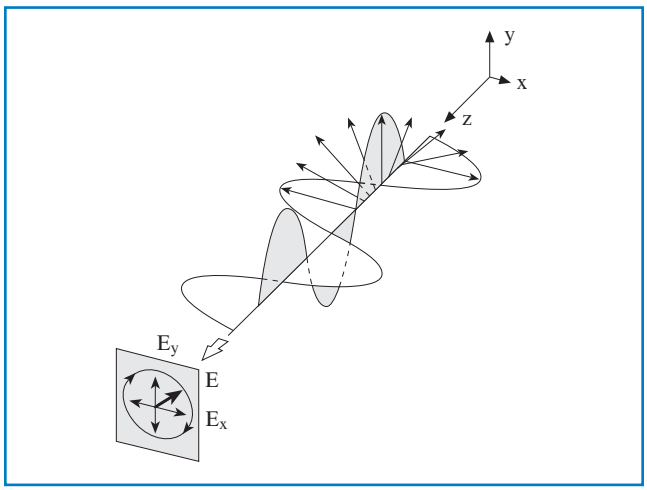

Figure 1.48 **Circularly polarized light. E_x and E_y are out of phase by angular frequency ω**

As in the case of the Cartesian representation, we write

$$E = (e_+ E_+ e^{i\phi +} + e_- E_- e^{i\phi -})\, e^{i(kz-\omega t)} \quad (1.79)$$

where E_+, E_-, ϕ_+, and ϕ_- are four real numbers describing the magnitudes and phases of the field components of the left and right circularly polarized components. Note that

$$E_+ = e_- \cdot E \quad (1.80)$$

$$E_- = e_+ \cdot E \quad (1.81)$$

3. ELLIPTICAL REPRESENTATION

An arbitrary polarization state is generally elliptically polarized. This means that the tip of the electric field vector will describe an ellipse, rotating once per optical cycle.

Let a be the semimajor and b be the semiminor axis of the polarization ellipse. Let ψ be the angle that the semimajor axis makes with the x axis.

Let ξ and η be the axes of a right-handed coordinate system rotated by an angle $+\psi$ with respect to the x axis and aligned with the polarization ellipse as shown in Figure 1.49.

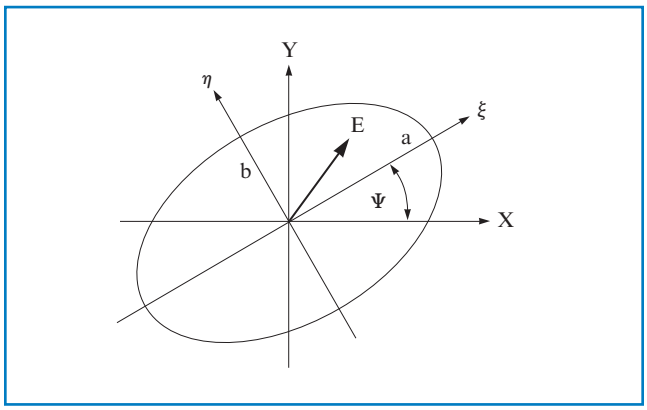

Figure 1.49 **The polarization ellipse**

The elliptical representation is:

$$E = \left(a\hat{\xi} + b\hat{\eta}\right) e^{i\delta_0} e^{i(kz-\omega t)} \quad (1.82)$$

Note that the phase shift δ_0 above is required to adjust the time origin, and the parameter ψ is implicit in the rotation of the ξ and η axes with respect to the x and y axes.

CONVERSIONS BETWEEN REPRESENTATIONS

For brevity, we will provide only the Cartesian to circular and Cartesian to elliptical transformations. The inverse transformations are straightforward. We define the following quantities:

$$g_1 = E_x \cos\phi_x - E_y \sin\phi_y \quad (1.83)$$

$$g_2 = E_x \sin\phi_x + E_y \cos\phi_y \quad (1.84)$$

$$g_3 = E_x \cos\phi_x + E_y \sin\phi_y \quad (1.85)$$

$$g_4 = E_x \sin\phi_x - E_y \cos\phi_y \quad (1.86)$$

$$u = \left(g_1^2 + g_2^2\right)^{1/2} \quad (1.87)$$

$$v = \left(g_3^2 + g_4^2\right)^{1/2} \quad (1.88)$$

$$\phi_{12} = \text{atan}\,(g_1, g_2) \quad (1.89)$$

$$\phi_{34} = \text{atan}\,(g_3, g_4) \quad (1.90)$$

In the above, atan(x,y) is the four quadrant arc tangent function. This means that atan(x,y) = atan(y/x) with the provision that the quadrant of the angle returned by the function is controlled by the signs of both x and y, not just the sign of their quotient; for example, if $g_2 = g_1 = -1$, then ϕ_{12} above is $5\pi/4$ or $-3\pi/4$, not $\pi/4$.

A. CARTESIAN TO CIRCULAR TRANSFORMATION

$$E_+ = v/\sqrt{2} \quad (1.91)$$

$$E_- = u/\sqrt{2} \quad (1.92)$$

$$\phi_+ = \phi_{34} \quad (1.93)$$

$$\phi_- = \phi_{12} \quad (1.94)$$

B. CARTESIAN TO ELLIPTICAL TRANSFORMATION

$$a = (v+u)/2 \quad (1.95)$$

$$b = (v-u)/2 \quad (1.96)$$

$$\psi = (\phi_{12} - \phi_{34})/2 \quad (1.97)$$

$$\delta_0 = (\phi_{12} + \phi_{34})/2 \quad (1.98)$$

LINEAR POLARIZERS

A linear polarizer is a device that creates a linear polarization state from an arbitrary input. It does this by removing the component orthogonal to the selected state. Unlike plastic sheet polarizers which absorb the rejected beam (which turns into heat), cube polarizers and thin-film plate polarizers reflect the rejected beam, creating two usable beams. Still others may refract the two polarized beams at different angles, thereby separating them. Examples are Wollaston and Rochon prism polarizers.

Suppose the pass direction of the polarizer is determined by unit vector p. Then the transmitted field E_2, in terms of the incident field E_1, is given by

$$E_2 = p(p \bullet E_1) \tag{1.99}$$

where the phase shift of the transmitted field has been ignored.

A real polarizer has a pass transmission, $T_{\|}$, less than 1. The transmission of the rejected beam, $T_{\perp}$, may not be 0. If r is a unit vector along the rejected direction, then

$$E_2 = (T_{\|})^{1/2} p(p \bullet E_1) e^{i\phi_{\|}} + (T_{\perp})^{1/2} r(r \bullet E_1) e^{i\phi_{\perp}} \tag{1.100}$$

In the above, the phase shifts along the two directions must be retained. Similar expressions could be arrived at for the rejected beam. If θ is the angle between the field E_1 and the polarizer pass direction p, the above equation predicts that

$$T = T_{\|} \cos^2\theta + T_{\perp} \sin^2\theta \tag{1.101}$$

The above equation shows that, when the polarizer is aligned so that $\theta = 0$, $T = T_{\|}$. When it is "crossed", $\theta = \pi/2$, and $T = T_{\perp}$. The extinction ratio is $\epsilon = T_{\|} / T_{\perp}$. A polarizer with perfect extinction has $T_{\perp} = 0$, and thus $T = T_{\|}\cos^2\theta$ is a familiar result. Because $\cos^2\theta$ has a broad maximum as a function of orientation angle, setting a polarizer at a maximum of transmission is generally not very accurate. One has to either map the $\cos^2\theta$ with sufficient accuracy to find the $\theta = 0$ point, or do a null measurement at $\theta = \pm\pi/2$.

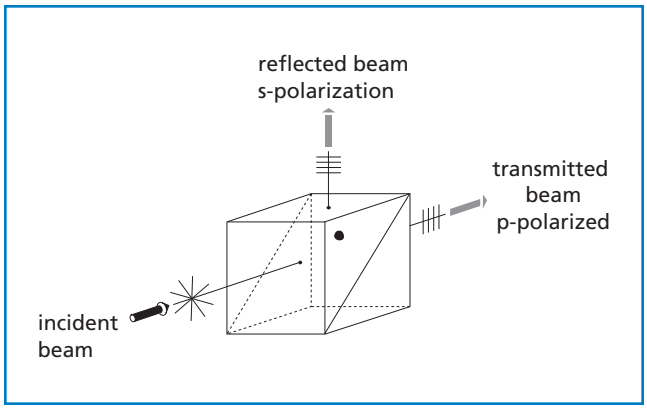

Figure 1.50 **At CVI Melles Griot, the DOT marks preferred input face. This is the tested direction for transmitted wavefront. Damage threshold is also higher for this orientation as well.**

Polarization Definitions

BIREFRINGENCE

A birefringent crystal, such as calcite, will divide an entering beam of monochromatic light into two beams having opposite polarization. The beams usually propagate in different directions and will have different speeds. There will be only one or two optical axis directions within the crystal in which the beam will remain collinear and continue at the same speed, depending on whether the birefringent crystal is uniaxial or biaxial.

If the crystal is a plane-parallel plate, and the optical axis directions are not collinear with the beam, radiation will emerge as two separate, orthogonally polarized beams (see Figure 1.51). The beam will be unpolarized where the beams overlap upon emergence. The two new beams within the material are distinguished from each other by more than just polarization and velocity. The rays are referred to as extraordinary (E) and ordinary (O). These rays need not be confined to the plane of incidence. Furthermore, the velocity of these rays changes with direction. Thus, the index of refraction for extraordinary rays is also a continuous function of direction. The index of refraction for the ordinary ray is constant and is independent of direction.

The two indexes of refraction are equal only in the direction of an optical axis within the crystal. The dispersion curve for ordinary rays is a single, unique curve when the index of refraction is plotted against wavelength. The dispersion curve for the extraordinary ray is a family of curves with different curves for different directions. Unless it is in a particular polarization state, or the crystalline surface is perpendicular to an optical axis, a ray normally incident on a birefringent surface will be divided in two at the boundary. The extraordinary ray will be deviated; the ordinary ray will not. The ordinary ray index n, and the most extreme (whether greater or smaller) extraordinary ray index n_e, are together known as the principal indices of refraction of the material.

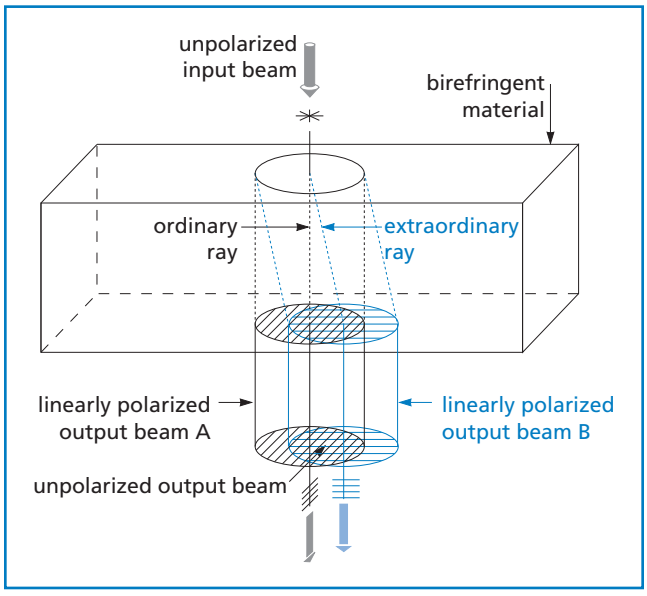

Figure 1.51 **Double refraction in a birefringent crystal**

If a beam of linearly polarized monochromatic light enters a birefringent crystal along a direction not parallel to the optical axis of the crystal, the beam will be divided into two separate beams. Each will be polarized at right angles to the other and will travel in different directions. The original beam energy, which will be divided between the new beams, depends on the original orientation of the vector to the crystal.

The energy ratio between the two orthogonally polarized beams can be any value. It is also possible that all energy will go into one of the new beams. If the crystal is cut as a plane-parallel plate, these beams will recombine upon emergence to form an elliptically polarized beam.

The difference between the ordinary and extraordinary ray may be used to create birefringent crystal polarization devices. In some cases, the difference in refractive index is used primarily to separate rays and eliminate one of the polarization planes, for example, in Glan-type polarizers. In other cases, such as Wollaston and Thompson beamsplitting prisms, changes in propagation direction are optimized to separate an incoming beam into two orthogonally polarized beams.

DICHROISM

Dichroism is selective absorption of one polarization plane over the other during transmission through a material. Sheet-type polarizers are manufactured with organic materials imbedded into a plastic sheet. The sheet is stretched, aligning molecules and causing them to be birefringent, and then dyed. The dye molecules selectively attach themselves to aligned polymer molecules, so that absorption is high in one plane and weak in the other. The transmitted beam is linearly polarized. Polarizers made of such material are very useful for low-power and visual applications. The usable field of view is large (up to grazing incidence), and diameters in excess of 100 mm are available.

POLARIZATION BY REFLECTION

When a beam of ordinary light is incident at the polarizing angle on a transmissive dielectric such as glass, the emerging refracted ray is partially linearly polarized. For a single surface (with n=1.50) at Brewster's angle, 100 percent of the light whose electric vector oscillates parallel to the plane of incidence is transmitted. Only 85 percent of the perpendicular light is transmitted (the other 15 percent is reflected). The degree of polarization from a single-surface reflection is small.

If a number of plates are stacked parallel and oriented at the polarizing angle, some vibrations perpendicular to the plane of incidence will be reflected at each surface, and all those parallel to it will be refracted. By making the number of plates within the stack large (more than 25), high degrees of linear polarization may be achieved. This polarization method

is utilized in CVI Melles Griot polarizing beamsplitter cubes which are coated with many layers of quarter-wave dielectric thin films on the interior prism angle. This beamsplitter separates an incident laser beam into two perpendicular and orthogonally polarized beams.

THIN METAL FILM POLARIZERS

Optical radiation incident on small, elongated metal particles will be preferentially absorbed when the polarization vector is aligned with the long axis of the particle. CVI Melles Griot infrared polarizers utilize this effect to make polarizers for the near-infrared. These polarizers are considerably more effective than dichroic polarizers.

Polarizing thin films are formed by using the patented Slocum process to deposit multiple layers of microscopic silver prolate spheroids onto a polished glass substrate. The exact dimensions of these spheroids determine the optical properties of the film. Peak absorption can be selected for any wavelength from 400 to 3000 nm by controlling the deposition process. Contrast ratios up to 10,000:1 can be achieved with this method. Other CVI Melles Griot high-contrast polarizers exhibit contrasts as high as 100,000:1.

CALCITE

Calcite, a rhombohedral crystalline form of calcium carbonate, is found in various forms such as limestone and marble. Since calcite is a naturally occurring material, imperfections are not unusual. The highest quality materials, those that exhibit no optical defects, are difficult to find and are more expensive than those with some defects. Applications for calcite components typically fall into laser applications or optical research. CVI Melles Griot offers calcite components in two quality grades to meet those various needs.

There are three main areas of importance in defining calcite quality.

Spectral Properties

Trace amounts of chemical impurities, as well as lattice defects, can cause calcite to be colored, which changes absorption. For visible light applications, it is essential to use colorless calcite. For near-infrared applications, material with a trace of yellow is acceptable. This yellow coloration results in a 15-percent to 20-percent decrease in transmission below 420 nm.

Wavefront Distortion (Striae)

Striae, or streaked fluctuations in the refractive index of calcite, are caused by dislocations in the crystal lattice. They can cause distortion of a light wavefront passing through the crystal. This is particularly troublesome for interferometric applications.

Scatter

Small inclusions within the calcite crystal account for the main source of scatter. They may appear as small cracks or bubbles. In general, scatter presents a significant problem only when the polarizer is being used with a laser. The amount of scatter centers that can be tolerated is partially determined by beam size and power.

CVI MELLES GRIOT CALCITE GRADES

CVI Melles Griot has selected the most applicable calcite qualities, grouped into two grades:

Laser Grade

Calcite with a wavefront deformation of $\lambda/4$ at 633 nm or better due to striae only.

Optical Grade

Calcite with a wavefront deformation of 1λ to $\lambda/4$ at 633 nm due to striae only.

Waveplates

Waveplates use birefringence to impart unequal phase shifts to the orthogonally polarized field components of an incident wave, causing the conversion of one polarization state into another.

There are two types of birefringence. With linear birefringence, the index of refraction (and hence the phase shift) differs for two orthogonally polarized linear polarization states. This is the operation mode of standard waveplates. With circular birefringence, the index of refraction and hence phase shift differs for left and right circularly polarized components. This is the operation mode of polarization rotators.

STANDARD WAVEPLATES: LINEAR BIREFRINGENCE

Suppose a waveplate made from a uniaxial material has light propagating perpendicular to the optic axis. This makes the field component parallel to the optic axis an extraordinary wave and the component perpendicular to the optic axis an ordinary wave. If the crystal is positive uniaxial, $\eta_e > \eta_o$, then the optic axis is called the slow axis, which is the case for crystal quartz. For negative uniaxial crystals $\eta_e < \eta_o$, the optic axis is called the fast axis.

The equation for the transmitted field E_2, in terms of the incident field E_1 is:

$$E_2 = s(s \bullet E_1)e^{i\phi_s} + f(f \bullet E_1)e^{i\phi_f} \qquad (1.102)$$

where s and f are unit vectors along the slow and fast axes. This equation shows explicity how the waveplate acts on the field. Reading from left to right, the waveplate takes the component of the input field along its slow axis and appends the slow axis phase shift to it. It does a similar operation to the fast component.

The slow and fast axis phase shifts are given by:

$$\phi_s = \eta_s(\omega)\omega t/c = 2\pi\eta_s(\lambda)t/\lambda \qquad (1.103)$$

$$\phi_f = \eta_f(\omega)\omega t/c = 2\pi\eta_f(\lambda)t/\lambda \qquad (1.104)$$

where η_s and η_f are, respectively, the indices of refraction along the slow and fast axes, and t is the thickness of the waveplate.

To further analyze the effect of a waveplate, we throw away a phase factor lost in measuring intensity, and assign the entire phase delay to the slow axis:

$$E_2 = s(s \bullet E_1)e^{i\phi} + f(f \bullet E1) \qquad (1.105)$$

$$\phi = \phi_s - \phi_f = 2\pi\left[\eta_s(\lambda) - \eta_f(\lambda)\right]t/\lambda \qquad (1.106)$$

$$\phi = 2\,\pi\,\Delta\eta(\lambda)t/\lambda \qquad (1.107)$$

In the above, $\Delta\eta(\lambda)$ is the birefringence $\eta_s(\lambda)$ - $\eta_f(\lambda)$. The dispersion of the birefringence is very important in waveplate design; a quarter waveplate at a given wavelength is never exactly a half waveplate at half that wavelength.

Let E_1 be initially polarized along x, and let the waveplate slow axis make an angle θ with the x axis. This orientation is shown in Figure 1.52.

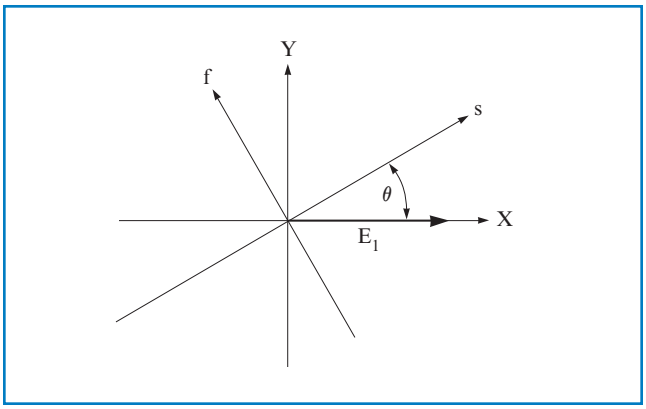

Figure 1.52. Orientation of the slow and fast axes of a waveplate with respect to an x-polarized input field

When the waveplate is placed between parallel and perpendicular polarizers the transmissions are given by:

$$T_{\parallel} \propto |E_2 x|^2 = 1 - \sin^2\ 2\theta \sin^2 \phi/2 \qquad (1.108)$$

$$T_{\perp} \propto |E_2 y|^2 = \sin^2\ 2\theta \sin^2 \phi/2 \qquad (1.109)$$

Note that θ is only a function of the waveplate orientation, and ϕ is only a function of the wavelength, the birefringence is a function of wavelength and the plate thickness.

For a full-wave waveplate:

$\phi = 2m\pi$, $T_{\parallel} = 1$, and $T_{\perp} = 0$, regardless of waveplate orientation.

For a half-wave waveplate:

$$\phi = (2m\ +\ 1)\pi,\ T_{\parallel} = \cos^2 2\theta, \text{ and } T_{\perp} = \sin^2 2\theta. \qquad (1.110)$$

This transmission result is the same as if an initial linearly polarized wave were rotated through an angle of 2θ. Thus, a half-wave waveplate finds use as a polarization rotator.

For a quarter waveplate,

$$\phi = (2m\ +\ 1)\pi/2 \text{ (i.e., an odd multiple of } \pi/2). \qquad (1.111)$$

To analyze this, we have to go back to the field equation. Assume that the slow and fast axis unit vectors s and f form a right handed coordinate system such that s x f = + z, the direction of propagation. To obtain circularly polarized light, linearly polarized light must be aligned midway between the slow and fast axes. There are four possibilities listed in the table below.

Phase Shift	Input Field Along $(\mathbf{s} + \mathbf{f})/\sqrt{2}$	Input Field Along $(\mathbf{s} - \mathbf{f})/\sqrt{2}$
$\phi = \pi/2 + 2m\pi$	RCP	LCP
$\phi = 3\pi/2 + 2m\pi$	LCP	RCP

Sometimes, waveplates described by the second line above are called 3/4 waveplates. For multiple order waveplates, CVI Melles Griot permits the use of either of the above classes of waveplates to satisfy the requirements of a quarter-wave waveplate.

MULTIPLE-ORDER WAVEPLATES

For the full-, half-, and quarter-wave waveplate examples given in standard waveplates, the order of the waveplate is given by the integer m. For m > 0, the waveplate is termed a multiple-order waveplate. For m = 0, we have a zero order waveplate.

The birefringence of crystal quartz near 500 nm is approximately 0.00925. Consider a 0.5-mm-thick crystal quartz waveplate. A simple calculation shows that this is useful as a quarter waveplate for 500 nm; in fact, it is a 37 λ/ 4 waveplate at 500 nm with m = 18. Multiple-order waveplates are inexpensive, high-damage-threshold retarders. Further analysis shows that this same 0.5mm plate is a 19 λ/2 half waveplate at 488.2 nm and a 10λ full-wave waveplate at 466.5 nm. The transmission of this plate between parallel polarizers is shown in Figure 1.53 as a function of wavelength. The retardance of the plate at various key points is also shown. Note how quickly the retardance changes with wavelength. Because of this, multiple-order waveplates are generally useful only at their design wavelength.

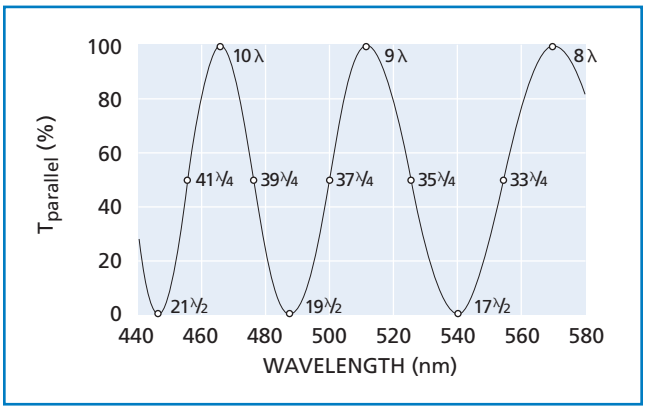

Figure 1.53 **Transmission of a 0.5-mm-thick crystal quartz waveplate between parallel polarizers**

ZERO-ORDER WAVEPLATES

As discussed above, multiple-order waveplates are not useful with tunable or broad bandwidth sources (e.g., femtosecond lasers). A zero-order waveplate can greatly improve the useful bandwidth in a compact, high-damage-threshold device.

As an example, consider the design of a broadband half-wave waveplate centered at 800 nm. Maximum tuning range is obtained if the plate has a single π phase shift at 800 nm. If made from a single plate of crystal quartz, the waveplate would be about 45 μm thick, which is too thin for easy fabrication and handling. The solution is to take two crystal quartz plates differing in thickness by 45 μm and align them with the slow axis of one against the fast axis of the other. The net phase shift of this zero-order waveplate is π. The two plates may be either air-spaced or optically contacted. The transmission of an 800-nm zero-order half-wave waveplate between parallel polarizers is shown in Figure 1.54 using a 0-10% scale. Its extinction is better than 100:1 over a bandwidth of about 95 nm centered at 800 nm.

CVI Melles Griot produces multiple order and zero order crystal quartz waveplates at any wavelength between 193 nm and 2100 nm. Virtually all popular laser wavelengths are kept in stock, and custom wavelength parts are available with short delivery time.

Mica waveplates are an inexpensive zero-order waveplate solution for low-power applications and in detection schemes.

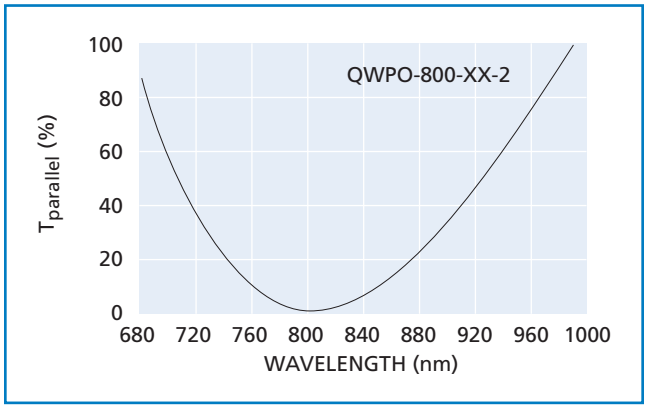

Figure 1.54 **Zero-order crystal quartz half-wave waveplate for 800 nm**

POLYMER WAVEPLATES

Polymer waveplates offer excellent angular field of view since they are true zero-order waveplates. Figure 1.55 compares the change in retardance as function of incidence angle for polymer and quartz waveplates. A polymer waveplate changes by less than 1% over a ±10° incidence angle.

Retardance accuracy with wavelength change is often of key concern. For example, an off-the-shelf diode laser has a center wavelength tolerance of ±10 nm. Changes with temperature and drive conditions cause wavelength shifts which may alter performance. These polymer waveplates maintain excellent waveplate performance even with minor shifts in the source wavelength. The temperature sensitivity of laminated polymer waveplates is about 0.15 nm/°C, allowing operation over moderate temperature ranges without significantly degrading retardance accuracy. A comparison of different waveplate types and their dependence on wavelength is shown in figure 1.56.

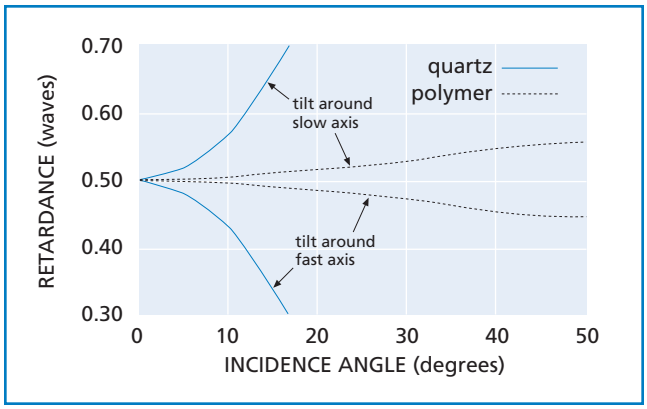

Figure 1.55 **Retardance vs incidence angle for quartz and polymer waveplates**

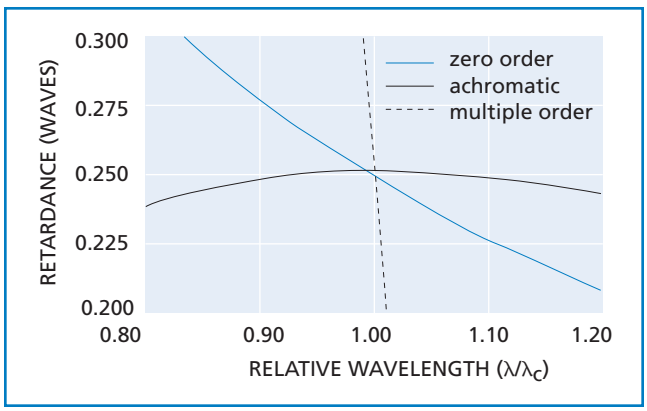

Figure 1.56 **Wavelength performance of common quarter wave retarders.**

ACHROMATIC WAVEPLATES

At 500 nm, a crystal quartz zero-order half-wave waveplate has a retardation tolerance of λ/50 over a bandwidth of about 50 nm. This increases to about 100 nm at a center wavelength of 800 nm. A different design which corrects for dispersion differences over the wavelength range is required for bandwidths up to 300 nm.

If two different materials are used to create a zero-order or low-order waveplate, cancellation can occur between the dispersions of the two materials. Thus, the net birefringent phase shift can be held constant over a much wider range than in waveplates made from one material. ACWP-series achromatic waveplates from CVI Melles Griot (see Figure 1.57) are comprised of crystal quartz and magnesium fluoride to achieve achromatic performance.

Three wavelength ranges are available in both quarter and half wave retardances. Retardation tolerance is better than λ/100 over the entire wavelength range.

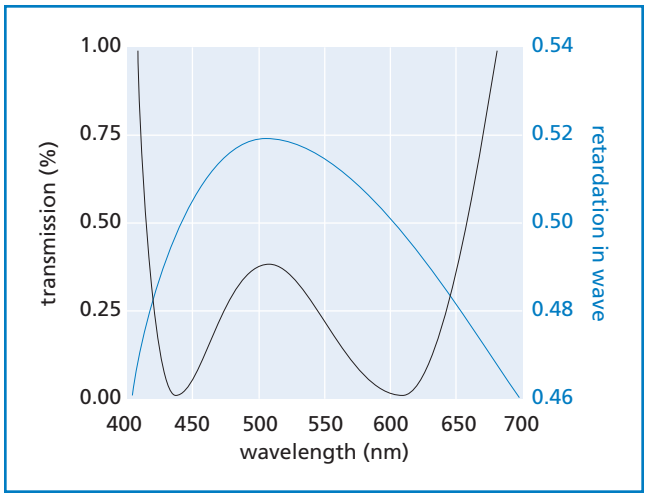

Figure 1.57 **ACWP-400-700-10-2**

For quarter-wave waveplates, perfect retardance is a multiple of 0.25 waves, and transmission through a linear polarizer must be between 33% and 67%. (In all but the shortest wavelength design, quarter-wave retardation tolerance is better than λ/100.) For half-wave waveplates, perfect retardance is 0.5 waves, while perfect transmission through a linear polarizer parallel to the initial polarization state should be zero. A high degree of achromatization is achievable by the dual material design. In addition, we manage low group velocity dispersion for ultrashort pulse applications through the use of thin plates.

DUAL-WAVELENGTH WAVEPLATES

Dual-wavelength waveplates are used in a number of applications. One common application is separation of different wavelengths with a polarizing beamsplitter by rotating the polarization of one wavelength by 90°, and leaving the other unchanged. This frequently occurs in nonlinear doubling or tripling laser sources such as Nd:YAG (1064/532/355/266).

One way to achieve the multiple retardation specifications is through careful selection of multiple-order waveplates which meet both wavelength and retardation conditions. This often results in the selection of a relatively high order waveplate. Therefore, these dual-wavelength waveplates operate best over a narrow bandwidth and temperature range.

Another approach is to combine two quartz waveplates with their optical axes orthogonal to one another, effectively creating a zero-order waveplate. In this configuration, the temperature dependence is a function of the thickness difference between the waveplates, resulting in excellent temperature stability. The retardation of the compound waveplate is also a function of the thickness difference enabling wide bandwidth performance.

Etalons

Etalons are most commonly used as line-narrowing elements in narrow-band laser cavities or as bandwidth-limiting and coarse-tuning elements in broadband and picosecond lasers. Further applications are laser line profile monitoring, diagnosis.

The etalons described in this section are all of the planar Fabry-Perot type. Typical transmission characteristics for this type etalon are shown in Figure 1.58.

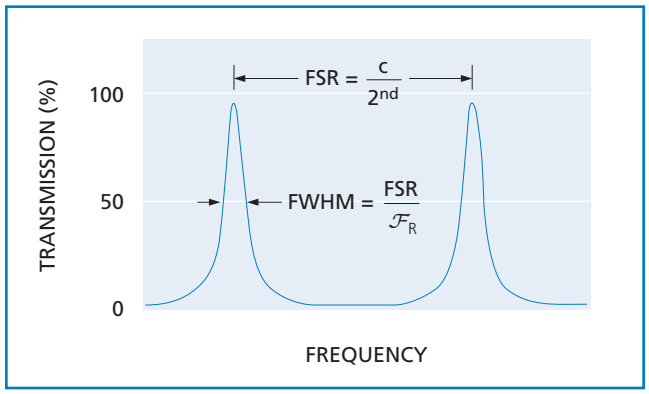

Figure 1.58 **Transmission characteristics of a Fabry-Perot etalon**

Air-Spaced Etalons consist of pairs of very flat plano-plano plates separated by optically contacted spacers. The inner surfaces of the plates are coated with partially reflecting coatings, the outer surfaces are coated with antireflection coatings.

Solid Etalons are made from a single plate with parallel sides. Partially reflecting coatings are then deposited on both sides. The cavity is formed by the plate thickness between the coatings.

Deposited Solid Etalons are a special type of solid etalon in which the cavity is formed by a deposited layer of coating material. The thickness of this deposited layer depends on the free spectral range required and can range from a few nanometers up to 15 micrometers. The cavity is sandwiched between the etalon reflector coatings and the whole assembly is supported on a fused-silica base plate.

Etalon plates need excellent surface flatness and plate parallelism. To avoid peak transmission losses due to scatter or absorption, the optical coatings also have to meet the highest standards.

For a plane wave incident on the etalon, the transmission of the etalon is given by:

$$T = \frac{I_{trans}}{I_{inc}} = \frac{1}{1 + \frac{4R}{(1-R)^2}\sin^2(\delta/2)} \qquad (1.112)$$

Here, R is the reflectance of each surface; δ is the phase shift

$$\delta = \frac{2\pi}{\lambda}\eta d\cos\theta \qquad (1.113)$$

where,

η is the refractive index (e.g., 1 for air-spaced etalons)

d is the etalon spacing or thickness

θ is the angle of incidence

The free spectral range (FSR) of the etalon is given by

$$\text{FSR} = \frac{c}{2\eta d} \text{ in Hz} \qquad (1.114)$$

$$= \frac{1}{2\eta d} \text{ in cm}^{-1}$$

$$= \frac{\lambda^2}{2\eta d} \text{ in nm}$$

The reflectivity finesse, $\mathcal{F}_R$ is given by

$$\mathcal{F}_R = \frac{\pi\sqrt{R}}{1-R} \qquad (1.115)$$

Figure 1.59 shows the reflectivity finesse as a function of the coating reflectivity.

The bandwidth (FWHM) is given by

$$\text{FWHM} = \frac{\text{FSR}}{\mathcal{F}_R} \qquad (1.116)$$

However, the above applies to theoretical etalons which are assumed to be perfect. In reality, even the best etalon will show defects that limit theoretically expected performance. Therefore, in a real etalon, the actual finesse will usually be lower than the reflectivity finesse.

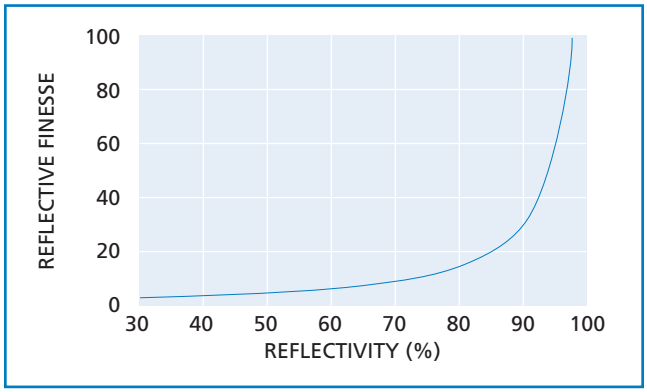

Figure 1.59 **Reflectivity finesse vs. coating reflectance of each surface**

$$\mathcal{F}_R = \frac{\pi\sqrt{R}}{1-R} \quad (1.117)$$

$$\mathcal{F}_S = \frac{M}{2}\frac{\lambda}{633\ \text{nm}} \quad (1.118)$$

$$\mathcal{F}_\theta = \frac{\lambda}{d\tan^2\theta} \quad (1.119)$$

$$\mathcal{F}_D = \frac{CA^2}{2d\lambda} \quad (1.120)$$

where $\mathcal{F}_R$ is the reflectivity finesse, $\mathcal{F}_s$ is the plate spherical deviation finesse coefficient, $\mathcal{F}_\theta$ is the incident beam divergence finesse coefficient, and $\mathcal{F}_d$ is the diffraction-limited finesse coefficient.

The defects that contribute to this reduction are as shown in Figure 1.60 (graphical representations are exagerated for clarification).

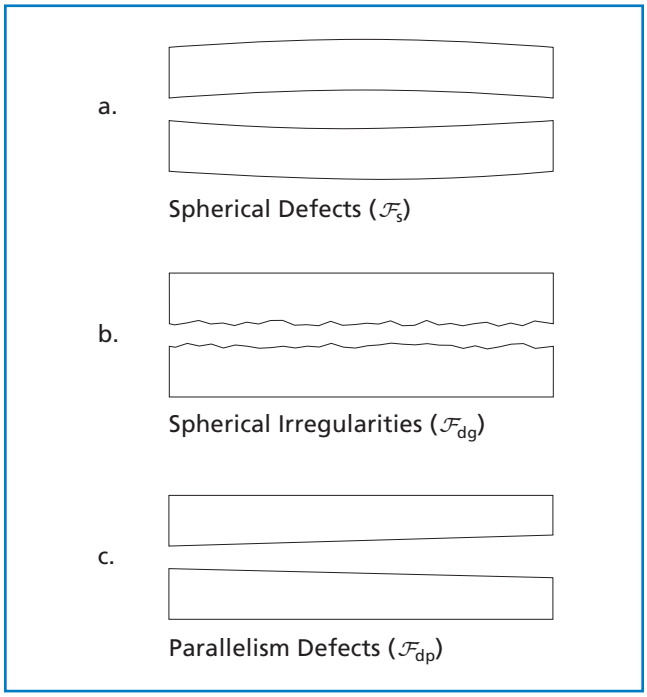

Figure 1.60 **Three types of defects contributing to the total defect finesse**

All three types of defects contribute to the total defect finesse $\mathcal{F}_d$:

$$\frac{1}{\mathcal{F}_d^2} = \frac{1}{\mathcal{F}_S^2} + \frac{1}{\mathcal{F}_{dg}^2} + \frac{1}{\mathcal{F}_{dp}^2} \quad (1.121)$$

The beam divergence also influences the actual finesse of an etalon.

Taking into account all these contributions, the effective finesse ($\mathcal{F}_e$) of an etalon (with $\mathcal{F}_R$ being the reflectivity finesse and $\mathcal{F}_\theta$ the divergence finesse) is:

$$\frac{1}{\mathcal{F}_e} = \sqrt{\frac{1}{\mathcal{F}_R^2} + \frac{1}{\mathcal{F}_D^2} + \frac{1}{\mathcal{F}_\theta^2} + \frac{1}{\mathcal{F}_S^2}} \quad (1.122)$$

The effective finesse a user sees when using the etalon depends not only on the absolute clear aperture, but also on the used aperture of the etalon, especially when a high finesse is required.

The examples below show how the effective finesse varies with plate flatness and clear aperture.

Example 1: Air-spaced etalon,

$R = 95\%\ (\pm 1\%)$ at 633 nm

CA = 25 mm

Used aperture = 20 mm

Spacer (air gap) = 1 mm

Spherical / parallelism defects = $<\lambda/20$

Plate rms = 0.80 nm

Beam divergence = 0.1 mRad

$\mathcal{F}_R = 61$, $\mathcal{F}_e = 10$

Example 2: Air-spaced etalon,

Same parameters as example 1 except:

Used aperture = 5 mm

$\mathcal{F}_R = 61$, $\mathcal{F}_e = 40\ (\pm 4)$

Example 3: Air-spaced etalon,

Same parameters as example 1 except:

Spherical / parallelism defects = $\lambda/100$

Plate rms = 0.40 nm

Beam divergence: 0.1mRad

$\mathcal{F}_R = 61$, $\mathcal{F}_e = 40\ (\pm 8)$

These examples illustrate that, for large-aperture applications, it is important to use very high-quality plates to ensure a high finesse and good transmission values.

TUNING AN ETALON

Etalons can be tuned over a limited range to alter their peak transmission wavelengths. These techniques are:

Angle tuning or tilting the etalon: As the angle of incidence is increased, the center wavelength of the etalon can be tuned down the spectrum.

Temperature tuning: Primarily used for solid etalons, temperature-tuning changes both the actual spacing of the reflective surfaces via expansion and the index of refraction of the material, which changes the optical spacing. The tuning result can be given by

$$\frac{\partial(\mathrm{FSR})}{\partial T} = -(\mathrm{FSR})\left[\frac{1}{\mathrm{n}}\frac{\partial \eta}{\partial T} + \frac{1}{d}\frac{\partial d}{\partial T}\right] \qquad (1.123)$$

Pressure tuning: Air-spaced etalons can be tuned by increasing the pressure in the cavity between the optics, thereby increasing the effective index of refraction, and thus the effective spacing.

The above examples illustrate how critical the optical surface flatness, plate parallelism and surface quality are to the overall performance of an etalon. At CVI Melles Griot we have developed sophisticated software that allows us to simulate all effects that influence the performance of an etalon. To order an etalon, FSR, finesse and used aperture are required.

Ultrafast Theory

The distinguishing aspect of femtosecond laser optics design is the need to control the phase characteristic of the optical system over the requisite wide pulse bandwidth. CVI Melles Griot has made an intensive theoretical study of these effects. Certain coating designs have been modified with control of the phase characteristics in mind. New proprietary designs have been created with desirable characteristics for femtosecond researchers. All optics in this section have been tested by researchers in the field and we are constantly fielding new requests.

Assume that the power, reflectivity, and polarization characteristics of a laser mirror are acceptable over the bandwidth of a femtosecond pulse. This means that, over the entire pulse bandwidth, a cavity mirror may have a reflectivity greater than 99.8%; a 50% beamsplitter may have a fairly constant reflection; a polarizer may maintain its rejection of one polarization with an acceptable transmission of the other. It is not enough, however, to simply preserve the power spectrum $S(\omega) = |E(\omega)|^2$ when dealing with femtosecond pulses. The phase relationship among the Fourier components of the pulse must also be preserved in order that the pulse not be broadened or distorted. What constraint on the performance of a mirror or transmissive optic does this imply?

Consider a general initial pulse shape $E_0(t)$. As a function of its Fourier components, it may be expressed as:

$$E_0(t) = \int E(\omega)^{-i\omega t}\, d\omega \qquad (1.124)$$

Suppose this pulse reflects off of a mirror. For this example, we assume the mirror is "ideal", and use the Fourier transform of its complex amplitude reflectance:

$$r(\omega) = re^{+i\Phi(\omega)} = re^{+i\omega t_d} \qquad (1.125)$$

For this "ideal" mirror, r is a real constant equal to the amplitude reflectivity that is assumed constant over the pulse bandwidth. All phase effects have been assumed to be describable by a single phase shift $\phi(\omega)$ that is linearly proportional to frequency with proportionality constant t_d. The reflected pulse is then:

$$\begin{aligned} E_r(t) &= r\int E(\omega)^{-i\omega(t-t_d)}\, d\omega \\ &= rE(t-t_d) \end{aligned} \qquad (1.126)$$

Thus, provided the phase shift is linear in frequency over the pulse bandwidth, the reflected pulse is scaled by the amplitude reflectance r, and delayed in time by the constant group delay t_d. It is, otherwise, an undistorted replica of the original pulse.

Examined over a large enough bandwidth, no optical system will exhibit the constant group delay over frequency needed for perfect fidelity. In general, the phase shift near some center frequency ω_0 may be expanded in a Taylor series for frequencies near ω_0:

$$\begin{aligned} \Phi(\omega) = \Phi(\omega_0) + \Phi'(\omega_0)(\omega-\omega_0) + \\ \Phi''(\omega_0)(\omega-\omega_0)^2/2! + \\ \Phi'''(\omega_0)(\omega-\omega_0)^3/3! \ldots \end{aligned} \qquad (1.127)$$

These derivatives are, respectively, the group delay $\Phi'(\omega_0)$, the group velocity dispersion $\Phi''(\omega_0)$, and the cubic term $\Phi'''(\omega_0)$, evaluated at a center frequency ω_0. This expansion is heuristically useful, in an exactly soluble model, for the propagation of a transform-limited Gaussian pulse. Note, however, that for extremely short pulses the expansion above may be insufficient. A full numerical calculation may have to be performed using the actual phase shift function $\Phi(\omega)$. CVI Melles Griot will be happy to assist those interested in the modeling of real optical elements.

To illustrate pulse distortion due to the dependence of the group delay on frequency, consider what happens when an unchirped, transform-limited Gaussian pulse passes through a medium, or is incident on a mirror whose dominating contribution to phase distortion is non-zero group velocity dispersion. The field envelope of the pulse is assumed to be of the form:

$$E(t) = \exp\left[-\left(2\ \ln 2 t^2/\tau_0^2\right)\right] \qquad (1.128)$$

where τ_0 is the initial pulse duration (FWHM of the pulse intensity). Let the pulse enter a medium or reflect off of a mirror with non-zero $\Phi''(\omega)$, measured in fsec^2 radians. (For a continuous medium-like glass, $\Phi''(\omega) = \beta''(\omega) \times z$ where $\beta''(\omega)$ is the group velocity dispersion (GVD) per centimeter of material, and z is the physical path length, in centimeters, traveled through the material.) The Gaussian pulse will be both chirped and temporally broadened by its encounter with group velocity dispersion. The power envelope will remain Gaussian; the result for the broadened FWHM is:

$$\tau_1 = \tau_0\left[1+\left(4\ln 2\Phi''(\omega)/\tau_0^2\right)^2\right]^{1/2} \qquad (1.129)$$

This result, valid only for initially unchirped, transform-limited Gaussian pulses, is nevertheless an excellent model to study the effects of dispersion on pulse propagation. The graphs shown in Figure 1.61 represent the theoretical broadening from dispersion for initial pulse widths ranging from 10 to 100 femtoseconds.

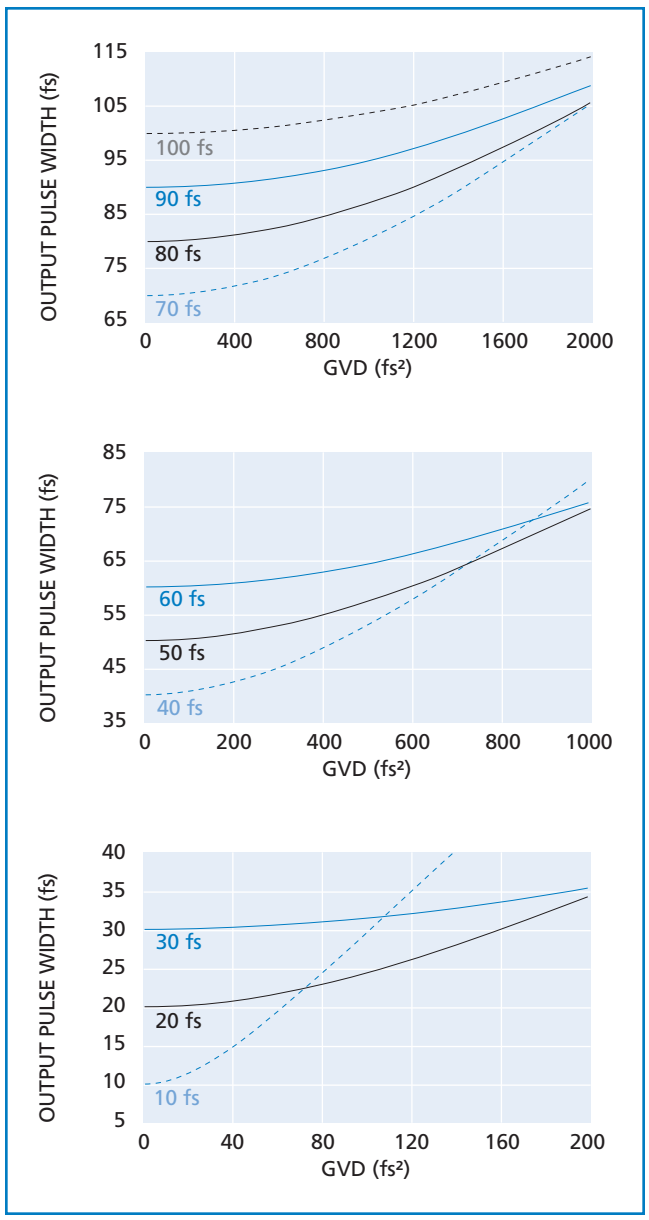

Figure 1.61 **Output pulse width vs. GVD**

GROUP-VELOCITY & CUBIC DISPERSION FOR VARIOUS OPTICAL MATERIALS

Figures 1.62 and 1.63 show the GVD and cubic dispersion respectively for some common used glasses. Some of the glasses can be used in the UV region. They should be useful in estimating material dispersion and pulse distortion effects. Please check these calculations independently before using them in a final design.

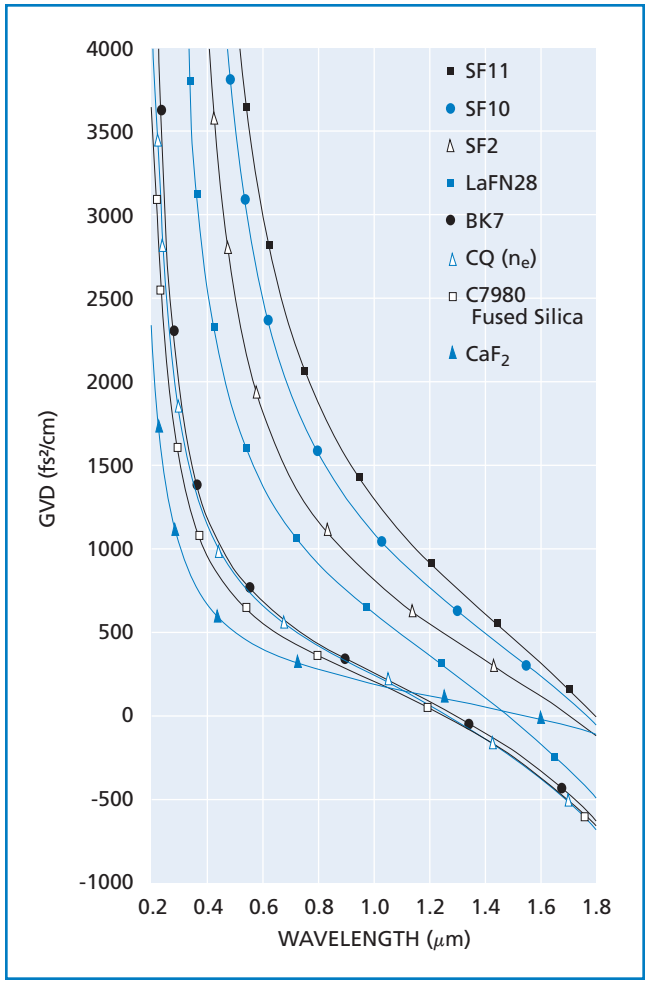

Figure 1.62 **GVD for common glasses**

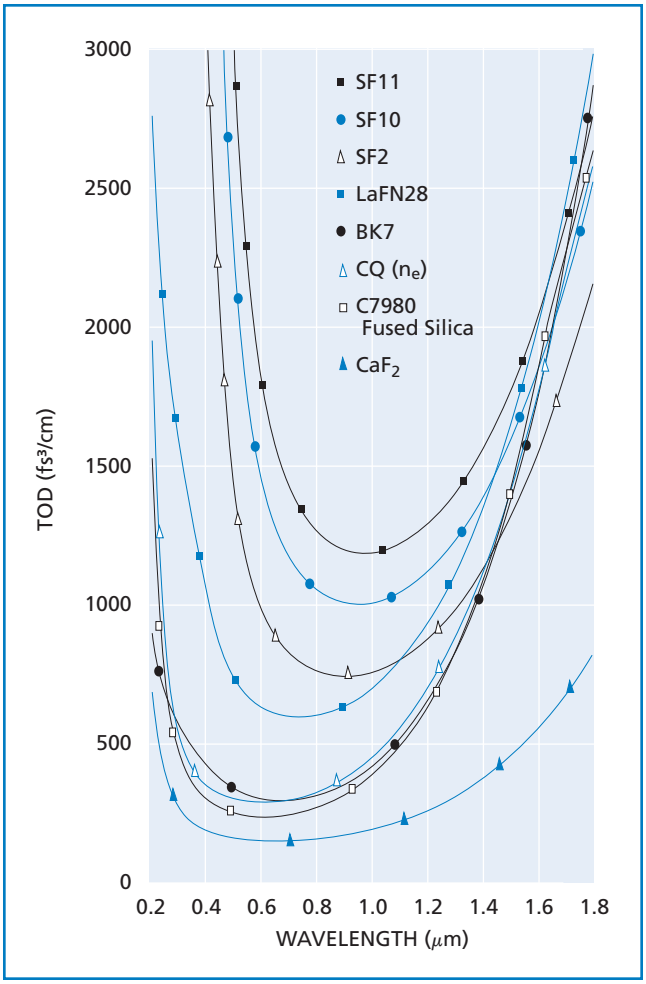

Figure 1.63 **Cubic dispersion for common glasses**

DISPERSIVE PROPERTIES OF MIRRORS

CVI Melles Griot uses three basic designs; TLM1 mirrors for energy fluence greater than 100 mJ/cm^2, TLM2 mirrors for cw oscillators and low-fluence pulses, and TLMB mirrors which are a hybrid of the two. The reflectivity, GVD parameter, and cubic dispersion parameter for TLM2 high reflectors are shown in Figure 1.64. In these examples, the mirrors are centered at 800 nm and are designed for use at normal incidence and at 45 degrees. Note that, at the design wavelength, (a) GVD is zero, (b) the cubic term is minimized, and (c) at 45° incidence, the GVD of the *p*-polarization component is very sensitive to wavelength, while the GVD for *s*-polarization component is nearly zero over a broad wavelength range. Thus one should avoid using mirrors at 45° incidence with the *p*-polarization. On the other hand, at 45° incidence, *s*-polarization provides very broad bandwidth and minimizes pulse distortion problems and should be used whenever possible.

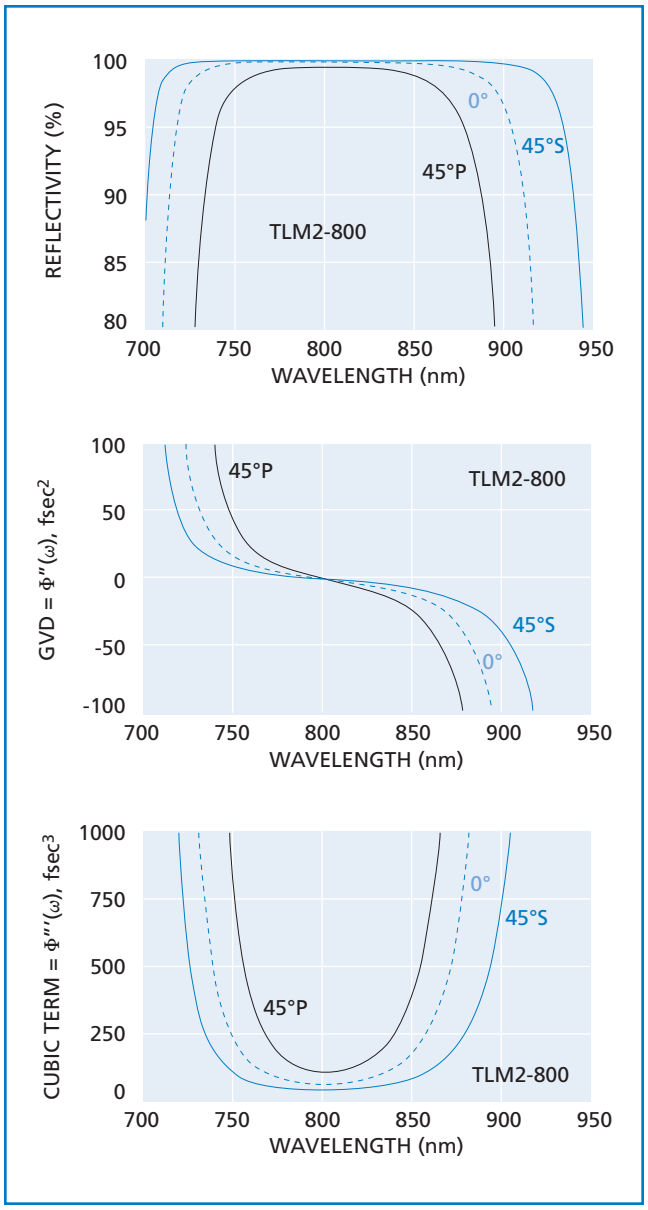

Figure 1.64 **Dispersion and reflectivity for mirrors TLM2-800-0 and TLM2-800-45**

Ti:Sapphire and other femtosecond laser systems need prismless compensation of the built-in positive chirp encountered in the laser optical circuit. This becomes mandatory in industrial and biomedical applications where the laser must provide a compact, stable, and reliable solution.

Negative Group Velocity Dispersion Mirrors (TNM2) meet these needs with off-the-shelf availability, and can be employed both intracavity and extracavity to satisfy chirp control requirements.

In experiments using CVI Melles Griot TNM2 negative group velocity dispersion mirrors, 200-mW, 80-fsec pulses centered at 785 nm were achieved in a simple, prismless, Ti:Sapphire oscillator. The configuration is shown in Figure 1.65.

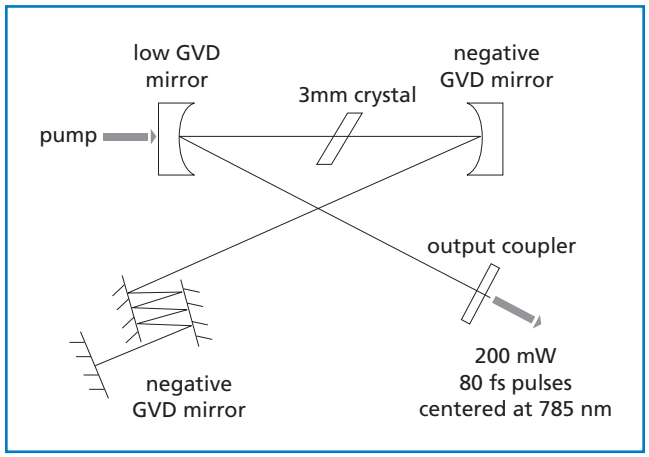

Figure 1.65 **Typical optical setup incorporating low GVD and Negative GVD mirrors in an ultrafast application**

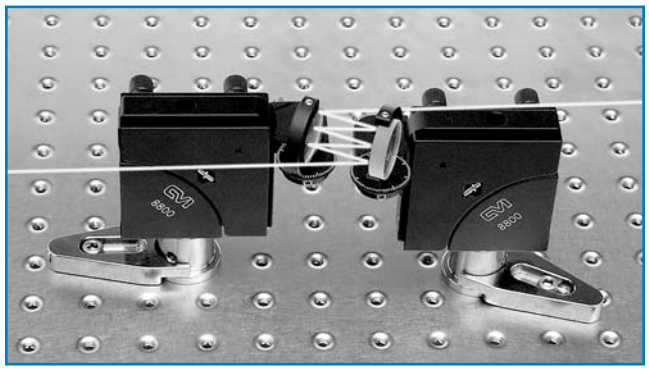

Figure 1.66 **Typical optical set-up of negative GVD mirrors**

OUTPUT COUPLERS AND BEAMSPLITTERS

Output-coupler partial reflectors and beamsplitters behave similarly; however, here is an additional consideration in their analysis. The behavior of the transmitted phase of the coating and the effect of material dispersion within the substrate on the transmitted beam have to be taken into account in a detailed analysis. In general, the coating transmitted phase has similar properties and magnitudes of GVD and cubic to the reflected phase. As usual, centering is important. As a beamsplitter, we recommend the 1.5 mm thick fused silica substrate PW-1006-UV. As an output coupler substrate, we recommend the 3.0 mm thick, 30 minute wedge fused silica substrate IF-1012-UV.

CVI Melles Griot has developed the TFPK Series Broadband Low Dispersion Polarizing Beamsplitters to satisfy requirements for very-high-power, short-pulse lasers. These optics are ideal for intracavity use in femtosecond regenerative amplifiers. The main emphasis is on linear phase characteristics. See Chapter 9 of Lasers, A. E. Siegman (University Science Books, Mill Valley, California, 1986), for a good discussion of linear pulse propagation.

In chirped pulse regenerative amplification, the pulse may have to pass through one or two polarizers twice per round trip. There can be 10 to 20 round trips before the gain is saturated and the pulse is ejected. At this stage the pulse is long (100–1000 psec); however the phase shift at each frequency must still be maintained to minimize the recompressed pulse width. The many round trips of the pulse in the regenerative amplifier put stringent requirements on the phase characteristics of the coatings.

Figure 1.67 shows the power transmission curves for both *s*- and *p*-polarization and the transmitted phase characteristics of the *p* component for a TFPK optimized at 800 nm. (Users may specify any wavelength

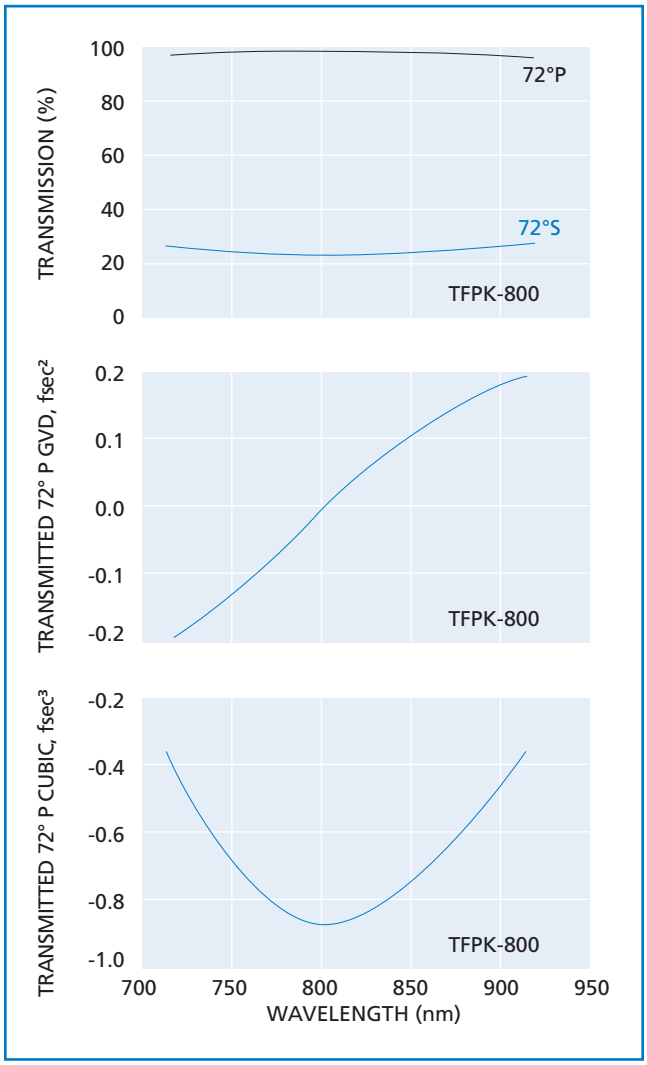

Figure 1.67 **Properties for one coated side of a TFPK polarizing beamsplitter optimized for 800 nm. Both sides are coated for these properties.**

from 250 nm to 1550 nm.) The phase characteristics shown are the GVD and the cubic phase term. Not shown are the reflected phase characteristics for *s*-polarization; they are similar to the *p*-polarization transmission curves, and have the same low nonlinearity and broad bandwidth. Note that both sides of the optic have the coating whose properties are described in Figure 1.67. Therefore, the *s*- and *p*-polarization transmissions per surface should be squared in determining the specifications. The phase characteristics show that in all modes of operation, the TFPK polarizer performance is dominated by the substrate.

There are some subtleties associated with the TFPK. The near 72° angle has to be set properly and optimized. Some thought has to be given to mechanical clearances of the laser beam at such a steep incidence angle. The reflectivity for *s*-polarization is limited to 75%. Variant designs can increase this at a slight loss in bandwidth, increase in incidence angle, and increase in insertion loss for the transmitted *p*-polarized component.

The FABS autocorrelator beamsplitters from CVI Melles Griot are broadband, 50% all-dielectric beamsplitters. They are useful in many types of pump-probe experiments and in the construction of antiresonant ring configurations. They are essentially lossless and extremely durable. Both have advantages over partially reflecting metal coatings.

Power transmission curves for the *s*- and *p*-polarized versions of the FABS, along with the corresponding reflected phase characteristics for beamsplitters optimized at 800 nm, are shown in Figures 1.68 and 1.69. The linear pulse propagation properties of these beamsplitters are dominated by the substrate material dispersion. As with virtually all dielectric coated optics, the *s*-polarized version is broader than *p*-polarized version. CVI Melles Griot can produce FABS in other than 50:50 with excellent phase characteristics.

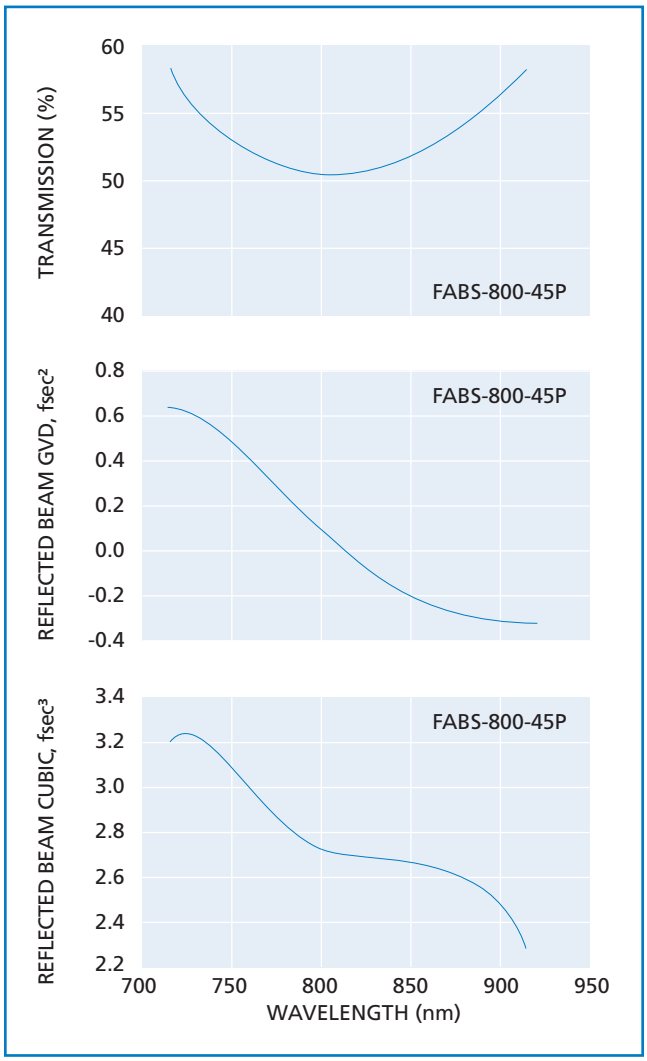

Figure 1.68 **Transmission characteristics for FABS series polarizers with *p*-polarized light**

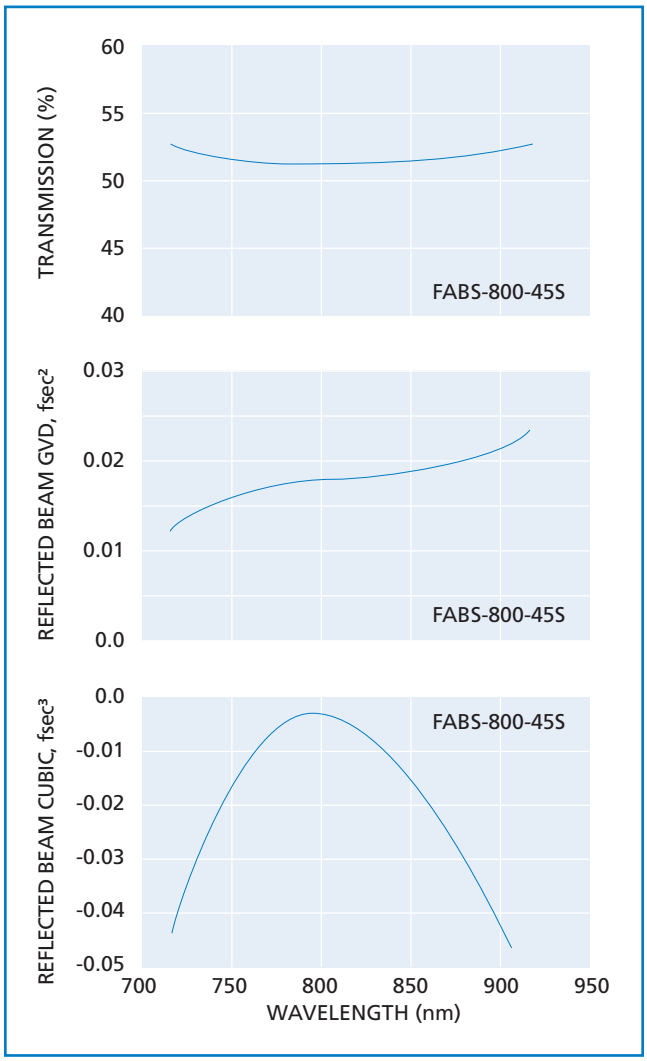

Figure 1.69 **Transmission characteristics for FABS series polarizers with *s*-polarized light**

ANTIREFLECTION COATINGS

All CVI Melles Griot antireflection coating designs work well in femtosecond operation as the forward-going phasor is the dominant contribution to the phase shift; the AR coating is very thin and simply "fixes" the small Fresnel reflection of the substrate.

PRISMS

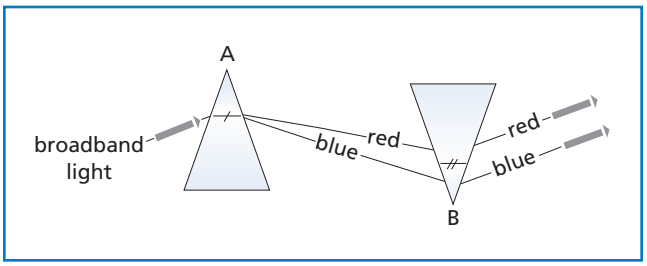

Figure 1.70 **Brewster prism**

Very-high-quality isosceles Brewster's angle prisms for intra and extracavity use are available from CVI Melles Griot. The design of these prisms satisfies the condition of minimum loss due to entrance and exit at Brewster's angle. To calculate GVD at Brewsters angle, refer to Figure 1.70 and use the following equation:

$$\mathrm{GVD} = \frac{d^2}{d\omega^2}\,\psi\Big|_{\omega=\omega_l} \approx \frac{\lambda_l^3}{2\pi c^2}\left[\mathrm{L}\,\frac{d^2\eta}{d\lambda^2}\Big|_{\lambda_l} - 4l\left(\frac{d\eta}{d\lambda}\Big|_{\lambda_l}\right)^2\right] \qquad (1.130)$$

where

η = refractive index of the prisms (assuming the same material)
l = tip to tip distance ($\overline{AB}$)
L = total avg. glass path
ψ = spectral phase of the electric field
$\omega_l \lambda_l = 2\pi_c$ (assumes Brewster prism at minimum deviation).

For more on the Ultrafast phenomena, see J.C. Diels and W. Rudolph, Ultrashort Laser Pulse Phenomena, Academic Press, 1996.

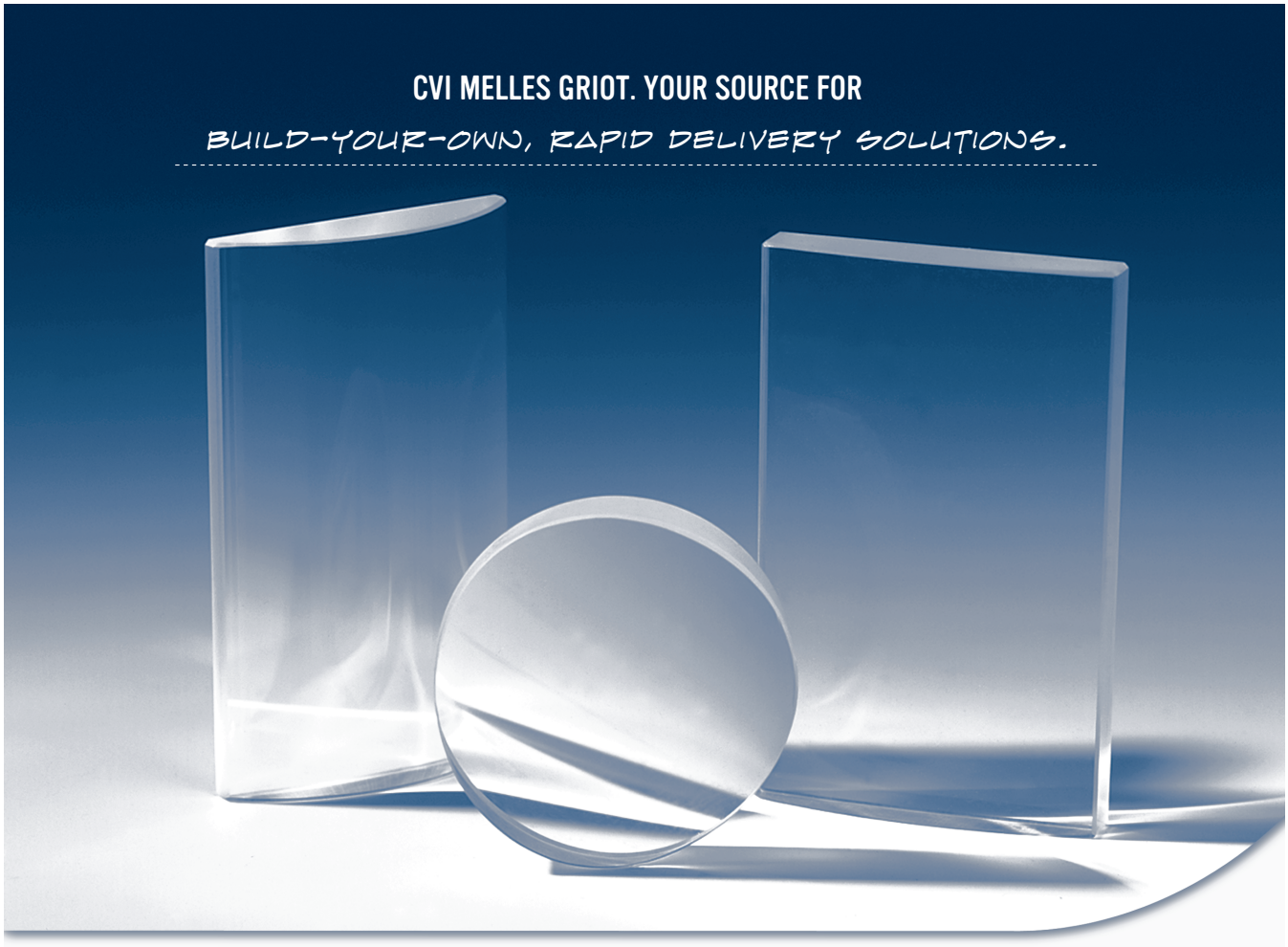

CVI Melles Griot offers two-week delivery of optics at catalog prices.

- 4000 uncoated substrates
- 2500 coating options
- A wide variety of in-stock substrates available (curves, flats, prisms, waveplates)
- Coatings from 193 nm to 2300 nm
- Your order ships in two weeks or less

How can we help you make your project a success?

Lasers | Lenses | Mirrors | Assemblies | Windows | Shutters | Waveplates | Mounts